The Astrophysical Journal, 587:278–311, 2003 April 10

NEUTRAL ATOMIC PHASES OF THE INTERSTELLAR MEDIUM IN THE GALAXY

Mark G. Wolfire
Department of Astronomy, University of Maryland, College Park, MD 20742-2421; mwolfire@astro.umd.edu

Christopher F. McKee
Departments of Physics and Astronomy, University of California at Berkeley, Berkeley, CA 94720;
cmckee@astron.berkeley.edu

David Hollenbach
NASA Ames Research Center, MS 245-3, Moffett Field, CA 94035; hollenbach@ism.arc.nasa.gov

and

A. G. G. M. Tielens
Kapteyn Astronomical Institute, P.O. Box 800, 9700 AV Groningen, Netherlands; tielens@astro.rug.nl
Received 2002 July 2; accepted 2002 December 13

ABSTRACT

Much of the interstellar medium in disk galaxies is in the form of neutral atomic hydrogen, H I. This gas can be in thermal equilibrium at relatively low temperatures, $T \lesssim 300$ K (the cold neutral medium [CNM]), or at temperatures somewhat less than 10^4 K (the warm neutral medium [WNM]). These two phases can coexist over a narrow range of pressures, $P_{\rm min} \leq P \leq P_{\rm max}$. We determine $P_{\rm min}$ and $P_{\rm max}$ in the plane of the Galaxy as a function of Galactocentric radius R using recent determinations of the gas heating rate and the gas-phase abundances of interstellar gas. We provide an analytic approximation for $P_{\rm min}$ as a function of metallicity, far-ultraviolet radiation field, and the ionization rate of atomic hydrogen. Our analytic results show that the existence of $P_{\rm min}$, or the possibility of a two-phase equilibrium, generally requires that H^+ exceed C^+ in abundance at $P_{\rm min}$. The abundance of H^+ is set by EUV/soft X-ray photoionization and by recombination with negatively charged polycyclic aromatic hydrocarbons. In order to assess whether thermal or pressure equilibrium is a realistic assumption, we define a parameter $\Upsilon \equiv t_{\rm cool}/t_{\rm shock}$, where $t_{\rm cool}$ is the gas cooling time and $t_{\rm shock}$ is the characteristic shock time or "time between shocks in a turbulent medium." For $\Upsilon < 1$ gas has time to reach thermal balance between supernova-induced shocks. We find that this condition is satisfied in the Galactic disk, and thus the two-phase description of the interstellar H I is approximately valid even in the presence of interstellar turbulence. Observationally, the mean density $\langle n_{\rm H\,I} \rangle$ is often better determined than the local density, and we cast our results in terms of $\langle n_{\rm H\,I} \rangle$ as well. Over most of the disk of the Galaxy, the H I must be in two phases: the weight of the H I in the gravitational potential of the Galaxy is large enough to generate thermal pressures exceeding $P_{\rm min}$, so that turbulent pressure fluctuations can produce cold gas that is thermally stable; and the mean density of the H I is too low for the gas to be *all* CNM. Our models predict the presence of CNM gas to $R \simeq 16$–18 kpc, somewhat farther than previous estimates. An estimate for the typical thermal pressure in the Galactic plane for 3 kpc $\lesssim R \lesssim$ 18 kpc is $P_{\rm th}/k \simeq 1.4 \times 10^4 \exp(-R/5.5\ {\rm kpc})$ K cm^{-3}. At the solar circle, this gives $P_{\rm th}/k \simeq 3000$ K cm^{-3}. We show that this pressure is consistent with the C I*/C $_{\rm tot}$ ratio observed by Jenkins & Tripp and the CNM temperature found by Heiles & Troland. We also examine the potential impact of turbulent heating on our results and provide parameterized expressions for the heating rate as a function of Galactic radius. Although the uncertainties are large, our models predict that including turbulent heating does not significantly change our results and that thermal pressures remain above $P_{\rm min}$ to $R \simeq 18$ kpc.

Subject headings: ISM: clouds — ISM: general — ISM: structure

1. INTRODUCTION

The interstellar medium (ISM) has a complex thermal and ionization structure. Much of the neutral atomic gas is observed to be either warm neutral medium (WNM) with $T \sim 10^4$ K or cold neutral medium (CNM) with $T \sim 100$ K (Kulkarni & Heiles 1987; Dickey & Lockman 1990). Some of the warm gas is partially ionized, the warm ionized medium (WIM), which also has $T \sim 10^4$ K (McKee & Ostriker 1977, hereafter MO; Reynolds 1983; Haffner, Reynolds, & Tufte 1999). A small mass fraction of the gas is in the form of hot ionized medium (HIM) with $T \sim 10^6$ K (Cox & Smith 1974; MO). Inside the solar circle, about half the interstellar gas is molecular (Scoville & Sanders 1987; Bronfman et al. 1988, 2000).

A significant simplification occurs if one focuses on the neutral atomic gas, the CNM and WNM. Some decades ago, Field, Goldsmith, & Habing (1969) demonstrated that the CNM and WNM could coexist in pressure equilibrium, so that the neutral atomic gas could be considered to be a two-phase medium. They assumed that cosmic rays dominate the heating, but it was subsequently realized that UV starlight dominates the heating due to photoelectric emission from the dust grains in the gas (Watson 1972). Using the photoelectric heating rates calculated by Bakes & Tielens (1994), Wolfire et al. (1995a, hereafter WHMTB) investigated the thermal balance of the WNM and CNM phases in the local ISM and showed that the two-phase model is in good agreement with a wide variety of data on the ISM in the solar vicinity.

What is the evidence for a two-phase medium elsewhere in the Galaxy? In the inner Galaxy, Garwood & Dickey (1989) found that there is H I emission (which can originate from both CNM and WNM) at all velocities allowed by Galactic rotation. On the other hand, they found that absorption (which originates only from CNM at their sensitivity) is somewhat less pervasive, particularly within 2 kpc of the Galactic center. Liszt, Braun, & Greisen (1993) suggested that the H I absorption in the inner Galaxy at $R > 2$ kpc is much higher than that reported by Garwood & Dickey (1989). Kolpak et al. (2002) recently repeated the earlier H I absorption study and confirmed the presence of cold gas in the inner Galaxy with an absorption coefficient at $R = 5$ kpc approximately 5 times higher than reported by Garwood & Dickey (1989). In the outer Galaxy, the presence of WNM is reasonably well established (Kulkarni & Heiles 1987), whereas that of a widely distributed CNM is less so. Carilli, Dwarakanath, & Goss (1998) have measured the temperature of the WNM in absorption features seen toward Cygnus A at distances of 9 and 12 kpc (and z height of $\sim$1 kpc) using the Westerbork Synthesis Radio Telescope. They find gas temperatures of $\sim$6000 and $\sim$4800 K, respectively, which are consistent with the low-pressure and low-UV field models of WHMTB for atomic gas above the plane. Several high-velocity absorption components have been observed in H I (Colgan, Salpeter, & Terzian 1988) and Na I (Sembach & Danks 1994) that arise from CNM clouds at Galactic radii $R \lesssim 14$ kpc. Kolpak et al. (2002) show H I absorption to $R \lesssim 17$ kpc. Molecular clouds, which presumably form from the CNM phase, are traced to at least $R \sim 20$ kpc (Wouterloot & Brand 1989; Heyer, Carpenter, & Snell 2001) with an extremely distant H II region and molecular cloud complex at $R = 28$ kpc (Digel, de Geus, & Thaddeus 1994). Wouterloot et al. (1990) and Bronfman et al. (2000) show that the molecular surface density can be fitted by a radial exponential in the outer Galaxy to $\sim$18 kpc (see also Williams & McKee 1997). In their study of the Perseus arm, Heyer et al. (1998), however, find that the molecular gas disk is effectively truncated at $R \sim 13.5$ kpc. These two results could be consistent if molecular gas extends to greater radii in directions other than those studied by Heyer et al. (1998) or if isolated molecular clouds extend to distances much greater than the molecular surface density can be reliably measured from CO surveys.

Thus, direct observations of cold H I or molecular gas extend to at least $R \sim 18$ kpc. Star formation provides an indirect test for the presence of CNM, since the gas that forms stars presumably goes through the stage of being cold H I. In the Galaxy, near-infrared sources, *IRAS* sources, and H II regions (Wouterloot et al. 1990; Rudolph et al. 1996; Kobayashi & Tokunaga 2000; Snell, Carpenter, & Heyer 2002) are seen out to $R \sim 17$–20 kpc, suggesting that CNM extends out to at least that distance.

What can be learned from observations of H I in other galaxies? Two-phase atomic gas has been observed using 21 cm absorption techniques in several extragalactic systems including M31 (Dickey & Brinks 1993; Braun & Walterbos 1992), M33 (Dickey & Brinks 1993), the LMC (Mebold et al. 1997), and the SMC (Dickey et al. 2000). Braun (1997), using the VLA, examined the neutral hydrogen emission in 11 nearby spirals. By associating high brightness, narrow emission components with cold gas, he finds that the fraction of cold gas remains relatively constant until the B-band surface brightness falls to $\mu_B \sim 25$ mag arcsec^{-2}, i.e., the R_{25} radius. At larger radii, the fraction drops, although in some systems more than 10% of the H I is in the form of cold gas out to $(1.5–2)R_{25}$. Since the extinction-corrected radius of the Galaxy is $R_{25} = 12.25$ kpc (de Vaucouleurs 1983), cold gas in the Galaxy could extend out to $(1.5–2)R_{25}$, or $R \sim 18.4$–24.5 kpc. Sellwood & Balbus (1999) interpret the line width of H I in the outer parts of galaxies as being due to CNM that is being stirred by the magnetorotational instability. Evidence for recent star formation in the outer disk of M31 is presented by Cuillandre et al. (2001), who find a population of B stars at $1.7R_{25}$, pointing toward the presence of cold gas in the outer parts of galaxies.

The fact that the neutral atomic gas in the Galactic ISM is in two phases is a powerful result, since two phases can coexist only over a narrow range of pressure, $P_{\max} > P > P_{\min}$ with $P_{\max} \lesssim 3P_{\min}$ (Field et al. 1969; see § 6). It is thus possible to estimate the thermal pressure of the H I with reasonable accuracy (when it is in two phases) from knowing the gas-phase abundances, the dust properties, and the intensity of the radiation field. We used this property to study gas in the Galactic halo and constrain the properties of the high-velocity clouds in Wolfire et al. (1995b). Corbelli & Salpeter (1988) have argued that achieving the condition for a two-phase equilibrium is a necessary step in initiating star formation in young galaxies, while Parravano (1988, 1989) has suggested that two-phase equilibria play a key role in regulating the rate of star formation in disk galaxies.

The primary goal of this paper is to predict the average thermal pressure of the ISM as a function of position in the Galaxy using the two-phase criteria. To do this, we shall extend the models of WHMTB to the inner and outer Galaxy. In light of the observational evidence that cold gas exists in the outer Galaxy, we shall carry out our model calculations for Galactic radii between 3 and 18 kpc. Knowing the thermal pressure allows one to predict the intensities of the dominant cooling lines of the gas, such as that of C II 158 μm, and examine the heating and cooling routes that determine the energy budget. Locally, the thermal pressure in the ISM is measured through ultraviolet absorption line studies (Jenkins, Jura, & Loewenstein 1983; Jenkins & Tripp 2001). In the near future, telescopes such as ALMA, SOFIA, and Herschel will provide additional measurements of the thermal pressure and dominant cooling lines throughout the Galaxy and in other galaxies. These will test our model for the gas thermal balance and check the importance of thermal instability.

We also can calculate whether the ISM could exist as pure WNM at various positions in the Galaxy by comparing the weight of the H I layer with $P_{\max}$. The problem of determining the phase structure of the H I in the outer Galaxy has been considered previously by Elmegreen & Parravano (1994), who find a transition to mainly WNM at $R \gtrsim 12$–14 kpc. Our results are compared with theirs in § 8.3.

Although the focus of this paper is on the determination of the thermal pressure in Galactic H I, it is well known that the thermal pressure is only a small part of the total pressure in the gas; in particular, the turbulent pressure is considerably greater than the thermal pressure (Boulares & Cox 1990). In § 2 we discuss the relation between the turbulent pressure and the thermal pressure and determine the conditions under which it makes sense to consider multiphase equilibria in a turbulent medium. We also discuss in Appendix B the dissipation of turbulent energy in the ISM and its potential effects on our results. In § 3 we discuss the

distribution of gas and dust in the Galaxy together with the abundances we have adopted. The heating and ionization in the gas are governed by energetic photons and particles, which are discussed in § 4. The thermal and chemical processes in our model are slightly modified from those discussed by WHMTB; the differences are briefly described in § 5. The results of our calculations are presented in § 6. We then construct a simple analytic model of a two-phase equilibrium that shows how the properties
of the equilibrium scale with the input parameters (§ 7). We compare our model with local and extragalactic observations in § 8 and discuss our results in § 9.

2. TURBULENT PRESSURE IN THE MULTIPHASE INTERSTELLAR MEDIUM

The ISM is observed to be highly turbulent (Larson 1979). When averaged over the vertical structure of the Galactic disk, the turbulent velocity dispersion exceeds the thermal velocity dispersion, and correspondingly the turbulent pressure exceeds the thermal pressure (Boulares & Cox 1990). Theoretical arguments (Spitzer 1968, 1978; MO) and numerical simulations (Bregman, Parriott, & Rosen 1999; Korpi et al. 1999) show that these turbulent motions can be accounted for by the injection of energy by supernovae.

Insofar as the disk of the Galaxy is in approximate hydrostatic equilibrium, the total pressure in the midplane of the disk must balance the weight of the material above it (Parker 1969; Boulares & Cox 1990), and the turbulent motions are an important contributor to the total pressure. In the solar neighborhood, the total pressure at the midplane is about $P/k \simeq 2.8 \times 10^4$ K cm^{-3} (Boulares & Cox 1990), about 10 times greater than the median thermal pressure of $\sim$3000 K cm^{-3} (Jenkins & Tripp 2001).[1] A similar situation occurs in molecular clouds, where the total pressure can also be about an order of magnitude greater than the thermal pressure (depending on scale; see Larson 1981). If the thermal pressure is such a small fraction of the total, why are arguments based on thermal pressure equilibrium relevant in the ISM?

The answer is that *the turbulent motions determine the temporal and spatial structure of the thermal pressure.* A key feature of turbulence is that the motions are spatially correlated, so that the rms velocity increases with scale; i.e., there is a relation between the line width and the size of a region,

$$\sigma = \sigma(1)\ell_{\rm pc}^{q} , \qquad (1)$$

where $\sigma(1)$ is the one-dimensional turbulent velocity on the scale of 1 pc and $\ell_{\rm pc}$ is the scale in units of parsecs. Larson's (1979) data on H I clouds give $\sigma(1) = 0.64$ km s^{-1} and $q = 0.37$ over the range $1 \lesssim \ell_{\rm pc} \lesssim 1000$. (Larson 1981 subsequently found a similar line width–size relation for molecular clouds.) We can estimate $\sigma(1)$ from a more homogeneous data set by using the recent H I study by Heiles & Troland (2003). They find that the mass-weighted velocity dispersion is 7.1 km s^{-1} for CNM clouds and 11.4 km s^{-1} for WNM clouds. The typical line of sight in this survey is at a Galactic latitude slightly greater than 30°, so the typical path length is about twice the half-height of the disk, i.e., the full disk thickness. From Dickey & Lockman's (1990) model for the vertical distribution of the H I, we infer that the FWHM of the CNM is 212 pc, whereas that for the WNM is 530 pc. We assume that the outer scale of the turbulence is greater than the disk thickness, so that the power-law behavior extends over this length scale; this assumption is consistent with the results of Larson (1979), who did not find a break in the power-law behavior out to 1 kpc in the Galaxy, and with the results of Lazarian & Pogosyan (2000), who did not find a break between 40 pc and 4 kpc in the data for the SMC. We shall set $q = \frac{1}{3}$, as expected for subsonic turbulence. On scales large enough for the turbulence to be supersonic, q is expected to be somewhat larger: Larson (1979) suggested that q would approach $\frac{1}{2}$, whereas Boldyrev (2002) finds $q \simeq 0.37$–0.38 (where σ is interpreted as an rms velocity). For the CNM, we then find $\sigma(1) = 1.2$ km s^{-1}, whereas for the WNM we find $\sigma(1) = 1.4$ km s^{-1}. The value of q is likely to be closer to the assumed $\frac{1}{3}$ on the smaller length scales associated with the CNM, so we shall adopt $\sigma(1) = 1.2$ km s^{-1} for the H I in the solar neighborhood. Although this value was determined from the velocity dispersion of different H I clouds, we shall assume that it applies within individual H I clouds as well. We note that this assumption is consistent with the results of Linsky & Wood (1996), who found that the velocity dispersion within the H I toward the nearby star α Cen is about 1.2 km s^{-1}, corresponding to $\sigma(1) = 1.1$ km s^{-1}. The use of a single turbulent velocity law in both the CNM and the WNM is undoubtedly an oversimplification; in particular, there is a range of scales over which the turbulence is supersonic in the CNM and subsonic in the WNM, and q might be expected to have different values within individual clouds of CNM and WNM over this range.

Let ℓ_P be the scale on which the turbulent pressure begins to dominate the thermal pressure; on scales less than ℓ_P the gas typically will be in approximate thermal pressure equilibrium. To estimate ℓ_P, we equate the thermal velocity dispersion, $\sigma_{\rm th} = 0.80 T_2^{1/2}$ km s^{-1}, with the turbulent velocity dispersion, so that

$$\ell_P = \left[\frac{\sigma_{\rm th}}{\sigma(1)}\right]^{1/q} \text{pc} \rightarrow 0.3 T_2^{3/2} \text{ pc} , \qquad (2)$$

where $T_2 \equiv T/(100\ {\rm K})$ and the numerical evaluation is for our fiducial case. Because ℓ_P depends on the cube of the uncertain quantity $\sigma(1)$, the numerical value of ℓ_P is quite uncertain. Bearing this in mind, we find that the CNM should be in approximate thermal pressure equilibrium on scales $\ell < \ell_P({\rm CNM}) \sim 0.3$ pc. For the WNM, with a typical temperature of about 8000 K, we find $\ell_P({\rm WNM}) \simeq 215$ pc. This is somewhat larger than the size of the turbulent cells in the warm gas, 60 pc, found in the three-dimensional numerical simulations of the ISM by Korpi et al. (1999).

In a multiphase medium, the CNM is embedded in warm gas, either predominantly neutral (WNM) or ionized (WIM), which in turn may be embedded in hot gas, the HIM. Since the sound speed in the WIM exceeds that in the WNM, ℓ_P(WIM) is somewhat larger than ℓ_P(WNM); both are much larger than the typical size of a CNM cloud, which is $\sim$1–2 pc (MO). As a result, the CNM clouds should typically be embedded in a medium that is spatially isobaric. The surface layers of the cloud [i.e., those layers within a

[1] The mean pressure quoted by Jenkins & Tripp (2001) is $P/k = 2240$ K cm^{-3} based on data from the Space Telescope Imaging Spectrograph. In § 8 we find that corrections for gas temperature and atomic constants raise the pressure derived from the observations to $\sim$3000 K cm^{-3}.

distance ℓ_P(CNM) of the surface] should typically have the same thermal pressure as the ambient warm medium, whereas the inner regions of the cloud should have the time-averaged value of the ambient thermal pressure. Elmegreen (1997) shows that in a one-dimensional simulation of interacting magnetized clouds the gas maintains approximate phase equilibrium with the intercloud medium.

This description of the relative roles of thermal and turbulent pressures in the ISM is consistent with the three-phase model of the ISM by MO. In their model, the supernova-generated HIM is pervasive and sets the thermal pressure in the embedded clouds of CNM and WNM. The ISM is viewed as the superposition of many supernova remnants (SNRs); as a result, there are substantial fluctuations in the thermal pressure, in qualitative agreement with observations (Jenkins et al. 1983; Jenkins & Tripp 2001). The turbulent motions provided by supernovae are consistent with observations of H I velocities in the Galactic plane. Turbulent pressure is the single largest contributor to the support of the ISM in the gravitational field of the disk (Boulares & Cox 1990), and McKee (1990) has argued that the turbulent motions that produce this pressure are produced by supernovae. Slavin & Cox (1993) and Cox (1995) have argued that magnetic fields in the ISM limit the size of SNRs so that they occupy only a small fraction of the volume. Such a model cannot account for the observed level of turbulence, however.

Under what conditions is the turbulence in the ISM weak enough that a two-phase description of the H I is valid? We first consider the cooling time $t_{\rm cool}$ for an element of gas to return to thermal equilibrium after a significant perturbation. From our numerical results presented in § 6, we find that the cooling rate at a constant thermal pressure of $P_{\rm th}/k = 3000$ K cm^{-3} is given by

$$\Lambda = 5.7 \times 10^{-26} T_4^{0.8} \text{ ergs cm}^3 \text{ s}^{-1} , \qquad (3)$$

where $T_4 \equiv T/(10^4 \text{ K})$ and where the fit is accurate to within a factor of 1.35 for temperatures between $T = 55$ and 8500 K. With this cooling rate, $t_{\rm cool}$ is given by

$$t_{\rm cool} = \left[\frac{(5/2)1.1nkT}{n^2\Lambda}\right] \simeq 7.7 \times 10^6 T_4^{1.2} \left(\frac{P_{\rm th}/k}{3000 \text{ K cm}^{-3}}\right)^{-0.8} \text{ yr} , \qquad (4)$$

where n is the hydrogen nucleus density ($n = n_{\rm H\,I} + n_{\rm H^+} + 2n_{\rm H_2}$). The fit to the pressure term results in an overall accuracy within a factor of 1.5 for temperatures between $T = 55$ and 8000 K and thermal pressures between $P_{\rm th}/k = 1000$ and 6000 K cm^{-3}. In order for a two-phase description to be valid, this time must be less than the characteristic time $t_{\rm shock}$ for a shock to induce motions of order $\sigma_{\rm th}$ or, equivalently (for an isothermal shock), to double the pressure.[2] One method of estimating $t_{\rm shock}$ is based on observations of interstellar turbulence. In order to induce motions of $\sigma_{\rm th}$, the velocity of an isothermal shock must be $\sqrt{2}\sigma_{\rm th}$. The time interval between shocks in a turbulent medium is then $t_{\rm shock} \sim \ell_P/\sqrt{2}\sigma_{\rm th}$, where, as discussed above, the value of ℓ_P is quite uncertain. Defining a dimensionless parameter Υ that measures the strength of the turbulence, we obtain

$$\Upsilon \equiv \frac{t_{\rm cool}}{t_{\rm shock}} \sim 0.3 T_4^{0.2} \left(\frac{P_{\rm th}/k}{3000 \text{ K cm}^{-3}}\right)^{-0.8} \left[\frac{\sigma(1)}{1.2 \text{ km s}^{-1}}\right]^3 . \qquad (5)$$

So long as $\Upsilon \lesssim 1$, a two-phase description of the H I is approximately valid, since the gas has time to reach thermal balance between shocks. This condition is well satisfied for the CNM ($\Upsilon \simeq 0.1$) but only marginally satisfied for the WNM ($\Upsilon \simeq 0.3$).

We can also estimate $t_{\rm shock}$ and Υ analytically under the assumption that the shocks are produced by SNRs, although this estimate is necessarily uncertain. Let $M_{\rm shock}(> v_s)$ be the mass of interstellar gas per supernova that suffers a shock with a shock velocity greater than v_s. Since the shock must have a velocity $\sqrt{2}\sigma_{\rm th}$ in order to induce motions of $\sigma_{\rm th}$, we have

$$t_{\rm shock} \simeq \frac{\Sigma_{\rm WNM}}{\dot{\varsigma}_{\rm SN,eff} M_{\rm shock}(> \sqrt{2}\sigma_{\rm th})} , \qquad (6)$$

where $\Sigma_{\rm WNM}$ is the surface density of WNM gas and $\dot{\varsigma}_{\rm SN,eff}$ is the effective supernova rate per unit area. Allowing for the clustering of supernovae in associations, McKee (1989) estimated that the effective supernova rate is only about 36% of the actual rate. For a two-phase ISM, he also estimated $M_{\rm shock} = 2460 n_{\rm WNM}^{-0.1} (v_s/100 \text{ km s}^{-1})^{-9/7} \; M_\odot$, where $n_{\rm WNM}$ is the H nucleus density in the WNM and where we have assumed that a typical SNR has an energy of 10^{51} ergs. (The results for a three-phase ISM with a substantial WNM filling factor should not differ qualitatively from the two-phase results.) At the solar circle, the supernova rate per unit area is about 3.8×10^{-11} SNs pc^{-2} yr^{-1} (McKee & Williams 1997), so this gives $t_{\rm shock} \simeq 5.3 \times 10^6$ yr for a density $n_{\rm WNM} = 0.3$ cm^{-3}. The corresponding value of the turbulence parameter for the WNM is $\Upsilon \simeq 0.9$, somewhat larger than the value estimated above (and indicative of the uncertainty in this parameter). Both estimates of Υ suggest that the WNM will often exhibit nonequilibrium temperatures. Heiles & Troland (2003) find that about half the WNM is at temperatures below the minimum equilibrium value, which is qualitatively consistent with our estimate of Υ.

Recent papers by Mac Low et al. (2001), Vázquez-Semadeni, Gazol, & Scalo (2000), and Vázquez-Semadeni et al. (2003) argue that thermal instability is of less importance in determining the distribution of phases than is turbulent dynamics followed by cooling toward thermal equilibrium. To some extent, the difference between these conclusions and those in the present paper is a matter of perspective: these authors focus on the time-dependent aspects of a turbulent medium, whereas we emphasize the utility of the equilibrium aspects. (We also note that Mac Low et al. 2001 did not include heating sources in their calculations.) In terms of the turbulence parameter Υ introduced above, we choose to approximate the case $\Upsilon \sim 1$ for the WNM with the two-phase $\Upsilon \ll 1$ results, whereas they prefer to emphasize the case $\Upsilon \gg 1$. Furthermore, in contrast to Mac Low

[2] In fitting eqs. (3) and (4) we have assumed that ionization equilibrium holds although the recombination time in WNM gas is found to be comparable to, or up to 2 times greater than, the cooling time. Since the cooling time in the WNM is proportional to $1/n_e$ for Lyα cooling and proportional to $1/n_e^{0.6}$ for electrons recombining onto positively charged grains (see § 5), any lingering ionization after the passage of a shock will tend to decrease the cooling time. Thus, our fits provide a maximum cooling time in WNM gas.

et al. (2001), who concentrate on evaluating the thermal pressure distribution in the solar neighborhood, the focus of our work is on determining the mean (volume-averaged) thermal pressure in the ISM throughout the Galaxy, $P_{\rm th,ave}$. Unless $P_{\rm th,ave}$ is in, or close to, the range $P_{\rm min} \lesssim P_{\rm th,ave} \lesssim P_{\rm max}$, the gas will be almost all CNM or all WNM, and the complex interplay between cold and warm gas seen by these authors will not occur. By determining $P_{\rm min}$ and $P_{\rm max}$, we can determine the range of pressures in which cold and warm gas can coexist; furthermore, we shall argue that most of the Galactic disk *must* have a thermal pressure such that this is the case.

3. GAS AND DUST IN THE MILKY WAY

3.1. *Distribution of* H I

We require the azimuthally averaged H I surface density distribution, $\Sigma_{\rm H\,I}(R)$, the half-width to half-maximum of the H I emission above the plane, $H_z^{\rm H\,I}(R)$, and the mean H I density in the Galactic plane, $\langle n_{\rm H\,I}(R)\rangle \propto \Sigma_{\rm H\,I}(R)/H_z^{\rm H\,I}(R)$. These will be used to trace the opacity in order to determine the distribution of energetic photons and particles in the Galaxy as discussed in § 4.

Several surveys have been conducted of the Galactic H I distribution (e.g., Weaver & Williams 1973; Burton 1985; Kerr et al. 1986; Stark et al. 1992; Hartmann & Burton 1997). Lockman (2003) discusses several limitations in interpreting the observations, including velocity crowding, which renders $\Sigma_{\rm H\,I}(R)$ highly sensitive to the adopted rotation curve, optical depth effects, which introduce uncertainty in the volume and surface densities, and a low dynamic range in emission, which makes small variations in the brightness temperature difficult to measure. Thus, the distribution in $\Sigma_{\rm H\,I}(R)$ is not well determined. In addition, the derived scale height $H_z^{\rm H\,I}$ may depend on the method of analysis, which could be preferentially sensitive to the CNM or WNM component. With these caveats in mind, we use the published H I data to derive our distributions.

The distribution of H I in the outer Galaxy was presented by Wouterloot et al. (1990), who combined the northern hemisphere (Kerr et al. 1986; Burton 1985) and southern hemisphere (Kerr et al. 1986) data. They provide plots of the H I surface density, $\Sigma_{\rm H\,I}(R)$, from the second and third Galactic quadrants (northern and southern data) as well as the average surface density and find that the average radial distribution at $R > 13$ kpc is well fitted by an exponential, $\Sigma_{\rm H\,I}(R) \propto \exp(-R/H_R^{\rm H\,I})$, with $H_R^{\rm H\,I} = 4$ kpc. A relatively flat rotation curve was used, similar to that derived by Brand & Blitz (1993).

Dame (1993) and Lockman (1988) showed that minor (∼2%) differences in the rotation curve can greatly affect the surface density derived from the data with differences in the surface density amounting to ∼50%. Based on the northern hemisphere data, Dame (1993) found a peak in surface density near 12 kpc for a flat rotation curve but a nearly constant surface density out to 17 kpc when using the slightly rising rotation curve of Kulkarni, Blitz, & Heiles (1982). Wouterloot et al. (1990) attributed the peak in the H I surface density to gas associated with the Perseus arm and show that the average of the northern and southern data partially smooths the 12 kpc peak.

In addition to the surface density enhancement at 12 kpc, the Wouterloot et al. (1990) plots of the outer Galaxy show a dramatic rise as R decreases toward the solar circle, reaching $\Sigma_{\rm H\,I} = 8.6\ M_\odot\ {\rm pc}^{-2}$ at $R = 9$ kpc. (Note that in our notation $\Sigma_{\rm H\,I}$ does not include the mass associated with helium or the metals.) This surface density is inconsistent with the value of $\Sigma_{\rm H\,I}(R_0) = 5\ M_\odot\ {\rm pc}^{-2}$ at the solar circle determined by Dickey & Lockman (1990). Furthermore, the average surface density in the outer Galaxy does not seem to join smoothly onto the inner Galaxy where $\Sigma_{\rm H\,I}$ is also 5 $M_\odot$ pc^{-2}. The inferred pileup of H I toward the edge of the solar circle may be an artifact of a flat rotation curve with strictly circular velocities, and noncircular motions may alleviate this problem (Blitz & Spergel 1991). An example of the H I surface density retaining the peak at R_0 is shown in Olling & Merrifield (1998), who also argue for $R_0 \sim 7.1$ kpc. In our post-Copernican world, we believe that a narrow density enhancement centered at $R = 8.5$ kpc is unrealistic and have smoothly joined the Wouterloot et al. (1990) surface densities at $R > 10$ kpc onto the distribution for $R < 8.5$ kpc. We are mainly concerned with the disk properties in the inner and outer Galaxy, and thus errors less than a factor of 2 in a thin region between 8.5 and 10 kpc are not critical.

The observational evidence suggests that the H I surface density is constant in the inner Galaxy between 8.5 and ∼4 kpc and then drops by a factor of ∼3 by 1.5 kpc (Dickey & Lockman 1990; Liszt 1992; Dame 1993). Our piecewise analytic fit to the H I surface density data is shown in Figure 1 and is given by

$$\Sigma_{\rm H\,I}(R) = \begin{cases} 1.4R_k - 0.6\ M_\odot\ {\rm pc}^{-2} & (3 \le R_k < 4)\ , \\ 5\ M_\odot\ {\rm pc}^{-2} & (4 \le R_k < 8.5)\ , \\ -1.12 + \left[6.12\left(\dfrac{R_k}{8.5}\right)\right]\ M_\odot\ {\rm pc}^{-2} & (8.5 \le R_k < 13)\ , \\ 8.24e^{-(R_k-13)/4}\ M_\odot\ {\rm pc}^{-2} & (13 \le R_k < 24)\ , \end{cases} \tag{7}$$

where $R_k \equiv R/(1\ {\rm kpc})$ and where we use the conversion $1\ M_\odot\ {\rm pc}^{-2} = 1.25 \times 10^{20}\ {\rm H\,I\,cm}^{-2}$. Dame (1993) found that using the H I surface density given in Liszt (1992), the H I mass at $R < R_0$ (excluding the Galactic center) is $M_{\rm H\,I} \sim 1.7 \times 10^9\ M_\odot$, while our distribution gives a mass

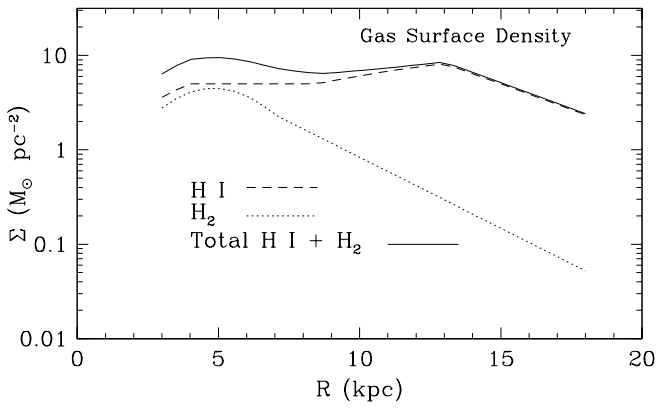

FIG. 1.—Azimuthally averaged H I surface density $\Sigma_{\rm H\,I}$ (*dashed curve*) and H_2 surface density $\Sigma_{\rm H_2}$ (*dotted curve*) in the Galactic disk vs. Galactocentric radius R. Total H I plus H_2 is shown as a solid curve. Mass does not include He.

$M_{\rm H\,I} \sim 1.0 \times 10^9\ M_\odot$ in this same range. A simple estimate of the maximum H I mass is $M_{\rm H\,I} < \pi R^2 \Sigma_{\rm H\,I}(R_0) \lesssim 1.2 \times 10^9\ M_\odot$, and our lower estimate seems reasonable. We find an H I mass of $M_{\rm H\,I} \sim 4.3 \times 10^9\ M_\odot$ in the range $8.5 < R < 18$ kpc, consistent with Wouterloot et al. (1990), who report $M_{\rm H\,I} = 5.3 \times 10^9\ M_\odot$ between $R = 8.5$ and 24 kpc.

The H I half-height, $H_z^{\rm H\,I}(R)$, at $R > R_0$ is taken from the data of Wouterloot et al. (1990). As for the surface density distribution, we assume that the data at 10 kpc should be smoothly joined to that at 8.5 kpc. With this assumption we find that the variation in the height over the entire range from 8.5 to 18 kpc can be reasonably well fitted by an exponential of scale length ~6.7 kpc. From Dickey & Lockman (1990) we assume that the half-height at $R < R_0$ is approximately constant and given by $H_z^{\rm H\,I}(R < R_0) = 115$ pc. We note that Malhotra (1995) finds a constant half-height of ~118 pc in the inner ($R < 5.1$ kpc) Galaxy, which rises to ~260 pc at the solar circle, a height that is nearly identical to that of the WNM (~265 pc) found by Dickey & Lockman (1990). Note that Malhotra (1995) fitted both the midplane height and the height of the H I above the midplane; thus, possible effects due to disk corrugation are removed from her results. The dramatic rise in height at the solar circle might be partly attributed to the correction for saturated H I emission by Dickey & Lockman (1990), which was not accounted for by Malhotra. Including this correction increases the intensity of the CNM component and tends to weight the height more toward the CNM height than the WNM height.

Figure 2 shows the H I height distribution with an analytic fit given by

$$H_z^{\rm H\,I}(R) = \begin{cases} 115 \text{ pc} & (3 \le R_k < 8.5)\ , \\ 115 e^{(R_k - 8.5)/6.7} \text{ pc} & (8.5 \le R_k \le 18)\ . \end{cases} \quad (8)$$

The H I surface density and height are used to scale the mean midplane density $\langle n_{\rm H\,I}(R) \rangle \propto \Sigma_{\rm H\,I}(R)/H_z^{\rm H\,I}(R)$. Liszt (1992) notes that with a density of $\langle n_{\rm H\,I} \rangle \sim 0.4$ cm^{-3} and a single temperature $T_{\rm spin} = 135$ K, both the emission and absorption characteristics of the H I in the plane can be simultaneously modeled. On the other hand, he points out that a higher density is required to match the observed H I surface density of Dickey & Lockman (1990), who find $\langle n_{\rm H\,I} \rangle \simeq 0.57$ cm^{-3}. With the mean density of hydrogen nuclei as derived from extinction studies $n_{\rm H\,I} + 2n_{\rm H_2} = 1.15$ H nuclei cm^{-3} (Bohlin, Savage, & Drake 1978), the Dickey & Lockman (1990) mean H I density requires a molecular density of $2n_{\rm H_2} \sim 0.58$ cm^{-3}, roughly consistent with the observations of Bronfman et al. (1988), who find $2n_{\rm H_2} \sim 0.5$ cm^{-3}. We adopt a local mean H I density of $\langle n_{\rm H\,I} \rangle = 0.57$ cm^{-3} and show the run of mean midplane H I density with R in Figure 3.

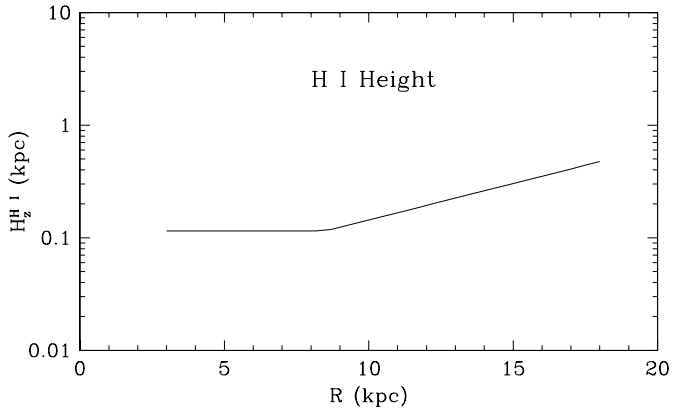

FIG. 2.—Azimuthally averaged H I half-width to half-maximum height $H_z^{\rm H\,I}$ vs. Galactocentric radius R.

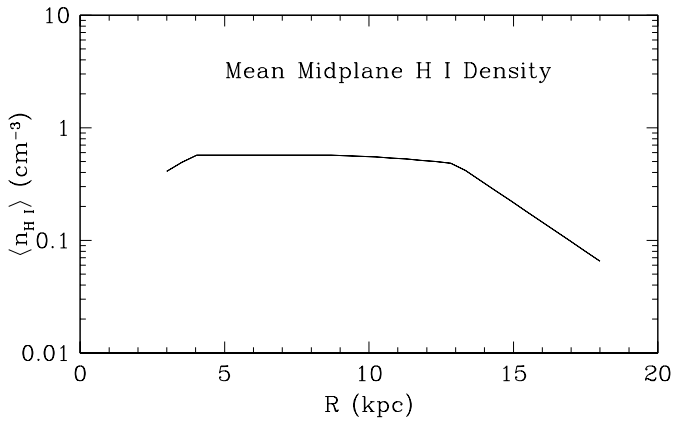

FIG. 3.—Mean H I density in the Galactic midplane vs. Galactocentric radius R. The value at $R = R_0$ is taken to be $\langle n_{\rm H\,I} \rangle = 0.57$ cm^{-3} and scaled by $\langle n_{\rm H\,I} \rangle \propto \Sigma_{\rm H\,I}/H_z^{\rm H\,I}$ at other radii.

Our H I distribution differs from that adopted by Ferrière (1998) for her global models of the Galactic ISM. Ferrière adopted a constant surface density $\Sigma_{\rm H\,I}(R) = 5\ M_\odot$ pc^{-2} to $R = 20$ kpc with a scale height that increases linearly with R at $R > 8.5$ kpc and a mean midplane density that decreases as $1/R$. Our surface density is thus equal to or higher than Ferrière (1998) out to a radius of $R = 15$ kpc and then drops to lower values. Our midplane density is slightly higher until $R = 14$ kpc and then drops to a factor of ~4 lower at $R = 18$ kpc.

3.2. *Distribution of* H_2

The distribution of the H_2 surface density in the Galaxy is required primarily as a cosmic-ray opacity source. We shall also use the distribution of H_2 height to estimate the height of OB stars in the Galactic plane. We use a surface density distribution from Bronfman et al. (2000) that is a Gaussian in Galactic radius in the inner Galaxy and a radial exponential in the outer Galaxy. The distribution has a peak value of 4.5 $M_\odot$ pc^{-2} centered on $R = 4.85$ kpc, an FWHM extent equal to 4.42 kpc, and a radial exponential of scale length $H_R^{\rm H_2} = 2.89$ kpc beyond $R \ge 6.97$ kpc. The H_2 surface density at the solar circle is $\Sigma_{\rm H_2}(R_0) = 1.4\ M_\odot$ pc^{-2}. These values are derived from an average of the data from both northern and southern Galactic quadrants. Bronfman et al. (2000) find an H_2 mass of $M({\rm H_2}) = 6.1 \times 10^8\ M_\odot$ for 1.7 kpc $< R <$ 8.5 kpc and $M({\rm H_2}) = 2 \times 10^8\ M_\odot$ for 8.5 kpc $< R <$ 14.5 kpc. By comparison, Williams & McKee (1997) adopted a simpler, purely exponential distribution for the H_2 and found $M({\rm H_2}) = 7.1 \times 10^8\ M_\odot$ for R between 1.7 and 8.5 kpc (their quoted value of $1.0 \times 10^9\ M_\odot$ included the He mass). Figure 1 shows the H_2 surface density distribution.

In the inner Galaxy, Bronfman et al. (2000) find that the H_2 height to half-maximum density is roughly constant at $H_z^{\rm H_2}(R \le R_0) \simeq 59$ pc. In the outer Galaxy we simply

scale the H_2 height by the H I height of Wouterloot et al. (1990) (eq. [8]).

3.3. *Distribution of Dust and Metals*

The photoelectric heating rate depends on the abundance of the smallest dust particles, which may primarily consist of polycyclic aromatic hydrocarbons (PAHs), while the radiative cooling rate depends mainly on the gas-phase abundances of carbon and oxygen. The photoelectric heating rate has been studied in detail by Bakes & Tielens (1994) using a realistic model for the PAH and grain size distribution. For the grains (i.e., particles with $a > 15$ Å), they adopted the MRN grain size distribution for spherical grains [i.e., $n(a)da \propto a^{-3.5}\,da$; Mathis, Rumpl, & Nordsieck 1977]. The PAH molecules ($a < 15$ Å) are assumed to be small disks. Their distribution is given by $n(N_C)dN_C = 1.15 \times 10^{-5} N_C^{-2.25} dN_C$ (with N_C the number of C atoms in the molecule), which ensures that the total volume in disks between 12 and 275 C atoms is equal to that of the MRN spherical grain size distribution between 3 and 15 Å. WHMTB have shown that this heating rate can adequately heat the local WNM and CNM phases. The characteristics of the PAH distribution adopted by WHMTB correspond to a total fraction of C in the form of PAHs of 14×10^{-6} relative to H. Recent analysis of *Infrared Space Observatory* (*ISO*) observations of the PAH emission in the galaxy concludes that this fraction is actually 22×10^{-6} relative to H (Tielens et al. 1999). We note that this corresponds to a total PAH abundance, n_{PAH}/n, of 6×10^{-7} as compared to 4×10^{-7} in WHMTB. We have adopted the former, higher value, which enters in the photoelectric heating rate and the chemical network. As will be discussed in § 8, these new values still reproduce the observed [C II] 158 μm cooling rates and the thermal pressures in the local ISM.

We use a local gas-phase abundance of metals consistent with the *Hubble Space Telescope* observations of Sofia et al. (1997), Cardelli et al. (1996), and Meyer, Jura, & Cardelli (1998) with $n_C/n = 1.4 \times 10^{-4}$ for carbon and $n_O/n = 3.2 \times 10^{-4}$ for oxygen. The gas-phase abundances of these elements are seen to be independent of the physical conditions in the diffuse medium, showing relatively constant values for fractional H_2 abundances between $\log[n_{H_2}/(n_{H_2} + n_{H\,I})] = -5.0$ and -0.2. Although of relatively minor importance in these calculations, we also include Si, S, Mg, and Fe and, with the exception of S, increase their depletions with gas density as in Jenkins (1987) and Van Steenberg & Shull (1988; see also WHMTB).

The optical and infrared line diagnostics seem to be converging on a value for the oxygen abundance gradient in the Galaxy that is roughly consistent with the early findings of Shaver et al. (1983), which were based on radio observations of the temperatures of H II regions (e.g., Torres-Peimbert & Peimbert 1977; Simpson et al. 1995; Afflerbach et al. 1996; Afflerbach, Churchwell, & Werner 1997; Gummersbach et al. 1998; Rolleston et al. 2000). We will use oxygen as our basis for the metallicity gradient $Z(R)$ and assume that both the elemental abundances and the gas-phase abundances of all elements scale similarly with $Z(R)$. Since both carbon and oxygen are primary elements, the elemental carbon abundance gradient is seen to closely follow the oxygen gradient (Rolleston et al. 2000). We further assume that the grain size distribution does not vary significantly with Galactic radius, but that the total dust abundance scales with $Z(R)$. Afflerbach et al. (1997) note that they do not observe a jump in the nitrogen-to-oxygen abundance ratio at $R \leq 6$ kpc as suggested by Simpson et al. (1995). In addition, Rolleston et al. (2000) find that their data can be fitted with a single slope of $d[O/H]/dR = -0.067 \pm 0.008$ dex kpc^{-1} without discontinuities (Twarog, Ashman, & Anthony-Twarog 1997) or a flattening of the gradient in the outer Galaxy as suggested by Fich & Silkey (1991). We take a constant gradient of $d[O/H]/dR = -0.07$ dex kpc^{-1} in the range 3 kpc $\leq R \leq$ 18 kpc. This slope corresponds to a radial exponential scale length of $H_R^Z = 6.2$ kpc.

3.4. *Distribution of Ionized Gas*

Although the ionized gas in the Galaxy does not enter into our analysis directly, we include a brief discussion of it for completeness. Most of the ionized gas in the Galaxy is produced by photoionization. Taylor & Cordes (1993) identified three components of ionized gas: a diffuse component that extends out to $R \gtrsim 20$ kpc, an annular component in the inner Galaxy centered at 3.7 kpc, and a component associated with spiral arms. Heiles, Reach, & Koo (1996) suggested that there are actually only two separate components, since the annular component is most likely due to spiral arms in the inner Galaxy.

Taylor & Cordes (1993) infer that the diffuse component has a mean electron density in the Galactic plane at the solar circle of 0.019 cm^{-3}, a vertical scale height of 0.88 kpc, and a radial distribution proportional to $\mathrm{sech}^2\,(R_k/20)$. Assuming that the ionization of He is similar to that of H (Slavin, McKee, & Hollenbach 2000), this corresponds to a surface density of diffuse ionized gas of $\Sigma_{H\,II,diff} = 0.89\,\mathrm{sech}^2\,(R_k/20)\ M_\odot$ pc^{-2} (not including He); at the solar circle, this is 0.75 $M_\odot$ pc^{-2}. In the Wolfire et al. (1995b) model of the Galactic halo, the surface density of H in the collisionally ionized, hot ISM (HIM) at the solar circle is 0.26 $M_\odot$ pc^{-2}, which accounts for about $\frac{1}{3}$ of the total diffuse ionized gas. We note that the HIM, however, has a much larger vertical scale height.

The photoionized gas in spiral arms is associated with the H II regions produced by OB associations. These H II regions typically have dense cores, which appear as radio H II regions, and much lower density envelopes, which absorb a significant fraction of the ionizing photons (Anantharamaiah 1985; McKee & Williams 1997). Most of the mass of the photoionized gas is in the envelopes, which have a surface density $\Sigma_{H\,II,env} = 3.5 \exp(-R_k/3.5)\ M_\odot$ pc^{-2} (McKee & Williams 1997), or 0.31 $M_\odot$ pc^{-2} at the solar circle.

4. DISTRIBUTION OF ENERGETIC PHOTONS AND PARTICLES

The distributions of far-ultraviolet (FUV; 6 eV $< h\nu <$ 13.6 eV) radiation, extreme ultraviolet (EUV, 13.5 eV $< h\nu \lesssim$ 100 eV) radiation, soft X-ray (100 eV $\lesssim h\nu \lesssim$ 1 keV) radiation, and cosmic rays are required to calculate the ionization fraction in the gas, the charge on grains, and the grain photoelectric heating rate. In the next three subsections we describe our adopted distributions.

4.1. *Far-Ultraviolet Radiation*

The FUV radiation field strength enters the photoelectric heating rate in two ways. First, it provides the total photon energy available for gas heating, and second, it governs the

grain charge and thus the efficiency at which photon energy is converted into gas heating (Watson 1972). We calculate the FUV radiation field by carrying out a simple radiative transfer calculation in an inhomogeneous medium. Note that we shall be scaling the numerical results to the measured value in the solar neighborhood and thus we need calculate only the variation from the local value. In addition, we are concerned with the *radial* variation of the mean intensity in the Galactic midplane and not the variation with height above the plane. Finally, we note that the vertical scale height of the H I and diffuse dust distribution, $H_z^{\rm H\,I}$, is always much greater than that of the OB stars that contribute to the FUV field. With these considerations, we assume that the FUV emissivity and opacity have a constant value between the midplane and the scale height of OB stars above the plane $H_z^{\rm OB}(R)$ and that the emissivity is zero at heights greater than $H_z^{\rm OB}(R)$. The mean intensity in the Galactic midplane at radius R is given by

$$4\pi J^{\rm FUV}(R) = \int_0^{2\pi} dl \int_0^{\pi/2} 2I^{\rm FUV}(R,l,b)\cos b\, db\ , \quad (9)$$

where b and l are Galactic latitude and longitude and $I^{\rm FUV}(R,l,b)$ is the FUV intensity in direction (l, b) at Galactocentric radius R. The expression for the intensity in direction (l, b) is given by

$$I^{\rm FUV}(R,l,b) = \int_0^{\tau_{\rm max}} \frac{j(R')}{\kappa(R')} e^{-\tau'}\, d\tau'\ , \quad (10)$$

where j and κ are the FUV emissivity and opacity, respectively, and $\tau_{\rm max}$ is the maximum optical depth along the line of sight (l, b) (see the discussion below eq. [12]). The FUV emissivity is determined by the distribution of OB stars in the Galactic plane, while the opacity is provided by dust, mainly in the diffuse atomic phases. Normalized to the local value in the solar neighborhood, the FUV emissivity scales as

$$\frac{j(R)}{j(R_0)} = \frac{\Sigma_{\rm OB}(R)}{\Sigma_{\rm OB}(R_0)} \frac{H_z^{\rm OB}(R_0)}{H_z^{\rm OB}(R)}\ , \quad (11)$$

where $\Sigma_{\rm OB}(R)$ is the surface density of OB stars. We assume that the vertical height $H_z^{\rm OB}(R)$ is given by the H_2 height in the inner Galaxy, i.e., $H_z^{\rm OB}(R \le R_0) = 59$ pc, and that it scales with the H_2 height at R greater than R_0.

To proceed further, we need to find how $\Sigma_{\rm OB}(R)$ scales with R, or equivalently, we require the radial exponential scale length, $H_R^{\rm OB}$, of the OB star surface density. McKee & Williams (1997) examined the Smith, Biermann, & Mezger (1978) catalog of giant radio H II regions and found that the surface density of the exciting OB associations between 3 kpc $< R <$ 11 kpc can be fitted with a scale length of roughly 3.5 kpc. They found no evidence for giant radio H II regions beyond 11 kpc and within 3 kpc (other than at the Galactic center). Bronfman et al. (2000) recently obtained a scale length of only $\sim$1.8 kpc for the surface density of embedded OB stars in the outer Galaxy (8.5 kpc $\lesssim R \lesssim$ 17 kpc). We note that the Bronfman et al. (2000) data can be fitted well by an $H_R^{\rm OB} = 3.5$ kpc scale length between 8.5 and $\sim$13 kpc, with a steeper slope at greater radii. The Bronfman et al. (2000) results are based on observations of far-infrared radiation from deeply embedded OB stars, but the embedded stage may last a shorter time in the outer Galaxy because molecular clouds are smaller there: Solomon et al. (1987) found no giant molecular clouds (GMCs) at $R > 10$ kpc (after correcting their distances to a Galactocentric distance of 8.5 kpc); Heyer et al. (2001) found no clouds more massive than $10^5\ M_\odot$ at $R > 11.6$ kpc, whereas half the molecular gas inside the solar circle is in clouds with $M > 10^6\ M_\odot$ according to Williams & McKee (1997). Thus, it is conceivable that the total OB star distribution extends beyond 13 kpc without a break in slope.

What do observations of other galaxies tell us about the radial distribution of OB stars? In M31, Cuillandre et al. (2001) have found B stars out to $\sim$33 kpc, or $1.7R_{25}$, a distance corresponding to $\sim$21 kpc in the Galaxy. Further evidence for star formation at large galactocentric distances is provided by Wang, Höflich, & Wheeler (1997), who found that the radial distribution of SNs in disk galaxies is exponential (with an average radial scale length of 3.5 kpc) with no evidence for an outer cutoff in the distribution. Ferguson et al. (1998) found that star formation in several disk galaxies extended out to at least $2R_{25}$ (corresponding to about 24.5 kpc in the Galaxy). They did find a break in the star formation rate, but the scale height in the outer parts of the disk ($R_{25} < R < 2R_{25}$) averages about $0.3R_{25}$, similar to the value found by McKee & Williams (1997) for the Galaxy between 3 and 11 kpc. The H II regions in the outer parts of these galaxies were substantially smaller than in the inner regions, consistent with the lack of giant H II regions in the Galaxy beyond 11 kpc. On the other hand, Martin & Kennicutt (2001) analyzed a larger sample of galaxies and found that most galaxies exhibit a strong cutoff in their star formation at a radius determined by the Toomre criterion; this cutoff radius is generally of order R_{25}. In view of the uncertainties in the distribution of star formation at large distances, we shall extend our analysis only out to 18 kpc, corresponding to about $1.5R_{25}$. Between 4 and 18 kpc, we shall adopt a scale length for the OB star surface density of $H_R^{\rm OB} = 3.5$ kpc, noting that the actual distribution beyond 13 kpc is uncertain and, if anything, is less than our adopted distribution. Between 3 and 4 kpc, we shall adopt a constant OB star surface density; since the H I and H_2 surface densities appear to drop toward the Galactic center in this range, it is unlikely that the OB star surface density would continue to rise at radii less than 4 kpc.

Using $H_R^{\rm OB} = 3.5$ kpc (at $R \ge 4$ kpc) and substituting $H_z^{\rm H_2}$ for the OB star vertical height, equation (11) can be simplified to

$$\frac{j(R)}{j(R_0)} = e^{-(R-R_0)/H_R^{\rm OB}} \frac{H_z^{\rm H_2}(R_0)}{H_z^{\rm H_2}(R)}\ . \quad (12)$$

With the adopted cutoff in the OB star distribution, the maximum path of integration $\tau_{\rm max}$ in equation (10) extends to $R = 18$ kpc in the plane or until the line of sight reaches the perpendicular height of $z = H_z^{\rm OB}(R') = H_z^{\rm OB}(R_0)[H_z^{\rm H_2}(R')/H_z^{\rm H_2}(R_0)]$.

The opacity to the FUV radiation $\kappa_{\rm FUV}(R)$ depends on the dust abundance, which in turn is proportional to the mean gas density and metallicity. The run of mean density $\langle n(R)\rangle$ and metallicity $Z(R)$ are discussed in §§ 3.1 and 3.3, respectively. Dust in the molecular phases is to a large extent shielded from the FUV radiation. Recent *ORFEUS I* observations (Dixon, Hurwitz, & Bowyer 1998) confirm the earlier *Copernicus* result that the H-to-H_2 transition in diffuse

gas occurs at $E(B-V) \approx 0.1$. For $R_V = 3.1$ this corresponds to $A_V \approx 0.3$ or $A_{\rm FUV} \approx 0.6$. Thus, the FUV field responsible for gas heating does not penetrate deeply into the molecular layer. In addition, the small volume filling factor of molecular gas ($f \sim 0.1\%$) means that the molecular component of the FUV opacity can be safely neglected.

The opacity at visual wavelengths is found from the local observed extinction [$A_V = N/(2 \times 10^{21}$ cm^{-2})] and mean H I density [$\langle n_{\rm H\,I}(R_0)\rangle = 0.57$ cm^{-3}] from Dickey & Lockman (1990), yielding $\kappa_V(R_0) = 0.88$ kpc^{-1} in the midplane. The FUV opacity for photoelectric heating is taken from the photodissociation region models of Tielens & Hollenbach (1985) and is based on the radiation transfer results of Flannery, Roberge, & Rybicki (1980). We use $\kappa_{\rm FUV}(R_0) = 1.8\kappa_V(R_0) = 1.6$ kpc^{-1}. The FUV opacity is then given by

$$\kappa_{\rm FUV}(R) = 1.6\frac{\langle n_{\rm H\,I}(R)\rangle}{\langle n_{\rm H\,I}(R_0)\rangle} e^{-(R-R_0)/H_R^Z} \text{ kpc}^{-1} , \quad (13)$$

with the radial metallicity scale length $H_R^Z = 6.2$ kpc. Since the scale height of diffuse gas is much greater than that of OB stars, we can consider the gas density in our integrations to be independent of height and a function of only the radial distance R. Figure 4 shows the FUV opacity as a function of R.

Locally, the FUV (6 eV $< h\nu <$ 13.6 eV) intensity has a measured strength of approximately $4\pi J(R_0) = 2.7 \times 10^{-3}$ ergs cm^{-2} s^{-1} (Draine 1978). This is a factor of 1.7 higher than the integrated field of Habing (1968), often used as a unit ($G_0 = 1$) of flux in models of photodissociation regions. Since the *local* FUV flux is observed, we find the distribution of flux in the Galaxy by scaling $j(R_0)$ in equation (10) so that the value of the integral at $R = R_0$ is given by the Draine field. Results are shown in Figure 5. The drop-off in intensity near 18 kpc is due to the abrupt cutoff in the OB star population that we have imposed in the outer Galaxy. The true intensity distribution should fall off more gradually.

We find that the calculated mean intensity at $R \geq 4$ kpc can be fitted by an exponential with a radial scale length of $H_R^J = 4.1$ kpc,

$$4\pi J^{\rm FUV}(R) = 4\pi J^{\rm FUV}(R_0) e^{-(R-R_0)/H_R^J} \quad (R \geq 4 \text{ kpc}) , \quad (14)$$

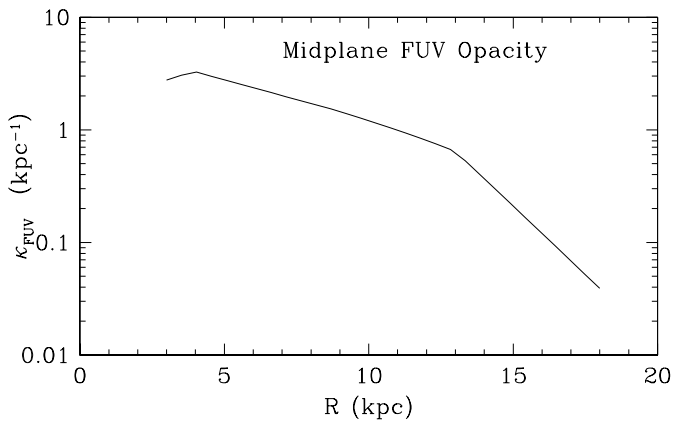

FIG. 4.—Calculated FUV opacity in the Galactic midplane vs. Galactocentric radius R.

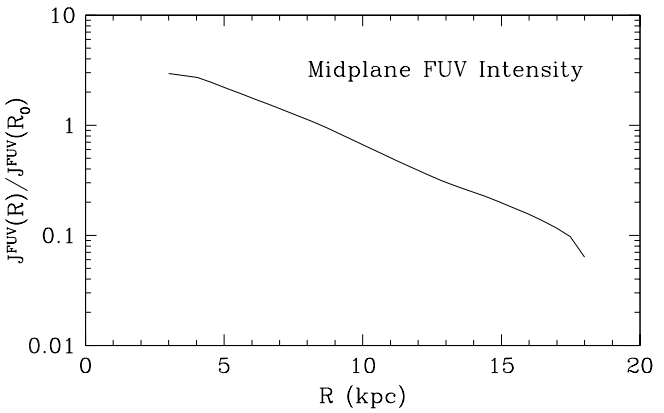

FIG. 5.—Calculated FUV field in the Galactic midplane vs. Galactocentric radius R normalized to the value at $R = R_0$. At $R = R_0$ the field strength is equal to $4\pi J^{\rm FUV}(R_0) = 2.7 \times 10^{-3}$ ergs cm^{-2} s^{-1}.

whereas for R between 3 and 4 kpc it is constant,

$$4\pi J^{\rm FUV}(R) = 4\pi J^{\rm FUV}(R_0) e^{-(4-R_0)/H_R^J} \quad (3 \geq R < 4 \text{ kpc}) . \quad (15)$$

These expressions are good to within 10% for R between 3 and 17 kpc.

4.2. *Cosmic Rays*

The low-energy ($E \lesssim 100$ MeV) cosmic rays that contribute to ionizing the CNM and WNM do not travel far from their point of origin (Kulsrud & Cesarsky 1971; Spitzer & Jenkins 1975). We obtain the cosmic-ray ionization rate as a function of position in the Galaxy by scaling the local primary rate (taken to be $\zeta_{\rm CR} = 1.8 \times 10^{-17}$ s^{-1}) by the production rate of cosmic rays per unit area (sources) divided by the mass per unit area (sinks). For the distribution of sources we use the surface density of OB stars (§ 4.1), and for the distribution of sinks we use the total surface density of molecular and neutral atomic (CNM+WNM) gas (§§ 3.1 and 3.2). This scaling differs from that adopted by Hunter et al. (1997) and Bertsch et al. (1993), who made the assumption that the cosmic-ray intensity is proportional to the surface density of gas alone; however, these authors were studying Galactic gamma-ray emission and were therefore interested in cosmic rays with higher energies than those that dominate the ionization. Such high-energy cosmic rays can travel more freely in the Galaxy and therefore acquire a fairly homogeneous distribution.

The surface density of WIM can potentially affect our cosmic-ray ionization rate by providing an additional sink for cosmic rays (the energy-loss rate for cosmic rays in ionized gas is several times that in neutral gas; Ginzburg & Syrovatskii 1964, p. 121). In order to simplify our model, we have chosen to neglect the effect of the WIM surface density in calculating the distribution of sinks of cosmic rays; note that this effect enters only insofar as the distribution of the WIM differs from that of the rest of the gas. Our neglect of the effect of the WIM will not strongly influence our results since EUV/X-ray radiation generally dominates the ionization and FUV radiation dominates the heating.

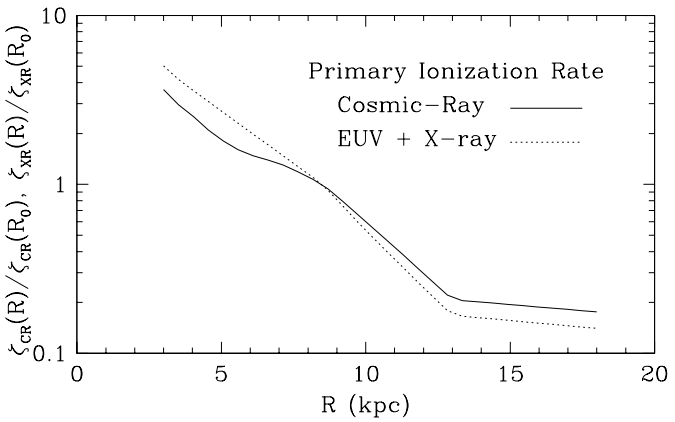

FIG. 6.—Primary cosmic-ray (*solid curve*) and EUV plus X-ray (*dotted curve*) ionization rates vs. Galactocentric radius R normalized to the value at $R = R_0$. At $R = R_0$ the primary cosmic-ray ionization rate is taken to be $\zeta_{CR}(R_0) = 1.8 \times 10^{-17}$ cm^{-3} s^{-1}. The EUV and X-ray rate depends on the adopted value of the WNM cloud column, N_{cl}. For $N_{cl} = 1.0 \times 10^{20}$ cm^{-2}, $\zeta_{XR}(R_0) = 8.9 \times 10^{-19}$ s^{-1}; for $N_{cl} = 1.0 \times 10^{19}$ cm^{-2}, $\zeta_{XR}(R_0) = 1.6 \times 10^{-17}$ s^{-1}; for $N_{cl} = 3.0 \times 10^{18}$ cm^{-2}, $\zeta_{XR}(R_0) = 7.6 \times 10^{-17}$ s^{-1}. Note that the EUV and X-ray rate always exceeds the cosmic-ray rate because of the effects of secondary ionizations. Typical values for N_{cl} are of order 10^{19} cm^{-2}.

The resulting primary cosmic-ray ionization rate is given by

$$\zeta_{CR} = 1.8 \times 10^{-17} e^{-(R-R_0)/H_R^{OB}} \left[\frac{\Sigma_{neutral}(R_0)}{\Sigma_{neutral}(R)}\right] \text{ s}^{-1} , \quad (16)$$

where $H_R^{OB} = 3.5$ kpc, $\Sigma_{neutral}(R) = \Sigma_{H_2}(R) + \Sigma_{H\,I}(R)$, and $\Sigma_{neutral}(R_0) = 6.4\ M_\odot$ pc^{-2}. The variation in the primary cosmic-ray ionization rate with Galactocentric radius R is shown in Figure 6.

4.3. *Soft X-Ray and EUV Radiation*

As demonstrated in WHMTB, the ionization of H and He by soft X-rays and EUV photons (13.6 eV $< h\nu \lesssim 10^3$ eV) provides a source of electrons in the local WNM amounting to an electron fraction of $n_e/n \sim 2\%$ (at $n = 0.3$ cm^{-3}), a fraction that depends on the column N_w of warm absorbing gas and dust traversed by the X-rays. These electrons neutralize the positive charging of grains caused by the FUV photoelectric effect and thereby help maintain a high photoelectric heating efficiency in the WNM phase. The local X-ray field arises from the Local Bubble and the Galactic halo plus an extragalactic background, with the low-energy (50 eV $\lesssim E \lesssim$ 100 eV) emission from the Local Bubble dominating the ionization at typical columns $N_w \approx 10^{19}$ cm^{-2}. WHMTB used a fit to the observed X-ray intensity from Garmire et al. (1992) to generate the X-ray spectrum incident on a WNM "cloud." The fit consisted of the temperature and emission measure in the Local Bubble and halo components, an absorbing layer through which the halo is seen, and an extragalactic component and absorbing layer. The ionization rate at a column N_w into the WNM cloud was then calculated by computing the attenuation of the incident X-ray flux by the column N_w.

The Garmire et al. (1992) fit was based on pre-*ROSAT* data. Snowden et al. (1998) and Kuntz & Snowden (2000) evaluated the *ROSAT* data to analyze the origin and distribution of the diffuse X-ray background. They find somewhat lower temperatures than Garmire et al. (1992) for the Local Bubble and argue that the $\frac{1}{4}$ and $\frac{3}{4}$ keV band observations can be fitted only if the halo is emitting at two or more temperatures. Using the observed ratios in the *ROSAT* R1, R2, R3, and R4 bands, Kuntz & Snowden (2000) find $\log T_b = 6.11$ for the bubble and $\log T_{h1} = 6.06$, $\log T_{h2} = 6.46$ for the two halo temperatures as compared with $\log T_b = 6.16$ and $\log T_h = 6.33$ from Garmire et al. (1992). (Note that there is an error in Table 1 of WHMTB in that the emission measures for the bubble and halo components are reversed.)

The fit to the *ROSAT* data provides the *local* soft X-ray flux. However, we know that the Sun is located in a bubble of hot gas that dominates the low-energy radiation and hence the ionization, and the local emission may differ from the average emission at the solar circle. We derive the average X-ray emission in the disk from the calculations of Slavin et al. (2000). They define the emissivity per unit area $\langle \epsilon_{\nu A} \rangle$ as

$$\langle \epsilon_{\nu A} \rangle = \int_{-\infty}^{\infty} dz \langle \epsilon_\nu \rangle , \quad (17)$$

where $\langle \epsilon_\nu \rangle$ is the volume emissivity and the integration is carried out perpendicular to the disk. The average value of the mean intensity is found from $\langle \epsilon_{\nu A} \rangle$ as

$$\langle J_\nu \rangle = \frac{(1 - \eta_\nu)}{\tau_{\nu,d}} \left(\frac{\langle \epsilon_{\nu A} \rangle}{4\pi}\right) , \quad (18)$$

where $\tau_{\nu,d}$ is the opacity through the disk and η_ν is the mean escape probability of soft X-rays out of the Galaxy. The opacity $\tau_{\nu,d}$ is taken to be that of a cloudy medium of column density through the disk $N_{WNM,d}$ with clouds of typical column density N_{cl}(H I). (These parameters appear as $\tau_{0\nu}$, $N_{H^0\perp}$, and $N_{H^0_c}$, respectively, in the Slavin et al. 2000 notation.) We consider WNM clouds only; the small filling factor of the CNM means that it does not contribute much to the opacity of very soft X-rays. The opacity is then given by $\tau_{\nu,d} = [N_{WNM,d}/N_{cl}(\text{H I})][1 - \exp(-\tau_{\nu,cl})]$, where $\tau_{\nu,cl}$ is the optical depth through a single WNM cloud and $N_{WNM,d}$ is the WNM column through the disk.

Slavin et al. (2000) determine the average emissivity produced by SNRs $\langle \epsilon_\nu^{SNR} \rangle$, which accounts for the time- and space-averaged emissivity produced as SNRs evolve into the ISM of ambient density n_a, although Slavin et al. (2000) show that the average emissivity is very insensitive to n_a. Slavin et al. (2000) applied their model to a specific line of sight toward a high-latitude cloud, calculated the ionizing flux as a function of height in the disk, and found that they could successfully match the observed fractional ionization.

In addition to the soft X-rays emitted by the SNRs, stellar EUV radiation also contributes to the ionization rate in the WNM. We use the stellar EUV spectrum shown by Slavin & Frisch (1998), which is derived from *Extreme Ultraviolet Explorer* observations (Vallerga 1996) and corrected for extinction by the local interstellar cloud [taken to be $N(\text{H I}) = 9 \times 10^{17}$ cm^{-2}]. While keeping the stellar EUV spectral shape fixed, we adjust the level of the stellar EUV emissivity $\langle \epsilon_\nu^* \rangle$ so that the total emissivity per unit area $\langle \epsilon_A \rangle = \int d\nu\, dz (\langle \epsilon_\nu^{SNR} \rangle + \langle \epsilon_\nu^* \rangle)$ provides the observed ionizing photon flux of the Galactic disk outside H II regions, as deduced from Hα observations ($\langle \epsilon_A \rangle \approx 4 \times 10^6$ photons cm^{-2} s^{-1}; Reynolds 1984, 1995). We find that approximately 43% of the EUV photon flux comes from stars; this is

consistent with the results of Slavin et al. (2000), who suggest that hot gas in SNRs produces about half the total number of ionizing photons in the diffuse ISM.

We adopt parameters for the total column density of WNM through the disk appropriate for the Galactic average at the solar circle. Dickey & Lockman (1990) fit the vertical distribution of H I in the solar neighborhood with three distinct components. Following Kulkarni & Heiles (1987), we identify the two components with the largest scale heights with the WNM. The total WNM column density through the disk is then $N_{\rm WNM,\it d}(R_0) = 3.45 \times 10^{20}$ cm^{-2}, or $\sim$56% of the total H I column at R_0. We also set the mean escape probability equal to zero ($\eta_\nu = 0$). For our standard model we set $N_{\rm cl}({\rm H\ I}) = 1 \times 10^{19}$ cm^{-2}, comparable to the column densities of the WNM clouds observed along the line of sight toward the halo star HD 93521 (Spitzer & Fitzpatrick 1993) and disk star γ^2 Vel (Fitzpatrick & Spitzer 1994; this line of sight contains four WNM clouds ranging in H I column density from 2.7×10^{18} to 4.5×10^{19} cm^{-2} with an average value of 1.5×10^{19} cm^{-2}). Note that in our formalism, $N_{\rm cl}$ is the WNM column density in a typical cloud that provides the opacity for the EUV and soft X-ray radiation. Note also that the phase diagrams and thermal processes presented in § 6 apply to the WNM/CNM boundary within a cloud and thus radiation incident upon the cloud must pass through an additional column $N_{\rm cl}$ (or N_w in WHMTB notation).

Using the flux at $z = 0$, we find that at a cloud column of $N_{\rm cl}({\rm H\ I}) = 10^{19}$ cm^{-2}, the primary EUV plus X-ray ionization rate of hydrogen is $\zeta_{\rm XR} = 1.6 \times 10^{-17}$ s^{-1}, a factor of $\sim$1.6 lower than that used by WHMTB. (This rate is approximately equal to the primary cosmic-ray ionization rate, 1.8×10^{-17} s^{-1}. The total ionization rate from either cosmic rays or EUV/soft X-rays is larger than the primary rate as a result of the effects of secondary ionizations. The secondary rate increases with the energy of the primary ejected electron and with decreasing ionization fraction. In the WNM at a cloud column of $N_{\rm cl} = 10^{19}$ cm^{-2} and density $n \sim 0.3$ cm^{-3} the total EUV/X-ray rate is $\sim 5.3 \times 10^{-17}$ s^{-1}, about 1.5 times higher than that from cosmic rays, while in the CNM at a density of $n \sim 33$ cm^{-3} the total EUV/X-ray rate is $\sim 7.5 \times 10^{-17}$ s^{-1}, or $\sim$2.7 times higher than that from cosmic rays.) The ionizing photon intensity incident on clouds is $\sim 9.4 \times 10^3$ cm^{-2} s^{-1} sr^{-1}. This is a factor of 2.2 larger than that obtained by Slavin et al. (2000) because (1) we are modeling a typical region of the ISM, which has a significant flux of stellar ionizing photons, and (2) we have adopted a somewhat smaller cloud column density.

Having determined the value for the soft X-ray ionization rate at $R = R_0$, we must now scale the results for other Galactic radii. The ultimate energy source for the hot gas that produces the X-ray flux is supernova explosions, while the opacity arises from the surface density of (WNM) H I gas. Thus, we assume that the X-ray ionization rate per hydrogen in the Galactic midplane scales as the OB star distribution divided by the H I surface density, $\zeta_{\rm XR}(R) \propto \Sigma_{\rm OB}(R)/\Sigma_{\rm H\,I}(R)$, as shown in Figure 6. We assume that the stellar EUV photoionization rate scales the same as the soft X-ray ionization rate. Because of the increased gas opacity to the EUV/X-ray radiation compared to FUV radiation, the mean free path for the EUV/X-ray photons is much shorter than for FUV. Thus, the dust in CNM clouds dominates the FUV opacity, but the gas in WNM clouds dominates the EUV/X-ray opacity. Since the fraction of WNM column to the total is unknown outside the solar neighborhood, we have assumed, for the purposes of estimating the X-ray distribution, that the fraction is always given by the value in the solar neighborhood. If the WNM fraction were to increase in the outer Galaxy, for example, the X-ray ionization rate would be lower than our adopted rates. We also include ionization by the extragalactic X-ray and EUV radiation field of Sternberg, McKee, & Wolfire (2002), which is based on the work of Haardt & Madau (1996) and Chen, Fabian, & Gendreau (1997). The extragalactic field passes through an absorbing column given by one-half of the total WNM column density. At the solar circle the extragalactic field provides $\sim$1% of the total ionization rate (for $N_{\rm cl} = 10^{19}$ cm^{-2}), while at $R = 18$ kpc the extragalactic rate rises to $\sim$12% of the total rate.

5. CHEMICAL AND THERMAL PROCESSES IN THE NEUTRAL PHASES

The chemical and thermal processes included in this work are slightly modified from those discussed in WHMTB. The main changes involve the PAH reaction network and PAH reaction rates. These rates are important because reactions with PAHs affect the PAH charge state and electron abundance, which in turn affects the photoelectric heating rate. We have simplified the PAH chemical reaction network compared to that used in WHMTB. Here we use rates appropriate for a single PAH size containing $N_{\rm C} = 35$ carbon atoms, the mean size in the distribution between 3 and 15 Å. We have also dropped the adsorption reactions used in WHMTB since these were found to be not important in determining the PAH charge.

For the PAH reaction rates we use the photoionization/photodetachment rates of Bakes & Tielens (1994) and a modified form of the Draine & Sutin (1987) formalism for the interaction between ions and electrons with neutral and charged PAHs in which we multiply all of the collisional rates by a factor $\phi_{\rm PAH} = 0.5$. There is considerable uncertainty in applying a classical treatment of the interaction between atoms and grains to the molecular regime. In particular, collision rates (using $\phi_{\rm PAH} = 1$) consistently overestimate the laboratory-measured rates for electron attachment to neutral PAHs and for electron recombination with PAH$^+$ (Allamandola, Tielens, & Barker 1989; Salama et al. 1996; Weingartner & Draine 2001b and references therein). We will consider $\phi_{\rm PAH}$ to be a parameter and rely on observation to guide us in its appropriate value. As noted by Lepp et al. (1988) and recently by Bakes & Tielens (1998), Welty & Hobbs (2001), and Weingartner & Draine (2001a), ion recombination on small grains and PAHs can be important in determining the neutral fraction of metals. (In Appendix C we also elucidate the conditions under which reactions of C$^+$ and H$^+$ with PAHs can affect the electron abundance.) Specifically, we find that the abundance of neutral carbon is sensitive to the rate of C$^+$ recombination with PAH$^-$. We find that the observed C I/C II column density ratio in diffuse clouds ($\lesssim 3 \times 10^{-3}$; Welty & Hobbs 2001; Jenkins & Tripp 2001) implies $\phi_{\rm PAH} = 0.5$, and we adopt this value for our standard model. In § 6.1 we discuss the effect of higher and lower values of $\phi_{\rm PAH}$ on the phase equilibrium of the ISM.

We have also updated the gas-phase chemical reaction rates according to the list of Millar, Farquhar, & Willacy (1997) and modified the H_2 formation and dissociation rate

according to the discussion in Kaufman et al. (1999). These additional chemical changes mainly affect the molecular pathways included in our network and are of minor consequence for the atomic phases discussed in this paper. Note, however, that the adopted gas-phase carbon and oxygen abundances have been modified from their WHMTB values (§ 3.3). The results of these changes are discussed in §§ 6.1 and 6.2.

The dominant heating process at $R = R_0$ in both the CNM and WNM phases is grain photoelectric heating. We use the heating rate determined by Bakes & Tielens (1994), modified by the higher PAH abundances as explained in § 3.3, and modified by the parameter $\phi_{\rm PAH}$, which scales the electron-PAH collision rates. For the same density, electron abundance, temperature, and incident FUV field, the higher abundances result in an increase in the heating rate by a factor of 1.3. The cooling rate due to electron recombination with PAHs increases similarly by a factor of 1.3. In Bakes & Tielens (1994) the heating/cooling rates were calculated self-consistently with the PAH ionization state as a function of the photo and collision rates. To maintain this self-consistency, the heating/cooling rates (and the fit to the rates) must be modified for the parameter $\phi_{\rm PAH}$. Including the correction for higher PAH abundances, the heating rate per unit volume is given by

$$n\Gamma_{\rm pe} = 1.3 \times 10^{-24} n\epsilon G_0 \text{ ergs cm}^{-3} \text{ s}^{-1} , \qquad (19)$$

where n is the hydrogen nucleus density and the heating efficiency ϵ is given by

$$\epsilon = \frac{4.9 \times 10^{-2}}{1 + 4.0 \times 10^{-3} (G_0 T^{1/2}/n_e \phi_{\rm PAH})^{0.73}} + \frac{3.7 \times 10^{-2} (T/10^4)^{0.7}}{1 + 2.0 \times 10^{-4} (G_0 T^{1/2}/n_e \phi_{\rm PAH})} . \qquad (20)$$

The cooling rate per unit volume is given by

$$n^2\Lambda = 4.65 \times 10^{-30} T^{0.94} \left(\frac{G_0 T^{1/2}}{n_e \phi_{\rm PAH}}\right)^{\beta} \times n_e \phi_{\rm PAH} n \text{ ergs cm}^{-3} \text{ s}^{-1} , \qquad (21)$$

with $\beta = 0.74/T^{0.068}$.

The dominant cooling process in the CNM is radiative line cooling in the [C II] 158 μm fine-structure transition. Cooling in the WNM is provided by several processes: radiative line cooling by [C II] 158 μm, [O I] 63 μm, and Lyα, as well as by electrons recombining onto grains (refer to details in WHMTB). In this paper we adjusted the collision rate for the excitation of C^+ by impacts with e^- to that of Blum & Pradhan (1992).

6. RESULTS

6.1. *Phase Diagrams*

Utilizing the results from the previous sections on the FUV intensity and ionization rates in the Galaxy as functions of R, we calculate phase diagrams—gas thermal pressure P versus hydrogen nucleus density n—for several Galactocentric distances R. The curves are generated by calculating, at constant n, the chemical equilibrium abundances and the thermal equilibrium temperature. We then step through n and plot the calculated thermal pressure, $P = \Sigma n_i kT$, where i ranges over all chemical species. The calculations are carried out for various WNM cloud columns $N_{\rm cl}$ and apply to the WNM/CNM boundary. An appropriate range is 3×10^{18} cm$^{-2} \le N_{\rm cl} \le 1 \times 10^{20}$ cm^{-2}. The upper limit is set by the size scale at which turbulent pressure begins to dominate. As discussed in § 2, we obtain l_P(WNM) $\sim$ 215 pc, or $N_{\rm cl} \sim 2 \times 10^{20}$ cm^{-2} for a typical density $n \sim 0.3$ cm^{-3}. The lower limit is set by the requirement that there be a substantial neutral fraction in the cloud. We note that the smallest neutral column density in the warm clouds along the line of sight to the disk star γ^2 Vel is 2.7×10^{18} cm^{-2} (Fitzpatrick & Spitzer 1994). The column density of the ionized clouds in the MO model of the ISM is 2.2×10^{18} cm^{-2}; since this model agrees with observations of Hα and pulsar dispersion measures in the disk, it is difficult to have predominantly neutral clouds that are smaller than this. We shall use $N_{\rm cl} = 10^{19}$ cm^{-2} as a standard and demonstrate the effects of both higher (1×10^{20} cm^{-2}) and lower (3×10^{18} cm^{-2}) columns.

We present in Figure 7 phase diagrams for Galactic radii $R = 3$, 5, 8.5, 11, 15, and 18 kpc. The model parameters are given in Tables 1 and 2. As demonstrated by Field (1965), the region of thermal stability in P versus n phase diagrams lies in the range where $dP/dn > 0$. Where $dP/dn < 0$ the gas is thermally unstable to isobaric perturbations. If the pressure curve has a characteristic shape shown in Figure 7, two thermally stable phases may coexist in pressure equilibrium within a range of gas pressures, $P_{\rm min}$ to $P_{\rm max}$. At thermal pressures greater than $P_{\rm max}$ only the cold phase (CNM) may be present, while at thermal pressures less than $P_{\rm min}$ only the warm phase (WNM) may exist (see also further discussions in reviews by Shull 1987; Begelman 1990).

We see that a two-phase (WNM+CNM) equilibrium is possible in the Galactic midplane at all Galactic radii between 3 and 18 kpc. The pressure ranges $P_{\rm min}$ and $P_{\rm max}$ are listed in Table 3 for each radius along with the range in gas temperature and density for WNM and CNM gas between $P_{\rm min}$ and $P_{\rm max}$. Also listed is the average pressure, where we adopt the geometric mean of $P_{\rm min}$ and $P_{\rm max}$ to

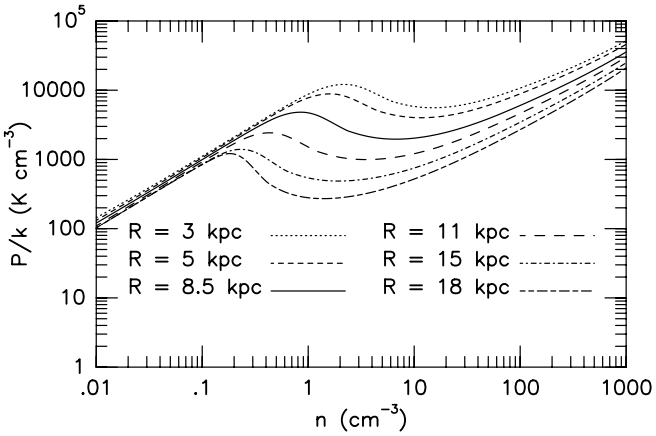

FIG. 7.—Phase diagrams showing thermal pressure P/k vs. hydrogen nucleus density n at Galactocentric radii $R = 3$, 5, 8.5, 11, 15, and 18 kpc. Curves apply to the WNM/CNM boundary at a depth of 1×10^{19} cm^{-2} through the WNM. Gas is thermally stable to isobaric perturbations where $dP/dn > 0$.

TABLE 1
MODEL PARAMETERS: LOCAL VALUES

Parameter	Value	Reference
$J^{FUV}(R_0)$[a] (ergs cm^{-2} s^{-1} sr^{-1})	2.2×10^{-4}	1, 2
ζ_{CR}[b] (s^{-1})	1.8×10^{-17}	3
ζ_{XR}[c] (s^{-1})	1.6×10^{-17}	4
$\mathscr{A}_C$[d]	1.4×10^{-4}	5, 6
$\mathscr{A}_O$[e]	3.2×10^{-4}	7
$\mathscr{A}_{PAH}$[f]	6×10^{-7}	4, 8
A_V[g]	$N/(2 \times 10^{21}$ cm$^{-2})$	9
$\Sigma_{H\,I}$[h] ($M_\odot$ pc^{-2})	5	10
Σ_{H_2}[i] ($M_\odot$ pc^{-2})	1.4	11
Σ_{WNM}[j] ($M_\odot$ pc^{-2})	2.75	10
$\langle n_{H\,I} \rangle$[k] (cm^{-3})	0.57	10
$H_z^{H\,I}$[l] (pc)	115	10
$H_z^{H_2}$[m] (pc)	59	11

NOTE.—Values at solar circle $R = R_0 = 8.5$ kpc.

[a] Intensity of FUV (6 eV $< h\nu <$ 13.6 eV) interstellar radiation field. This intensity is a factor of 1.7 higher than the integrated field of Habing 1968, which has a value of $J^{FUV}(R_0) = 1.3 \times 10^{-4}$ ergs cm^{-2} s^{-1} sr^{-1}. The interstellar field has a value of $G_0 = 1.7$ in units of the Habing field.

[b] Primary cosmic-ray ionization rate of hydrogen.

[c] Primary EUV plus soft X-ray ionization rate of hydrogen at a cloud depth of $N_{cl} = 10^{19}$ cm^{-2}. The primary rate depends on the adopted value of the WNM cloud column, N_{cl}. The total rate is higher than the primary rate as a result of secondary ionizations and increases with lower electron fraction. For our standard model, over the two-phase range, the total rate is a factor of 3–5 higher than the primary rate. For $N_{cl} = 1.0 \times 10^{20}$ cm^{-2}, $\zeta_{XR}(R_0) = 8.9 \times 10^{-19}$ s^{-1}; for $N_{cl} = 3.0 \times 10^{18}$ cm^{-2}, $\zeta_{XR}(R_0) = 7.6 \times 10^{-17}$ s^{-1}.

[d] Gas-phase carbon abundance per H nucleus.

[e] Gas-phase oxygen abundance per H nucleus.

[f] PAH abundance per H nucleus. This abundance gives a total number of C atoms in PAHs of 22×10^{-6} relative to hydrogen.

[g] Magnitudes of visual extinction per hydrogen column density.

[h] Atomic hydrogen surface density through full disk, $N(H\,I) = 6.25 \times 10^{20}$ cm^{-2}.

[i] Molecular hydrogen surface density through full disk, $2N(H_2) = 1.75 \times 10^{20}$ cm^{-2}.

[j] WNM column density through full disk, $N_{WNM,d} = 3.45 \times 10^{20}$ cm^{-2}.

[k] Mean H I density.

[l] H I half-height to half-intensity.

[m] H_2 half-height to half-intensity.

REFERENCES.—(1) Draine 1978. (2) Habing 1968. (3) WHMTB. (4) This paper. (5) Cardelli et al. 1996. (6) Sofia et al. 1997. (7) Meyer et al. 1998. (8) Tielens et al. 1999. (9) Bohlin et al. 1978. (10) Dickey & Lockman 1990. (11) Bronfman et al. 2000.

TABLE 2
MODEL PARAMETERS: GALACTIC VALUES

R (kpc)	G_0'[a]	ζ_{CR}'[b]	ζ_{XR}'[c]	$Z_d' = Z_g'$[d]
3	2.95	3.64	5.02	2.43
4	2.73	2.56	3.62	2.07
5	2.21	1.83	2.72	1.76
8.5 (=R_0)	1.00	1.00	1.00	1.00
11	0.509	0.424	0.359	0.668
15	0.198	0.194	0.156	0.351
17	0.116	0.182	0.145	0.254
18	0.0634	0.176	0.140	0.216

NOTE.—Values scaled to solar circle.

[a] Scaled intensity of FUV interstellar radiation field.

[b] Scaled primary cosmic-ray ionization rate.

[c] Scaled primary EUV and soft X-ray ionization rate.

[d] Scaled gas-phase metallicity, Z_g', and dust/PAH abundances, Z_d'.

represent the average,

$$P_{th,ave}(R) \equiv [P_{min}(R) P_{max}(R)]^{1/2} . \quad (22)$$

We also give the temperature and density at $P_{th,ave}$ for WNM and CNM gas. Compared to the results in WHMTB at $R = 8.5$ kpc, P_{min} is higher by a factor of $\sim$2.0 and P_{max} is higher by a factor of $\sim$1.3. The difference in P_{min} is mainly due to the revised (lower) gas-phase carbon and oxygen abundances from those in WHMTB. The lower abundance of coolants results in a higher gas temperature. The higher P_{max} is partly due to the lower abundance of coolants, but mitigated by the effects of the collision rate parameter ϕ_{PAH}. The collision parameter affects the electron fraction, the photoelectric heating rate, and the cooling rate as a result of electrons recombining onto positively charged grains. Lower values of ϕ_{PAH} result in a higher electron fraction in WNM gas. At P_{max}, higher electron fractions and enhanced recombination cooling play a role in limiting the maximum pressure.

We next examine the effects of the PAH collision rate parameter ϕ_{PAH} and the PAH abundance on the pressure curves. We show in Figure 8 and list in Table 4 results for $R = 8.5$ kpc and $\phi_{PAH} = 0.25$, 0.5, and 1.0, with the standard PAH abundance ($n_{PAH}/n = 6 \times 10^{-7}$ or an amount of C in PAHs of 22×10^{-6} relative to H). We also show results for $\phi_{PAH} = 0.5$ and a lower PAH abundance of $n_{PAH}/n = 4 \times 10^{-7}$ as used by WHMTB. Results for $G_0 = 1.1$, as is appropriate for the interstellar radiation field of Mathis, Mezger, & Panagia (1983), are also given in Table 4 but not shown in the figure since the resulting pressures are very similar to the case for low PAH abundance. Over the range of ϕ_{PAH} from 0.25 to 1, P_{min} changes by a factor of only 1.5 while P_{max} changes by 1.9 mainly because of the increased effects of recombination cooling. We conclude that the results for the phases of the ISM are very robust against variations in the PAH physical and chemical characteristics. For example, the average temperature hardly varies. The largest change occurs for $\phi_{PAH} = 0.25$ in which P_{max} decreases by $\sim$35%.

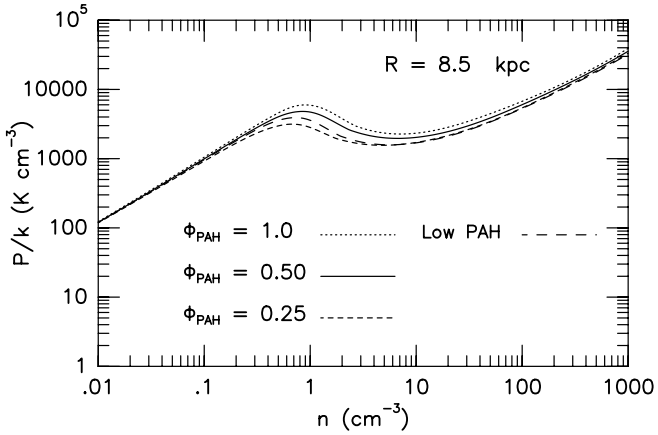

FIG. 8.—Thermal pressure P/k vs. hydrogen nucleus density n at $R = 8.5$ kpc showing the effects of varying the collision rate parameter ϕ_{PAH} and the PAH abundances. For the standard PAH abundances ($n_{PAH}/n = 6 \times 10^{-7}$), curves are shown for $\phi_{PAH} = 0.25$ (*dashed curve*), $\phi_{PAH} = 0.5$ (*solid curve*), and $\phi_{PAH} = 1.0$ (*dotted curve*). Our standard model uses $\phi_{PAH} = 0.5$. Also shown is a curve for $\phi_{PAH} = 0.5$ and a low PAH abundance of $n_{PAH}/n = 4 \times 10^{-7}$ (*long-dashed curve*).

TABLE 3
RANGE OF PHYSICAL CONDITIONS FOR TWO-PHASE MEDIUM

				WNM				CNM			
N_{cl} (cm^{-2})	R (kpc)	$P_{min}/k - P_{max}/k$ (K cm^{-3})	$P_{th,ave}/k$ (K cm^{-3})	T (K)	n (cm^{-3})	T_{ave} (K)	n_{ave} (cm^{-3})	T (K)	n (cm^{-3})	T_{ave} (K)	n_{ave} (cm^{-3})
1×10^{19}.....	3	5580–12100	8220	8530–5030	0.579–2.17	7960	0.922	345–88.8	14.6–124	124	60.2
	4	4910–10600	7210	8430–4930	0.516–1.93	7880	0.817	323–87.5	13.9–110	121	54.2
	5	4000–8850	5950	8410–4910	0.422–1.63	7880	0.675	312–80.6	11.6–100	111	48.6
	8.5	1960–4810	3070	8310–5040	0.209–0.860	7860	0.349	258–61.6	6.91–71.0	85.0	32.9
	11	995–2420	1550	8130–5080	0.109–0.430	7700	0.180	247–56.5	3.65–39.0	78.4	18.0
	15	487–1400	825	8080–5540	0.0534–0.227	7690	0.0958	229–43.8	1.93–29.0	62.3	12.0
	17	374–1360	713	8190–5690	0.0403–0.215	7800	0.0815	197–35.7	1.72–34.6	51.4	12.6
	18	272–1220	575	8320–6050	0.0287–0.180	7880	0.0648	180–30.7	1.37–36.0	44.1	11.8
1×10^{20}.....	3	3150–5330	4090	7820–4410	0.359–1.09	7080	0.519	411–136	6.95–35.5	180	20.6
	4	2800–4690	3620	7700–4360	0.325–0.971	6960	0.467	410–133	6.19–32.1	174	18.9
	5	2300–3910	3000	7670–4320	0.268–0.817	6950	0.387	401–122	5.20–29.1	161	17.0
	8.5	1240–2310	1690	7750–4300	0.142–0.485	7150	0.212	324–86.2	3.47–24.4	117	13.2
	11	652–1200	886	7560–4240	0.0770–0.257	6990	0.113	322–77.4	1.84–14.1	106	7.57
	15	329–674	471	7620–4470	0.0385–0.136	7170	0.0588	291–59.6	1.03–10.3	84.6	5.06
	17	253–629	399	7830–5260	0.0287–0.108	7440	0.0480	250–47.3	0.917–12.1	68.2	5.32
	18	179–548	313	8010–5760	0.0198–0.0855	7610	0.0367	223–39.3	0.727–12.7	57.4	4.96
3×10^{18}.....	3	7340–19900	12100	8800–5370	0.732–3.33	8320	1.29	280–66.6	23.8–271	95.0	115
	4	6490–17300	10600	8700–5260	0.655–2.97	8240	1.15	277–66.1	21.2–238	93.5	103
	5	5290–14500	8770	8670–5560	0.537–2.36	8210	0.950	269–61.9	17.8–214	87.0	91.6
	8.5	2560–7830	4480	8520–5650	0.264–1.25	8100	0.491	233–49.6	10.0–144	69.2	58.9
	11	1300–3940	2260	8330–5380	0.137–0.660	7940	0.253	223–46.0	5.29–77.8	64.3	31.9
	15	635–2300	1210	8240–5910	0.0678–0.349	7860	0.137	194–36.8	2.97–56.7	52.5	20.9
	17	495–2220	1050	8310–6040	0.0521–0.329	7890	0.118	180–31.1	2.50–64.8	44.4	21.5
	18	371–1970	856	8390–6020	0.0385–0.293	7940	0.0953	152–27.5	2.22–65.0	39.1	19.9

The phase diagrams presented in Figure 7 used a column of atomic gas $N_{cl} = 10^{19}$ cm^{-2}. We illustrate in Figure 9 the effects of higher ($N_{cl} = 10^{20}$ cm^{-2}) and lower ($N_{cl} = 3 \times 10^{18}$ cm^{-2}) column densities at $R = R_0 = 8.5$ kpc. As the column density decreases at a given Galactic radius, the electron abundance rises (as a result of hydrogen photoionization by EUV/X-rays). The increased electron abundance neutralizes the grains and enhances the rate of grain photoelectric heating. In addition, the EUV/X-ray heating rate rises. Therefore, lower column densities result

TABLE 4
DEPENDENCE ON MODEL PARAMETERS

Model	Standard[a]	Low ϕ_{PAH}[b]	High ϕ_{PAH}[c]	Low n_{PAH}/n[d]	Low G_0[e]
P_{min} (K cm^{-3}), $N = N_{cl}$[f]	1960	1560	2270	1580	1460
P_{max} (K cm^{-3}), $N = N_{cl}$[f]	4810	3150	5970	3920	3980
$P_{th,ave}$[g] (K cm^{-3}), $N = N_{cl}$[f]	3070	2220	3680	2490	2410
T_{ave}[h] (K), $N = N_{cl}$[f]	85	94	96	79	76
n_{ave}[i] (K), $N = N_{cl}$[f]	33	21	35	29	29
$n\Lambda$[j] (ergs s^{-1} H^{-1}), $N = N_{cl}$[f]	4.1×10^{-26}	3.2×10^{-26}	5.0×10^{-26}	3.3×10^{-26}	3.1×10^{-26}
C I*/C I_{tot}[k], $N = N_{cl}$[f]	0.190	0.145	0.205	0.168	0.167
T_{ave}[h] (K), 1×10^{20} (cm^{-2})[l]	71	67	84	64	65
$n\Lambda$[j] (ergs s^{-1} H^{-1}), 1×10^{20} (cm^{-2})[l]	3.6×10^{-26}	2.6×10^{-26}	4.3×10^{-26}	2.8×10^{-26}	2.7×10^{-26}
C I*/C I_{tot}[k], 1×10^{20} (cm^{-2})[l]	0.201	0.162	0.213	0.178	0.172
C I/C II[m], 1×10^{20} (cm^{-2})[l]	2.3×10^{-3}	7.1×10^{-4}	6.1×10^{-3}	1.5×10^{-3}	3.7×10^{-3}

[a] Standard model with $\phi_{PAH} = 0.5$, $n_{PAH}/n = 6 \times 10^{-7}$, $G_0 = 1.7$, $N_{cl} = 1 \times 10^{19}$ cm^{-2}.
[b] Low PAH collision rates with $\phi_{PAH} = 0.25$, $n_{PAH}/n = 6 \times 10^{-7}$, $G_0 = 1.7$, $N_{cl} = 1 \times 10^{19}$ cm^{-2}.
[c] High PAH collision rates with $\phi_{PAH} = 1.0$, $n_{PAH}/n = 6 \times 10^{-7}$, $G_0 = 1.7$, $N_{cl} = 1 \times 10^{19}$ cm^{-2}.
[d] Low PAH abundance with $\phi_{PAH} = 0.5$, $n_{PAH}/n = 4 \times 10^{-7}$, $G_0 = 1.7$, $N_{cl} = 1 \times 10^{19}$ cm^{-2}.
[e] Low FUV field with $\phi_{PAH} = 0.5$, $n_{PAH}/n = 6 \times 10^{-7}$, $G_0 = 1.1$, $N_{cl} = 1 \times 10^{19}$ cm^{-2}.
[f] Model result at cloud depth of $N_{cl} = 1 \times 10^{19}$ cm^{-2} and $P_{th,ave}$.
[g] $P_{th,ave} = (P_{max} P_{min})^{1/2}$.
[h] Temperature of CNM at $P_{th,ave}$.
[i] Density of CNM at $P_{th,ave}$.
[j] Gas cooling rate per hydrogen atom from [C II] 158 μm line emission in CNM.
[k] C I*/C I_{tot} population ratio.
[l] Model result at cloud interior at depth of 1×10^{20} cm^{-2} and $P_{th,ave}$.
[m] C I/C II abundance ratio.

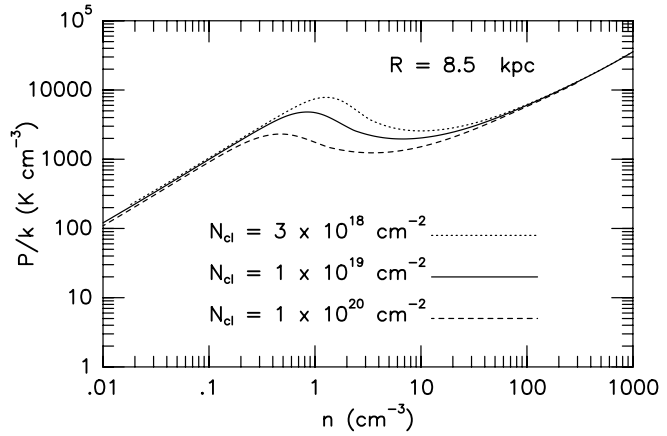

FIG. 9.—Thermal pressure P/k vs. hydrogen nucleus density n at Galactocentric radius $R = 8.5$ kpc. Curves are shown for various values of WNM atomic column density N_{cl} and apply to the WNM/CNM boundary.

in higher temperatures and pressures, P_{min} and P_{max}. At columns of $N_{cl} = 3 \times 10^{18}$ cm^{-2}, $P_{min}/k = 2560$ K cm^{-3}, and $P_{max}/k = 7830$ K cm^{-3}, while at the higher column of $N_{cl} = 1 \times 10^{20}$, $P_{min}/k = 1240$ K cm^{-3}, and $P_{max}/k = 2310$ K cm^{-3}. The calculated range in two-phase (CNM+WNM) thermal pressures over the column densities from $N_{cl} = 3 \times 10^{18}$ to 1×10^{20} cm^{-2} is in reasonably good agreement with the thermal pressures of $P/k = 10^3$–10^4 K cm^{-3} that are observed in the local ISM (Jenkins et al. 1983; Jenkins & Tripp 2001). For the fiducial case $N_{cl} = 10^{19}$ cm^{-2}, the average pressure at the solar circle is predicted to be 3070 K cm^{-3}, consistent with the C I population ratio observed by Jenkins & Tripp (2001) (see § 8.1).

6.2. *Thermal Processes*

Figures 10*a*–10*d* show the dominant thermal processes at Galactic radii of $R = 5$, 8.5, 11, and 17 kpc. We see that at all radii, photoelectric heating dominates in both the CNM and WNM phases. The [C II] 158 μm line emission dominates the cooling in the CNM and is generally a factor of $\sim$20 weaker (per H) in the WNM. The photoelectric heating rate per hydrogen is nearly the same as the results presented in WHMTB with the current rates approximately 20% lower at a density of 30 cm^{-3}. The higher PAH abundance used in this paper is offset by a lower gas-phase carbon abundance (and lower electron abundance in CNM gas), higher temperatures, and a $\phi_{PAH} = 0.5$ collision rate parameter, which decreases the photoelectric heating efficiency. Because of the higher CNM temperatures, however, we arrive at an average CNM density that is a factor of $\sim$2 lower than WHMTB (see Table 4), which results in an average C II cooling rate per hydrogen a factor of $\sim$1.5 lower than our previous result.

It is instructive to consider the total cooling luminosity of the ISM, which is dominated by the [C II] 158 μm line. The [C II] luminosity of the Milky Way has been measured by *COBE* to be 5×10^7 $L_\odot$ (Wright et al. 1991). Tielens (1995) considered the possible global sources of this emission. In the inner galaxy, much of it may originate in extended low-density H II regions (Heiles 1994), while most of this emission in the Galaxy as a whole has to stem from the CNM (WHMTB). The WNM cannot contribute much to the total [C II] luminosity as a result of the low emission rates in such tenuous gas. We consider the potential for mechanical heating by supernovae in Appendix B and conclude that neither the shock heating nor the turbulence generated by SNRs can contribute substantially to heating the H I gas. (Of course, mechanical energy dominates the energy balance of the HIM and coronal gas in the Milky Way.) Thus, the thermal structure of the ISM is largely dominated through the coupling of the gas to the stellar, nonionizing radiation field. The fraction of [C II] emission in the inner Galaxy that arises from CNM or warm ionized gas depends on the mass and density (or filling fractions) of these components. Fitting the observed profile of [C II] emission versus Galactic longitude may provide a test of the models presented here; however, a detailed model of the ionized gas (in pressure equilibrium and in overdense regions) is beyond the scope of this paper. We shall discuss in a future paper the implications of our [C II] emission rates for the filling fractions of the WNM and CNM gas and for the origin of the [C II] emission in the Galaxy.

6.3. *Predicted Infrared Radiation Field*

In this subsection we discuss a check on the distribution and local values of the model opacity and interstellar radiation field by comparing the calculated infrared intensity emitted by dust with observations from the *COBE* satellite.

We calculate the integrated infrared continuum intensity along a line of sight assuming that the predominantly far-infrared emission is optically thin,

$$I_{IR} = \int_{IR} d\nu\, I_\nu = \int_0^s ds' \int_{IR} d\nu \int da\, B_\nu[T(a)]\kappa_\nu(a)\ , \qquad (23)$$

where $B_\nu[T(a)]$ is the Planck function for the grain size–dependent temperature $T(a)$ and $\kappa_\nu(a)$ is the grain absorptive opacity for grains of size a. In thermal equilibrium, this emission just balances the heating by UV photons,

$$I_{IR} = \int_0^s ds' \int_{UV} d\nu \int da\, J_\nu^{ISRF} \kappa_\nu(a)\ , \qquad (24)$$

where J_ν^{ISRF} is the interstellar radiation field. We have ignored the small amount of energy that goes into photoelectric heating of the gas. We take the spectral energy distribution of the interstellar field to be that of Draine (1978) between 912 Å $\leq \lambda <$ 2000 Å, that of van Dishoeck & Black (1982) between 2000 Å $\leq \lambda <$ 3400 Å, and that of Mathis et al. (1983) for $\lambda \geq$ 3400 Å. The grain absorptive opacity κ_ν is calculated as in Wolfire & Cassinelli (1986) and Wolfire & Churchwell (1994) using a grain abundance and optical constants from Draine & Lee (1984, 1987) with grains distributed in size as a power law [$n(a)da \propto a^{-3.5}\, da$; Mathis et al. 1977]. The dust opacity is scaled with R in proportion to the mean H I density and metallicity,

$$\kappa_\nu(R) = \kappa_\nu(R_0) \frac{\langle n_{H\,I}(R)\rangle}{\langle n_{H\,I}(R_0)\rangle} e^{-(R-R_0)/H_R^Z}\ , \qquad (25)$$

while the interstellar radiation field is scaled with R according to results reported in § 4.1.

We show in Figure 11 the calculated IR emission compared with the *COBE* longitudinal profile reported by Sodroski et al. (1994). We obtain a reasonably good fit. We have not compared with the region within 3 kpc of the Galactic center, since we have not modeled the H I

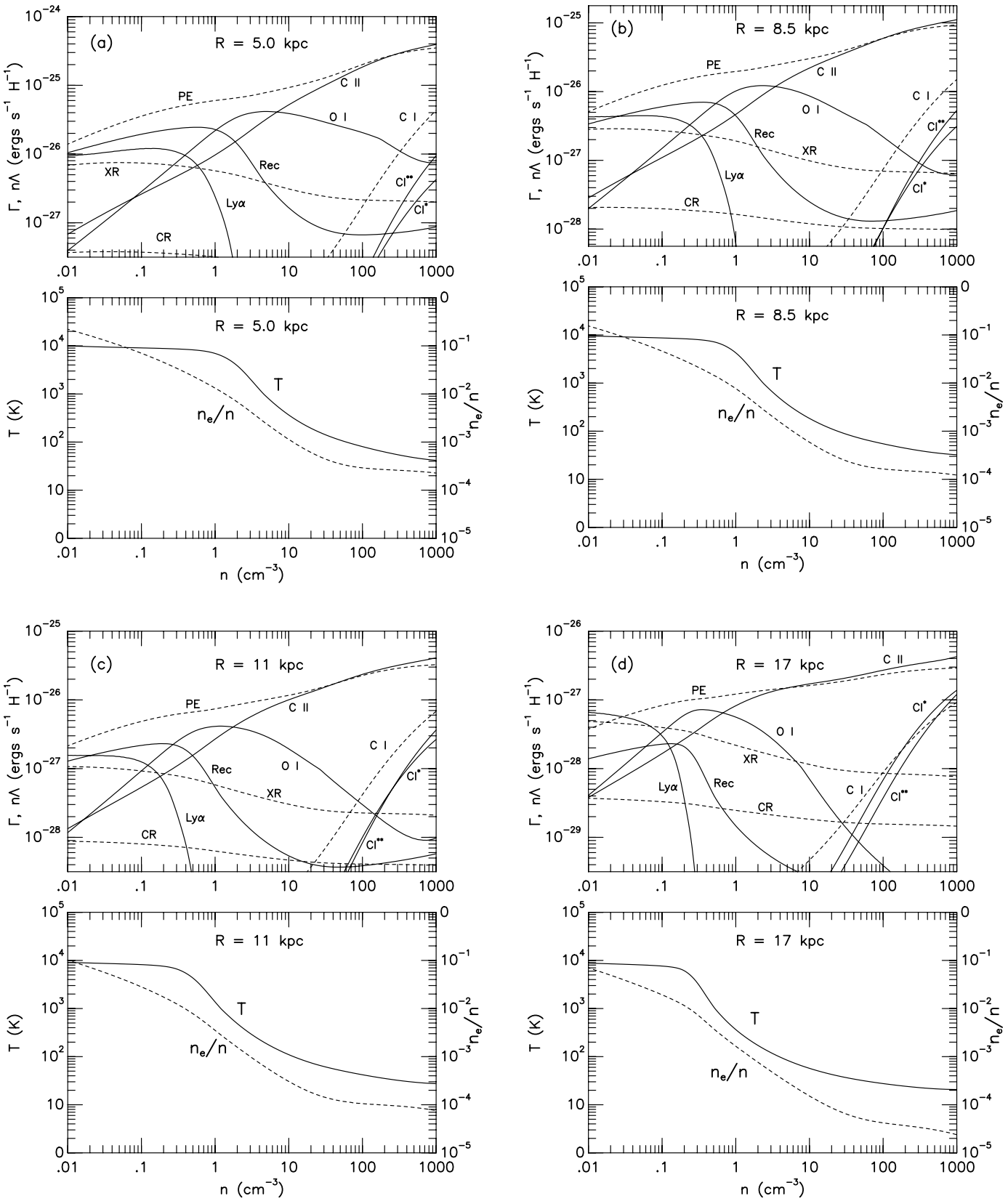

FIG. 10.—*Top panels:* Heating and cooling curves vs. hydrogen nucleus density n at various Galactic distances, R. Heating rates (*dashed curve*): photoelectric heating from small grains and PAHs ("PE"); EUV and X-ray ("XR"); cosmic ray ("CR"); photoionization of C ("C I"). Cooling rates (*solid curve*): C II 158 μm fine-structure ("C II"); O I 63 μm fine-structure ("O I"); recombination onto small grains and PAHs ("Rec"); Lyα plus metastable transitions ("Lyα"); C I fine-structure 609 μm ("C I*"); C I fine-structure 370 μm ("C I**"). *Bottom panels:* Gas temperature T (*solid curve*) and electron fraction n_e/n (*dashed curve*) vs. hydrogen nucleus density n. (*a*) $R = 5$ kpc. (*b*) $R = 8.5$ kpc. (*c*) $R = 11$ kpc. (*d*) $R = 17$ kpc.

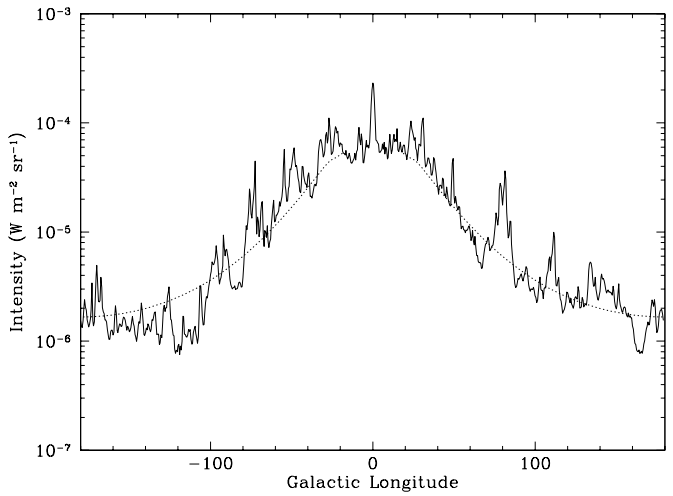

FIG. 11.—Infrared intensity in the Galactic midplane vs. Galactic longitude. *COBE* observations (*solid curve*) from Sodroski et al. (1994). Calculated dust emission (*dotted curve*) using the FUV opacity from Fig. 4 and the FUV field from Fig. 5.

there. The largest deviations occur at the locations of the spiral arms, where some of the FUV radiation is absorbed by molecular gas associated with star-forming regions; recall that we have not included this in our models, which are for the diffuse ISM. Integrating over Galactic longitude, but excluding the region near the Galactic center, the mean intensity from *COBE* is 1.4×10^{-5} W m^{-2} sr^{-1}, whereas our model gives 1.1×10^{-5} W m^{-2} sr^{-1}. According to Parravano, Hollenbach, & McKee (2003), about 80% of the FUV radiation is absorbed in the diffuse ISM and 20% is absorbed by the nearby natal GMC. Using the interstellar radiation field and opacity given in the preceding paragraph, we estimate that approximately half the dust heating is produced by the FUV radiation from OB stars and half by longer wavelength radiation from older stars generally located far from molecular clouds. Correcting for the OB starlight absorbed by nearby molecular clouds, our model gives 1.2×10^{-5} W m^{-2} sr^{-1} for the total IR emission, in reasonably good agreement with observation.

6.4. *Multiphase ISM*

We have presented phase diagrams that show $P_{\rm min}$ and $P_{\rm max}$ and have presented observational evidence that both CNM and WNM gas exists, but we have not yet tried to estimate the thermal pressure in order to make comparison to $P_{\rm min}$ or $P_{\rm max}$. One way to determine the pressure is from the density and volume filling factors of the H I gas. Our results are in terms of the local density n, but they can be recast in terms of the mean atomic hydrogen density $\langle n_{\rm H\,I}\rangle$, which is often better determined observationally. Let $n_{\rm WNM}(P_{\rm min})$ be the equilibrium density of the WNM at the pressure $P_{\rm min}$, etc. We generalize the treatment of Krolik, McKee, & Tarter (1981) (who used the notation $\bar{n}$ for the mean density) by allowing for the possibility that the two-phase medium fills only a fraction $f_{\rm H\,I}$ of the volume and by allowing for pressure fluctuations in the gas. We follow Krolik et al. (1981) in assuming that the gas is in thermal equilibrium, which is not strictly true in a turbulent medium.

The ratio of the CNM mass to the WNM mass is (Krolik et al. 1981)

$$\frac{M_{\rm CNM}}{M_{\rm WNM}} = \frac{[\langle n_{\rm H\,I}\rangle/(n_{\rm WNM} f_{\rm H\,I})] - 1}{1 - [\langle n_{\rm H\,I}\rangle/(n_{\rm CNM} f_{\rm H\,I})]} \ . \tag{26}$$

Similarly, one can show that the ratio of the volume filling factors is

$$\frac{f_{\rm CNM}}{f_{\rm WNM}} = \frac{1 - (n_{\rm WNM} f_{\rm H\,I}/\langle n_{\rm H\,I}\rangle)}{(n_{\rm CNM} f_{\rm H\,I}/\langle n_{\rm H\,I}\rangle) - 1} \ . \tag{27}$$

Let $\mathscr{R} \equiv n_{\rm CNM}(P_{\rm min})/n_{\rm WNM}(P_{\rm max})$; if $\mathscr{R}$ is large, then there is an extensive range of density in which the H I is thermally unstable. The cases summarized in Table 3 all have $\mathscr{R} \gtrsim 6$.

There are five regimes for two-phase media:

1. $\langle n_{\rm H\,I}\rangle/f_{\rm H\,I} < n_{\rm WNM}(P_{\rm min})$. Since the average density of the H I is less than the minimum required for CNM to exist, it follows that most, if not all, of the volume of H I is filled with WNM. If the gas is isobaric, the H I is all WNM.
2. $n_{\rm WNM}(P_{\rm min}) < \langle n_{\rm H\,I}\rangle/f_{\rm H\,I} < n_{\rm WNM}(P_{\rm max})$. Here again, most of the volume of H I must be filled with WNM [one can show from eq. (27) that $f_{\rm CNM}/f_{\rm WNM} < 1/(\mathscr{R} - 1)$], but even for the isobaric case some CNM can coexist with the WNM. In the presence of turbulent pressure fluctuations, some WNM will be driven into CNM, and both phases will occur.
3. $n_{\rm WNM}(P_{\rm max}) < \langle n_{\rm H\,I}\rangle/f_{\rm H\,I} < n_{\rm CNM}(P_{\rm min})$. If the local density n were in this regime, the gas would be thermally unstable and two phases would form. As a result, in this case two phases *must* exist.
4. $n_{\rm CNM}(P_{\rm min}) < \langle n_{\rm H\,I}\rangle/f_{\rm H\,I} < n_{\rm CNM}(P_{\rm max})$. In this regime, most of the mass must be CNM (one can show from eq. [26] above that $M_{\rm CNM}/M_{\rm WNM} > \mathscr{R} - 1$), but even for the isobaric case some WNM can occur. In the presence of turbulent pressure fluctuations (which are negative as well as positive), some CNM will be driven into WNM, and both phases will occur. However, in this regime, it is possible that all the neutral gas is CNM.
5. $n_{\rm CNM}(P_{\rm max}) < \langle n_{\rm H\,I}\rangle/f_{\rm H\,I}$. Finally, in this case most of, if not all, the H I must be in the form of CNM. If the gas is isobaric, all the H I must be CNM.

According to Table 3, the local ISM is characterized by $n_{\rm WNM}(P_{\rm min}) = 0.21$ cm^{-3}, $n_{\rm WNM}(P_{\rm max}) = 0.86$ cm^{-3}, $n_{\rm CNM}(P_{\rm min}) = 6.9$ cm^{-3}, and $n_{\rm CNM}(P_{\rm max}) = 71$ cm^{-3}. The locally observed value of the mean atomic hydrogen density $\langle n_{\rm H\,I}\rangle$ in the Galactic plane is 0.57 cm^{-3}. Therefore, if the H I is pervasive, the local ISM would be in the regime in which most of the volume of H I is primarily WNM. Observations show that most of the mass of the H I in the local plane is CNM (Dickey & Lockman 1990). Recently, Heiles & Troland (2003), utilizing H I 21 cm measurements, estimated a local value of $f_{\rm H\,I} = 0.5$ based on the assumption that the local thermal pressure of WNM is 2240 K cm^{-3} and $T_{\rm WNM} = 4000$ K so that $n_{\rm WNM} = 0.56$ cm^{-3}. In this paper we argue that the local WNM pressure is approximately 3100 K cm^{-3} and that $T_{\rm WNM} \simeq 8000$ K so that $n_{\rm WNM} \simeq 0.35$ cm^{-3}. The Heiles & Troland (2003) result then becomes $f_{\rm H\,I} \simeq 0.79$. These results lie close to the theoretical estimates, which range from $f_{\rm H\,I} = 0.4$ (MO) to 0.8 (Slavin & Cox 1993). If a substantial fraction of the volume of the ISM is hot, then $f_{\rm H\,I} \lesssim 0.5$ and the local ISM is marginally in the regime in which there *must* be two phases.

We extend our analysis to the inner and outer Galaxy by estimating the thermal pressure in the midplane in the limiting case in which the H I is entirely in the form of WNM. We derive a WNM pressure and check to see if it is self-consistent (i.e., is the thermal pressure less than $P_{\rm min}$ or $P_{\rm max}$) to assume that all the neutral gas is WNM. To calculate the thermal pressure, we rely on the assumption that the total pressure in the midplane is balanced by the weight of the overlying gas layers (i.e., hydrostatic equilibrium). We first consider the case in which the Galactic H I resides in a continuous, thermally supported WNM layer, and then we modify this thermal pressure calculation for the effects of nonthermal support, including cosmic rays, magnetic fields, and turbulence. We also estimate the thermal pressure by using the mean atomic hydrogen density $\langle n_{\rm H\,I}\rangle$ shown in Figure 3 to derive a "mean" thermal pressure, which we compare to $P_{\rm min}$ and $P_{\rm max}$ to find the region over which a two-phase medium must exist.

6.4.1. *Thermally Supported WNM*

For an isothermal gas in hydrostatic equilibrium in the Galactic gravitational field, the vertical density distribution is given by

$$n(R,z) = n_0(R) e^{[\Phi(R,0)-\Phi(R,z)]/\sigma_{\rm th}^2}\ , \qquad (28)$$

where $n(R,z)$ is the gas density at Galactic radius R and height above the plane z, $n_0(R) = n(R, z=0)$ is the density in the midplane, $\Phi(R,z)$ is the Galactic gravitational potential, and $\sigma_{\rm th}$ is the isothermal sound speed. We take $\Phi(R,z)$ from a variant of model 2b of Dehnen & Binney (1998), which has a disk mass of $5.3 \times 10^{10}\ M_\odot$ (by comparison, the disk model used by Wolfire et al. 1995b had a mass of $1.0 \times 10^{11}\ M_\odot$). The numerical code to calculate the potential was kindly provided by W. Dehnen. Each density component in the disk is assumed to be of the form

$$\rho = \frac{\Sigma_d}{2z_d} \exp\left(-\frac{R_m}{R} - \frac{R}{R_d} - \frac{|z|}{z_d}\right)\ , \qquad (29)$$

where z_d is the vertical scale height and R_d is the radial scale length of the disk. The parameter R_m allows for the depression in the gas density observed in the inner several kiloparsecs of the Galaxy; for the stellar disks, they set $R_m = 0$. Dehnen & Binney (1998) assumed that the gas in the disk could be described by a single component with $z_d = 40$ pc and, for model 2b, $R_d = 5.1$ kpc. A limitation of their model (which is relatively unimportant for their application) is that the vertical scale height z_d for each component is assumed to be independent of radius. We have altered their model for the gas to make it more consistent with the discussion in § 3, with one component for the molecular gas, two components for the H I in order to capture the radial variation, and one component for the H II. [We have included only the diffuse H II component discussed in § 3.4, since the ionized gas contributed by the envelopes of H II regions is always very small compared to the column density of stars plus H I. We have approximated $\mathrm{sech}^2\,(R_k/20)$ as $\exp(-R_k/30)$.] We have also altered their model for the thin stellar disk to allow the scale height to increase in the outer Galaxy. For Galactic radii $R > R_0$ we assume that $z_d \propto 1/\Sigma$, where Σ includes the total (gas plus stars) surface density, and then recalculate the potential for each radius R using the appropriate z_d. The parameters entering the fit are summarized in Table 5. The total surface density at the solar circle is 10.1 $M_\odot$ pc^{-2}.

TABLE 5

Parameters in Galactic Disk Potential Model

Component	Σ_d[a] ($M_\odot$ pc^{-2})	R_m (kpc)	R_d (kpc)	z_d (pc)
H I ($R \le 13$ kpc)	7.94	1.0	1000	178
H I ($R > 13$ kpc)	571	10	4.00	324
H_2	57.5	3.3	2.89	63.4
H II	1.39	0	30.0	880
Thin star disk ($R \le R_0$)	1058	0	2.55	180
Thin star disk ($R > R_0$)	1058	0	2.55	z_d^*[b]
Thick star disk	70.6	0	2.55	1000

Note.—Disk potential model based on Dehnen & Binney 1998. Each component has a density distribution given by the form $\rho(R) = \Sigma_d (2z_d)^{-1} \exp[-(R_m/R) - (R/R_d) - (|z|/z_d)]$. Bulge and halo components are the same as Dehnen & Binney 1998 model 2b.

[a] Includes He mass.

[b] Stellar disk height given by $z_d^* = 180\Sigma(R_0)/\Sigma(R)$ pc.

This is 2.5 $M_\odot$ pc^{-2} less than that of Dehnen & Binney (1998), so we added 2.5 $M_\odot$ pc^{-2} to the thin stellar disk in order to maintain the same value of the total surface density.

We wish to calculate the pressure that the WNM in the Galactic plane would have if all the H I in the disk were in the form of WNM and if the pressure support of the WNM were entirely thermal. We label this hypothetical pressure $P_{\rm WNM'}$. It is given in terms of the midplane H I density $n_{\rm H\,I,0}(R)$ by $P_{\rm WNM'}(R) = 1.1 n_{\rm H\,I,0}(R) kT$. To determine $n_{\rm H\,I,0}(R)$, we first calculate the column density from equation (28), noting that the velocity dispersion of the neutral WNM is $\sigma_{\rm th} = 7.2$ km s^{-1} ($T = 8000$ K). We then equate this theoretical column density to the observed column density, $N_{\rm H\,I}(R) = 2\int n_{\rm H\,I}(R,z)dz$, and solve for $n_{\rm H\,I,0}(R)$. Figures 12*a*–12*c* show the pressure obtained in this manner for $N_{\rm cl} = 1 \times 10^{19}$, 1×10^{20}, and 3×10^{18} cm^{-2}, respectively, compared to $P_{\rm min}$, $P_{\rm max}$, and the average thermal pressure $P_{\rm th,ave}(R)$. The kinks in $P_{\rm WNM'}$ are a reflection of the kinks in our adopted H I surface density (eq. [7]). In Appendix A we provide an analytic solution for $P_{\rm WNM'}$ at the solar circle that provides a value of $P_{\rm WNM'} = 7800$ K cm^{-3}, in good agreement with the numerical solution of $P_{\rm WNM'} = 8615$ K cm^{-3}. These values exceed $P_{\rm max}$ for $N_{\rm cl} \gtrsim 3.0 \times 10^{18}$ cm^{-2} (see Table 3), so we conclude that a thermally supported H I layer cannot be all in the form of WNM gas and some of the H I *must* be forced into the CNM phase, at least in the solar neighborhood. The numerical results (Figs. 12*a*–12*c*) show that this is true over most of the disk of the Galaxy.

6.4.2. *Turbulently Supported WNM*

The discussion in the previous section is based on a highly idealized model of the ISM, in which the gas is supported entirely by thermal pressure. In fact, turbulence makes a substantial contribution to the support of the gas; cosmic rays and magnetic fields appear to make less of a contribution to support of H I near the plane since their scale heights are much greater than that of the CNM and the gradient is therefore weak, although their substantial pressures must somehow be anchored by the weight of the ISM (Boulares & Cox 1990). The increase in the scale height reduces the mean density of the gas and hence the inferred thermal pressure. The turbulence leads to large pressure fluctuations, and these will drive some of the gas into the cold phase (e.g., Hennebelle & Pérault 1999, 2000). The condition for a

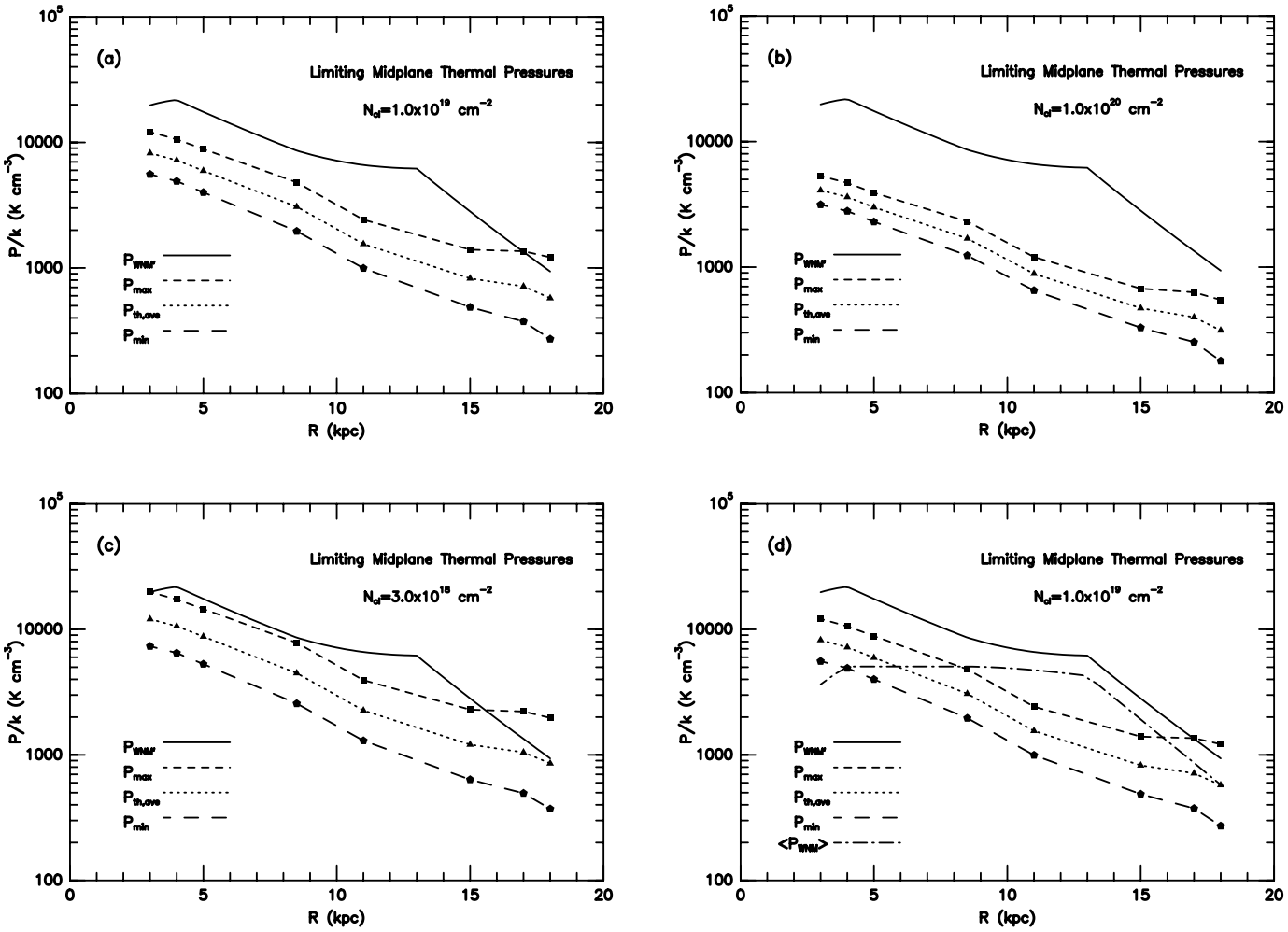

FIG. 12.—Limiting thermal pressures in the Galactic midplane vs. Galactocentric radius R. $P_{\rm WNM'}$ (*solid curve*) is the thermal pressure produced by the H I layer assuming that all of the gas is in the form of WNM and supported in hydrostatic equilibrium by thermal pressure. $P_{\rm max}$ (*short-dashed curve*) and $P_{\rm min}$ (*long-dashed curve*) are the maximum and minimum pressure range for a two-phase medium. $P_{\rm th,ave}$ (*dashed curve*) is the mean pressure $P_{\rm th,ave} = (P_{\rm min}P_{\rm max})^{1/2}$. Panels show the effects of different WNM columns. (*a*) $N_{\rm cl} = 1.0 \times 10^{19}$ cm^{-2}. (*b*) $N_{\rm cl} = 1.0 \times 10^{20}$ cm^{-2}. (*c*) $N_{\rm cl} = 3.0 \times 10^{18}$ cm^{-2}. (*d*) $N_{\rm cl} = 1.0 \times 10^{19}$ cm^{-2} curves with $\langle P_{\rm WNM}\rangle$ added. $\langle P_{\rm WNM}\rangle$ is the thermal pressure that would be present in the Galactic midplane if all of the H I had a temperature of 8000 K and a density given by the mean density shown in Fig. 3 (see § 6.4.2).

substantial amount of CNM in a turbulent ISM is therefore that the thermal pressure exceed $P_{\rm min}$, which ensures that the gas that is compressed into the CNM can remain there.

We analyze first the solar circle and compare the thermal pressure to $P_{\rm min}$ *assuming* that all H I is WNM. We redistribute the 2.75×10^{20} H I atoms cm^{-2} of CNM into the WNM components found by Dickey & Lockman (1990); the result is a gas with a central density of 0.31 cm^{-3}. This procedure should provide a lower bound on the thermal pressure of this hypothetical ISM in which the H I is pure WNM, since we are assuming that there is enough additional turbulent energy injection to lift the mass in CNM up to the height of the WNM. With this assumption, the resulting thermal pressure is $P/k = 2700$ K cm^{-3}. Since this significantly exceeds $P_{\rm min}/k = 1960$ K cm^{-3} and since the local ISM is turbulent, we conclude that it must be in two phases.

We can make analogous arguments to the rest of the Galaxy to show that, assuming that all of the H I were WNM, the thermal pressure would exceed $P_{\rm min}$, violating our assumption, and that therefore CNM must exist. We begin by determining a lower limit on the thermal pressure produced by WNM gas at other positions in the Galaxy. In § 3.1 we have presented the mean density $\langle n_{\rm H\,I}\rangle$ of H I in the plane rather directly derived from the observations. Assuming that the volume filling factor of WNM is much greater than that of the CNM,

$$\langle n_{\rm H\,I}\rangle = n_{\rm WNM}\left(1 + \frac{M_{\rm CNM}}{M_{\rm WNM}}\right) f_{\rm H\,I}\ , \tag{30}$$

where $M_{\rm CNM}/M_{\rm WNM}$ is evaluated in the midplane. The thermal pressure in the medium is given by

$$P_{\rm th,WNM} = 1.1 n_{\rm WNM} k T_{\rm WNM}\ . \tag{31}$$

In terms of the "observable" $\langle n_{\rm H\,I}\rangle$, $P_{\rm th,WNM}$ can be written as

$$P_{\rm th,WNM} = 1.1 \frac{\langle n_{\rm H\,I}\rangle k T_{\rm WNM}}{f_{\rm H\,I}(1 + M_{\rm CNM}/M_{\rm WNM})} \equiv \frac{\langle P_{\rm WNM}\rangle}{f_{\rm H\,I}(1 + M_{\rm CNM}/M_{\rm WNM})}\ . \tag{32}$$

The "mean" thermal pressure $\langle P_{\rm WNM}\rangle$, i.e., the thermal pressure assuming that the denominator is unity (for example, the observed mean density is all WNM and $f_{\rm H\,I}=1$), is shown in Figure 12*d* (assuming $T_{\rm WNM}=8000$ K) along with $P_{\rm min}$, $P_{\rm max}$, and $P_{\rm th,ave}$ for our standard $N_{\rm cl}=1.0\times10^{19}$ cm^{-2} case. Following the distribution of H I in the Galaxy, $\langle P_{\rm WNM}\rangle$ is flat with Galactocentric radius out to 13 kpc where it starts to drop exponentially.

As we did in the nonturbulent case, we can make the *Ansatz* that all the H I gas is WNM and ask whether the thermal pressure exceeds $P_{\rm min}$ or $P_{\rm max}$. In contrast to the argument above for the local ISM, we assume that there is no additional turbulent energy injection to raise the height of the converted CNM. In this case $\langle P_{\rm WNM}\rangle$ is a lower limit to the thermal pressure since $f_{\rm H\,I}$ may be less than unity (although it must be borne in mind that a hypothetical ISM in which the H I is pure WNM is likely to have $f_{\rm H\,I}$ closer to unity than the actual ISM). Comparing $\langle P_{\rm WNM}\rangle$ to the model thermal pressure curves, we conclude that in this case the thermal pressure would exceed $P_{\rm max}$ for Galactic distances 8 kpc $\lesssim R\lesssim$ 16 kpc, our *Ansatz* is violated, and a two-phase medium *must* exist in the outer Galaxy. Moreover, over much of the Galaxy $\langle P_{\rm WNM}\rangle$ exceeds $P_{\rm min}$; hence, pressure fluctuations in a turbulent ISM will produce a two-phase medium.

We also note in Figure 12*d* that $\langle P_{\rm WNM}\rangle$ falls everywhere below the nonturbulent pressure $P_{\rm WNM'}$ derived from the weight of the H I in the Galactic potential. Essentially, this high value of $P_{\rm WNM'}$ derives from the assumption of no turbulence and therefore has a thermal scale height of $\sim$80 pc (see Appendix A), whereas $\langle P_{\rm WNM}\rangle$ takes into account the observed half-height ($\sim$265 pc) of the H I and reflects the importance of turbulence for the dynamics of the interstellar gas.

7. AN ANALYTIC MODEL FOR TWO-PHASE EQUILIBRIA

In order to understand the physical reasons for the results just presented and to obtain scaling laws, it is convenient to have an approximate analytic model. The details of this model are presented in Appendix C; we summarize here our procedure and the results.

The thermal balance pressure P is found as a function of T by equating a simple analytic equation for the total ([C II] + [O I]) cooling to the analytic expression for grain/PAH photoelectric heating. The simple cooling equation holds for 100 K $< T <$ 1000 K, which marks the temperature range of validity of our analytic solutions. Several other parameters enter the pressure equation, including the FUV field G_0', the total gas ionization rate by cosmic rays and EUV/X rays ζ_t', the dust/PAH abundance Z_d', and the gas-phase metal abundance (especially of the coolants C and O) Z_g'. The primes denote normalization to the local values given in Table 1, so that all these parameters have value unity at the solar circle. In other words, $G_0'=G_0/1.7$ and $\zeta_t'=\zeta_t/10^{-16}$ s^{-1}, where ζ_t' includes primary and secondary ionizations. The grain photoelectric heating depends on the charge state of the PAHs/grains, which in turn depends on the electron density n_e in the gas. At a typical column $N_{\rm cl}=10^{19}$ cm^{-2}, H$^+$ (not C$^+$) supplies the electrons. Therefore, $n_e\simeq n({\rm H}^+)$ and we solve for $n({\rm H}^+)$. The source of H$^+$ is the photoionization of H by EUV/X-rays, and the sink is recombination with negatively charged PAHs, or PAH$^-$. PAH$^-$ is produced by electron attachment on neutral PAHs (neutral PAHs dominate the PAH population in the parameter space valid for our analytic P expression) and is destroyed by photodetachment in the FUV field (G_0').

With an analytical expression for P, we then take $dP/dT=0$ to find the temperature $T_{\rm (min)}$ at the pressure minimum, which substituted into our expression for P gives $P_{\rm min}$. We put the parentheses in the subscript for $T_{\rm (min)}$ to emphasize that this temperature is not a minimum temperature; in fact, it is the maximum temperature of the CNM! The hydrogen density at $P_{\rm min}$ is then $n_{\rm min}=P_{\rm min}/1.1kT_{\rm (min)}$. Appendix C describes all the essential and competing reactions and gives analytic expressions for the cooling, heating, PAH$^-$ abundance, n_e, and P. We summarize here the results for $P_{\rm min}$, $T_{\rm (min)}$, and $n_{\rm min}$, which we emphasize are valid over a range of parameter space centered on solar circle values, as discussed below. We find

$$\frac{P_{\rm min}}{k}\equiv 1.1 n_{\rm min}T_{\rm (min)} \simeq 8500\frac{G_0'\left(Z_d'/Z_g'\right)}{1+3.1\left(G_0'Z_d'/\zeta_t'\right)^{0.365}}\ {\rm cm^{-3}\ K}\ , \quad (33)$$

$$T_{\rm (min)}\simeq 243\ {\rm K}\ , \quad (34)$$

and

$$n_{\rm min}\simeq 31\frac{G_0'\left(Z_d'/Z_g'\right)}{1+3.1\left(G_0'Z_d'/\zeta_t'\right)^{0.365}}\ {\rm cm^{-3}}\ . \quad (35)$$

These equations are valid over the following range of parameters. The first condition is that

$$4.6\times10^{-2}\lesssim\frac{G_0'Z_d'}{\zeta_t'}\lesssim 11\ . \quad (36)$$

The lower limit is set so that the grain/PAH photoelectric heating is significantly affected by the positive charging of the grain/PAHs, which simplifies the analytic expression for the gas heating. It also ensures that most PAHs, and not PAH$^-$, are neutral and that FUV photodetachment, and not reaction with H$^+$, destroys PAH$^-$; these assumptions were made in deriving the analytic expression. The upper limit is set so that H$^+$ is destroyed by PAH$^-$, and not neutral PAHs. It also ensures the less restrictive condition that neutral PAHs, and not PAH$^+$, dominate the PAH population. The second condition is that

$$6.5\times10^{-3}Z_g'^2\lesssim\left(\frac{G_0'}{\zeta_t'}\right)^{0.27}Z_d'^{2.27}\phi_{\rm PAH}^2\lesssim 4.1\ . \quad (37)$$

The upper limit ensures that the gas-phase abundance of H$^+$ exceeds that of C$^+$ (H$^+$ supplies the electrons in the gas). As an interesting side note, we find that there is no $P_{\rm min}$ in the temperature range where [C II] 158 μm and [O I] 63 μm dominate the cooling, *if the electrons are supplied by* C$^+$ *and if the grain heating is significantly affected by positive charge*. The ionization of H and He is therefore generally critical to the two-phase phenomenon. The lower limit ensures that atomic hydrogen collisions, and not electrons, dominate the excitation of the [C II] line. The final condition is that

$$Z_g'Z_d'^{-1.635}\left(\frac{G_0'}{\zeta_t'}\right)^{0.365}\lesssim 38\phi_{\rm PAH}^2\ . \quad (38)$$

This condition assures that H$^+$ is destroyed by PAH$^-$, and

not by recombining with gas-phase electrons. We found it interesting that this is generally the case for the wide range of conditions centered on local values.

Given that all the above conditions are met, equations (33) and (34) give not only the absolute values of $P_{\rm min}$ and $T_{\rm (min)}$ but also the scaling of $P_{\rm min}$ with the parameters G_0', ζ_t', Z_d', and Z_g'. It might be noted that Z_d' and Z_g' may often scale linearly with respect to each other and with the total elemental metallicity Z. It is also noteworthy that in this simple analytic solution, $T_{\rm (min)}$ is independent of all the parameters Z_g', Z_d', G_0', and ζ_t'. It depends primarily on the gas temperature dependence of the cooling rates and the grain photoelectric heating rate. In much of parameter space, the numerical solution gives $T_{\rm (min)} \sim 180$–350 K, which lie within about $\pm 40\%$ of the constant 243 K analytic result. The numerical calculation of $T_{\rm (min)}$ is sensitive to small contributions from processes we have ignored or simplified in the analytic treatment (e.g., electrons supplied by C^+, our approximate cooling function, a simplification of the grain photoelectric heating). However, our analytic results for $P_{\rm min}$ and the scaling of $P_{\rm min}$ are much more robust; $P_{\rm min}$ is not sensitive to the exact value of $T_{\rm (min)}$, since it lies at a minimum with respect to changes in T.

Figure 13 illustrates the region of validity for the analytic solution for $P_{\rm min}$ (eq. [33]). We plot the conditions given in equations (36)–(38) as functions of $Z' = Z_g' = Z_d'$ and G_0'/ζ_t'. The constraint that hydrogen collisions dominate the excitation of [C II] (lower limit in eq. [37]) is readily met and not a factor as long as the other conditions are satisfied. We have performed several checks of the analytic solution for $P_{\rm min}$ and $T_{\rm (min)}$ against the detailed results of our numerical code. We held three of the parameters fixed at the local values (=1 in the notation of the analytic equations) and varied the fourth over a factor of 100 from 0.1 to 10. This test showed that over this range the absolute value of the analytic $P_{\rm min}$ was within $\pm 50\%$ of the numerical value as long as Z_g' was less than 3 and Z_d' was between 0.3 and 5.0. The scaling of $P_{\rm min}$ was accurate to about $\pm 45\%$, and $T_{\rm (min)}$ was accurate to about a factor of 2.5. In the numerical runs, $T_{\rm (min)}$ varied from 180 to 630 K, with a value of 258 K at the solar circle. This test, however, occasionally violated the conditions of validity. If we restrict the test strictly to the regime of validity, the agreement for $P_{\rm min}$ is unchanged, but the range of $T_{\rm (min)}$ in our numerical calculation is reduced to 180–465 K, with much of parameter space 180–350 K.

As another test of our analytic solution we compared $P_{\rm min}$ to our numerical results in which we varied $Z_g' = Z_d'$ from 0.01 to 10 and G_0'/ζ_t' from 0.1 to 300. The shaded region in Figure 13 shows the range in which the analytic solution agrees with the numerical results to within $\pm 50\%$. It is clear that the applicable range of validity extends well beyond that given by the restrictive conditions expressed in equations (36)–(38). As a final test we compared the analytic solution for $P_{\rm min}$ with the calculated $P_{\rm min}$ as a function of Galactic radius (§ 6.1 and Table 3). We find that the calculated $P_{\rm min}$ can be fitted with an exponential in Galactic radius as

$$P_{\rm min} = 1.1 \times 10^4 \exp\left(\frac{-R_k}{4.9}\right) \ {\rm K\ cm^{-3}}\ . \qquad (39)$$

This fit is good to within $\pm 17\%$ between $R_k = 3$ and 18 kpc. Substituting values for G_0', ζ_t', Z_d', and Z_g' from Table 2 into equation (33) yields analytical results that are good to within $\pm 15\%$ of the numerical results.

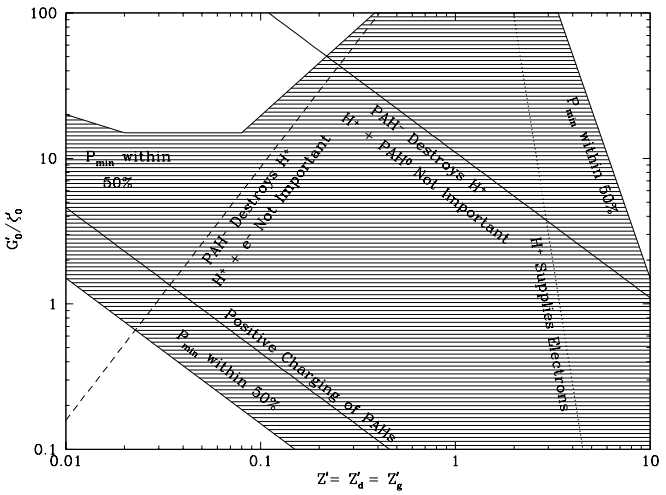

FIG. 13.—Region of validity for the analytic solution of $P_{\rm min}$ (eq. [33]) as a function of the dust abundance Z_d', gas-phase metal abundance Z_g', ionization rate ζ_t', and FUV radiation field G_0'. All parameters are scaled to their value in the solar neighborhood. The valid region is shown for the case of dust and metal abundances scaling linearly with the elemental abundance ($Z' = Z_d' = Z_g'$). The shaded region shows the range in which the analytic solution is good to within $\pm 50\%$ of the numerical results. Also shown are the more restrictive conditions derived in Appendix C and given in eqs. (36)–(38): PAHs are positively charged and the destruction of H^+ is dominated by reactions with PAH^- rather than with PAH^0 (eq. [36]; *solid line*); electrons are supplied by H^+ rather than C^+ (eq. [37]; *dotted line*); the destruction of H^+ is dominated by reactions with PAH^- rather than by electron recombination (eq. [38]; *dashed line*). The analytic solution is good to within $\pm 45\%$ of the numerical results within this region.

8. COMPARISON WITH OBSERVATIONS AND PREVIOUS WORK

8.1. *Comparison with Local Observations*

In this section we compare our model results with three critical observations of the CNM: the thermal pressure, the gas temperature, and the C^+ cooling rate per hydrogen atom. We also briefly examine the constraints imposed by the observed C I/C II ratio. Our model results for the local Galaxy and the effects of various model parameters are summarized in Tables 3 and 4. The results presented in this paper so far have been for the WNM/CNM interface at a cloud column of $N_{\rm cl}$. We also list in Table 4 results for a CNM cloud interior at a depth of 1×10^{20} cm^{-2}. The mean CNM column density measured by Heiles & Troland (2003) is 5×10^{20} cm^{-2}. For a slab cloud, a typical point is at a depth of one-fourth of the observed column density ($\sim 1.25 \times 10^{20}$ cm^{-2}), where half the mass is at greater column and half at lower column. For a spherical cloud, the average line of sight passes through a column of $2N/3$, where N is the column density through the cloud center and the half-mass depth is at $0.1N$ from the surface. This half-mass depth corresponds to $\sim 0.75 \times 10^{20}$ cm^{-2}. Our fiducial column is between the two limits for slab and spherical clouds.

The thermal pressure in the ISM has been measured through studies of the population distribution of the C I fine-structure levels based on FUV absorption lines originating from these levels (Jenkins et al. 1983; Jenkins & Tripp

2001). By necessity, such studies are largely limited to the local solar neighborhood. Jenkins & Tripp (2001) find a mean observed C I*/C I_{tot} ratio of 0.196 and derive a mean pressure of $P_{th} = 2240$ K cm^{-3} from this ratio. This pressure is somewhat lower than the previous result of Jenkins et al. (1983), who found $P_{th} \approx 4000$ K cm^{-3}. Our standard parameter set yields $P_{min} = 1960$ K cm^{-3}, $P_{max} = 4810$ K cm^{-3}, and $P_{th,ave} = 3070$ K cm^{-3}, and our average pressure would appear to be higher than the observed value. However, Jenkins & Tripp (2001) note that the derived pressure is sensitive to the CNM temperature and atomic constants where they used a CNM temperature of $T = 40$ K and radiative decay rates from Froese Fischer & Saha (1985). The more recent radiative rates of Galavis, Mendoza, & Zeippen (1997) are approximately 10% higher than those used by Jenkins & Tripp (2001), and our model temperature of 71 K in the CNM cloud interior (see Table 4) is considerably higher than 40 K. Both of the these differences tend to increase the derived thermal pressure for the same observed population ratio. (We note that the excitation rates of C I by collisions with H I from Launay & Roueff 1977 are expected to be accurate to within 10%; E. Roueff 2002, private communication.) Including the updated radiative rates, plus the optical/UV pumping of the C I lines as discussed in Jenkins & Tripp (2001) and Jenkins & Shaya (1979), we find a C I*/C I_{tot} population ratio of 0.190 at the CNM cloud surface and a C I*/C I_{tot} ratio of 0.201 in the cloud interior (Table 4). These values are within 3% of the observed ratio of 0.196. The "low-ϕ_{PAH}" ($\phi_{PAH} = 0.25$) model compares least favorably to the observations with a population ratio of between 0.145 and 0.162. Although the differences between models are not large, we conclude that our standard model with an average thermal pressure of $P_{th,ave} = 3070$ K cm^{-3} provides the best agreement with the observed C I*/C I_{tot} ratio.

In addition to the thermal pressure, observational tests are provided by the CNM temperature and C^+ cooling rate. Heiles (2001), using H I emission/absorption experiments along 19 lines of sight, found that of the total CNM column detected, most (~61%) lies in a narrow temperature range between 25 and 75 K, with a peak near 50 K. This value was recently revised by Heiles & Troland (2003) when an additional 60 lines of sight became available and it was possible to derive temperatures for separate low-latitude ($|b| < 10°$) and high-latitude ($|b| > 10°$) directions. They find a mean mass-weighted (low-latitude) CNM temperature of 99 K and a median temperature of 63 K with half the column density above and half below this temperature.

Additional measures of the gas temperature of diffuse clouds come from UV absorption line observations of the $J = 0$ and 1 level populations of H_2 in the ground vibrational state. The excitation temperature of these levels (sometimes denoted T_{01}) will equal the gas kinetic temperature as long as collisions with H^+ are sufficiently rapid to thermalize the H_2 ortho/para ratio and other processes (e.g., FUV pumping or H_2 formation) do not drive the ratio away from thermalization (see e.g., Dalgarno, Black, & Weisheit 1973; Black & van Dishoeck 1987; Burton, Hollenbach, & Tielens 1992; Sternberg & Neufeld 1999). We estimate that the ionization provided by the X-ray/EUV field provides sufficient H^+ so that T_{01} is a good measure of the gas kinetic temperature in CNM clouds. Early estimates of the gas temperature from *Copernicus* observations found $T_{01} = 77 \pm 17$ K (Savage et al. 1977), while recent estimates using the *Far Ultraviolet Spectroscopic Explorer* report $T_{01} = 68 \pm 15$ K (Rachford et al. 2002). Of the models shown in Table 4, the "high-ϕ_{PAH}" ($\phi_{PAH} = 1$) calculation has temperatures in the cloud interior more than 1 σ higher than the H_2 temperatures. Our CNM temperature of 71 K for the standard model lies between the median and mean H I temperatures of Heiles & Troland (2003) and is in good agreement with the H_2 measurements.

We note that Heiles & Troland (2003) found ~4% of the CNM column to lie at temperatures less than 25 K. Such extremely cold H I has been also reported, for example, by Gibson et al. (2000), who find local H I gas at $T = 16$–32 K, and by Knee & Brunt (2001), who find an H I supershell at $R = 16$ kpc with $T = 10$ K. Our standard model is unable to produce these low CNM temperatures. Such low temperatures might be produced in gas depleted in PAHs, which reduces the photoelectric heating (as suggested by Heiles & Troland 2003), or in gas that contains a sufficient molecular H_2 abundance to cool to these temperatures.

The reported [C II] 158 μm cooling rate per hydrogen atom varies widely depending on the method and direction of observation. The two main methods are derived from (1) UV absorption line measurements of the column density of C II*, N(C II*), where C II* means C^+ $^3P_{3/2}$, and (2) IR observations of the [C II] 158 μm line intensity I([C II]). From N(C II*) along a line of sight and the total (H I + H II + 2H_2) column of hydrogen nuclei, N(H), the cooling rate is found from $n\Lambda = E_{21}A_{21}N(\text{C II}^*)/N(\text{H})$, where E_{21} and A_{21} are the energy and radiative decay rate, respectively, for the [C II] 158 μm transition. The total hydrogen column is usually inferred from the column of S^+. For the IR method, the results are usually reported using H I 21 cm emission to obtain the column of neutral hydrogen N(H I). From the intensity of the [C II] line and N(H I), the average cooling rate is given by $n\Lambda = 4\pi I([\text{C II}])/N(\text{H I})$. Note that the UV and IR measures are not directly comparable since the former is per H nucleus and the latter is per H I atom. One source of uncertainty in both methods is the amount of WNM gas along a given line of sight. This is because the total column of hydrogen arises from both WNM and CNM gas whereas the C II* resides in mainly the CNM gas alone. Thus, the effect of WNM gas is to lead to an underestimate of the derived cooling rates in the CNM. This problem is especially severe for the high-latitude IR observations in which the H I column extends several hundred parsecs above the plane where there is not much cold gas. There are also processes that may lead to overestimates of the derived cooling rate. The UV absorption method can be influenced by radiation from the background stars that provides a UV radiation field and subsequent gas heating rate greater than the average interstellar field. The IR line and UV absorption methods can be contaminated by WIM gas, which has a cooling rate per hydrogen in the [C II] transition similar to the CNM so that the WIM contributes to both IR emission and UV absorption. (However, generally along a line of sight the column of WIM is much less than that of CNM.)

The UV absorption method was used in the Galactic plane by Pottasch, Wesselius, & van Duinen (1979), who found an average value of $n\Lambda \approx 1 \times 10^{-25}$ ergs s^{-1} H^{-1}, and by Gry, Lequeux, & Boulanger (1992), who reported $n\Lambda = 3.5^{+5.4}_{-2.1} \times 10^{-26}$ ergs s^{-1} H^{-1}. The Pottasch et al. (1979) value is probably biased toward higher rates as a result of UV illumination from background stars. On the

other hand, the Gry et al. (1992) results are probably biased toward lower rates. Their lines of sight were selected to have low column density and are thus expected to contain more WNM gas on average than a typical line of sight. The C II* columns have been determined for a few high-latitude lines of sight from which the cooling rate can be derived. For example, from Fitzpatrick & Spitzer (1997) we find $n\Lambda = (0.8\text{–}3.5) \times 10^{-26}$ ergs s^{-1} H^{-1} in the cool components toward HD 215733, and Savage et al. (1993) find $n\Lambda = 1.4 \times 10^{-26}$ ergs s^{-1} H^{-1} toward 3C 273. The Savage et al. (1993) observation is probably a lower limit to the CNM cooling rate. The direction toward 3C 273 is a well-studied line of sight with low mean density, and much of the C II* may reside in WNM gas. In addition, the hydrogen column (inferred from S^+) samples the entire column throughout the disk and halo and thus overestimates the column in CNM alone.

The IR line emission method has been applied to high-latitude directions. Bock et al. (1993) and Matsuhara et al. (1997), using a balloon borne experiment, measured the 158 μm line emission in a path covering Galactic latitudes $b = 33°\text{–}50°$. Matsuhara et al. (1997) obtain a cooling rate of $(1.6 \pm 0.4) \times 10^{-26}$ ergs s^{-1} (H I)$^{-1}$ (i.e., per neutral hydrogen) for columns $N(\text{H I}) < 2 \times 10^{20}$ cm^{-2}. Bock et al (1993), using the same C II observations, but for $N(\text{H I}) > 10^{20}$ cm^{-2} and excluding anomalously low C II/continuum ratios, found $(2.6 \pm 0.6) \times 10^{-26}$ ergs s^{-1} (H I)$^{-1}$. These rates are slightly lower than the *COBE* observations of 2.65×10^{-26} ergs s^{-1} (H I)$^{-1}$ (Bennett et al. 1994).

We can estimate the correction to these high-latitude IR observations as a result of WNM and WIM gas (see discussion in WHMTB). The C^+ line intensity arising in the ionized gas can be estimated from the Hα line intensity available from the WHAM data set (Reynolds et al. 1999).[3] We find that the Hα line intensity varies from about 0.5 R to 1 R over the path of the Bock et al (1993) experiment, where 1 R = $10^6/4\pi$ photons cm^{-2} s^{-1} sr^{-1}. Using $I(\text{H}\alpha) = 1$ R and the conversion between $I(\text{H}\alpha)$ and $I([\text{C II}])$ (e.g., Reynolds 1992), we find $I([\text{C II}]) = 1.5 \times 10^{-7}$ ergs s^{-1} cm^{-2} sr^{-1} from the ionized gas. Subtracting this from the Matsuhara et al. (1997) cooling rate, we get roughly 1.1×10^{-26} ergs s^{-1} (H I)$^{-1}$. Following WHMTB, we use the average WNM and CNM columns derived from the observations of Kulkarni & Fich (1985) yielding $N_{\text{CNM}} = 0.4 \times 10^{20}$ csc$|b|$ cm^{-2} and $N_{\text{WNM}} = 1.0 \times 10^{20}$ csc$|b|$ cm^{-2}. From equation (12) of WHMTB and neglecting the neutral component of the WIM, we find a cooling rate in CNM of 3.9×10^{-26} ergs s^{-1} H^{-1}. We conclude that although the rates are quite uncertain as a result of contributions from WNM and WIM gas, a conservative lower limit is that the [C II] cooling rate in the CNM is $\gtrsim 3.0 \times 10^{-26}$ ergs s^{-1} H^{-1}. All of the models presented in Table 4 satisfy this constraint although the low-ϕ_{PAH}, low PAH abundance, and low-G_0 cases barely do so.

We finally consider the model constraints imposed by the C I/C II ratio. From the C I and H I data compiled in Welty & Hobbs (2001) and assuming a constant C II/H I ratio of 1.4×10^{-4}, we find that C I/C II $\lesssim 3 \times 10^{-3}$. The abundance of neutral metals, as typified by the C I/C II ratio, strongly rises with increasing ϕ_{PAH} through the direct recombination of C^+ on PAH^-, and the C I/C II ratio increases by a factor of 8.2 as ϕ_{PAH} increases from 0.25 to 1. The effect of a lower PAH abundance is to diminish both the ion recombination on grains and the photoelectric heating rate, resulting in both lower thermal pressures and lower C I/C II ratios. Decreasing the FUV field from 1.7 to 1.1 decreases the rate of photoionization of C I and the C I/C II ratio rises by a factor of 1.6. We find that the "high-ϕ_{PAH} and "low-G_0" models can be safely ruled out by the required C I/C II ratio. We shall present in a future paper a more detailed analysis of the implications of the C I/C II ratio for translucent cloud models. In summary, we find that the average thermal pressures are not dramatically affected by the range of parameters shown in Table 4; however, in a detailed comparison with observations we find that (1) "low-ϕ_{PAH}" models poorly match the C I*/C_{tot} ratio and C^+ cooling rate, with values lower than observed, (2) "high-ϕ_{PAH}" models produce temperatures and C I/C II ratios higher than observed, (3) "low-PAH" models produce low values for the C I*/C_{tot} ratios and C^+ cooling rate, and (4) "low-G_0" models produce low values for the C I*/C_{tot} ratios and C^+ cooling rate and high values for the C I/C II ratio.

The discussion in this section highlights the need for more observational and laboratory study in the areas of PAH chemistry and thermal processes in the diffuse ISM. In the near future several ground-based, airborne, and space-based telescopes (ALMA, SOFIA, Herschel) may enable us to measure C I fine-structure level populations throughout the Milky Way, as well as in other galaxies. These observations will provide stringent tests for our model and for the general importance of the thermal instability for the two-phase medium of interstellar gas. We note that SOFIA and Herschel will also allow us to study the [C II] 158 μm emission along specific sight lines in the Milky Way at high spatial and spectral resolution. Together, this will provide a powerful way to study the physical conditions in the ISM and the processes that dominate its structure.

8.2. *Comparison with Extragalactic Observations*

In comparison to the Braun (1997) observations, we find that based on a phase diagram analysis alone we do not expect a strict cutoff in the cold gas at the Galactic R_{25} radius ($R_{25} = 12.25$ kpc). We also find a CNM temperature that decreases in the outer Galaxy, whereas Braun (1997) finds peak brightness temperatures to increase. To reconcile these differences, we suggest that Braun (1997) is mainly detecting the photodissociated outer envelopes of molecular clouds. The inferred high column densities ($N \gtrsim 3 \times 10^{21}$ cm^{-2}) and temperatures ($T \sim 80\text{–}150$ K) reported by Braun (1997) are more typical of photodissociated gas near star-forming regions than of the diffuse CNM clouds illuminated by the general interstellar radiation field on which we have been concentrating. A similar interpretation of the H I emission in M101 has been proposed by Smith et al. (2000).

Using the photodissociation region models of Kaufman et al. (1999), modified by the chemistry and thermal processes discussed in this paper, we find that if the gas density and UV field illumination are fixed, the H I brightness temperature increases if the metallicity (and therefore the gas-phase coolants and grain abundances) decreases as expected

[3] Available at http://www.astro.wisc.edu/wham/index.html.

in the outer portions of galaxies. Near regions of star formation, the UV radiation field does not drop with the disk radial scale length but remains relatively constant and depends mainly on the illumination from the nearest star-forming region. For local ISM metallicities, the H I 21 cm line is only marginally opaque, so that the maximum brightness temperature is set by the cool interior regions of H I clouds. However, at lower metallicities (and lower dust-to-gas ratios) the same visual optical depth is achieved at larger H I columns and thus the H I–to–H_2 transition is pushed deeper into the cloud. The larger H I column forces the 21 cm transition to become optically thick while still within the warm regions, thereby increasing the H I brightness temperature. For metallicities as low as 0.2–0.3 times cosmic, typical of those at the R_{25} radius in M101 and other spirals (Garnett et al. 1997), we find that the temperature increases by 40–60 K, comparable to that seen by Braun (1997).

As discussed by Sellwood & Balbus (1999), a fairly uniform H I 21 cm line width of $\sim$6 km s^{-1} is seen in the outer disk of spiral galaxies. Instead of indicating WNM gas, Sellwood & Balbus (1999) suggest that the dispersion arises from a cold, MHD-driven turbulent gas. Based on the results of WHMTB, they argue that a 5000 K gas inferred from the line width would be thermally unstable. Our temperature results for WNM in the outer Galaxy shown in Table 3 confirm that 5000 K gas is indeed thermally unstable there. Furthermore, our thermal pressure arguments for cold gas in the outer Galaxy are also consistent with their turbulence hypothesis. However, we also anticipate that the H I in the outer Galaxy is a two-phase medium with a substantial amount of WNM.

8.3. *Comparison with Previous Work*

Our results differ from those reported in Elmegreen & Parravano (1994), who found that CNM gas extends to only $\sim$12–14 kpc in the Galactic plane. Using the thermal processes and chemistry from Parravano (1987), they estimated the range of thermal pressures ($P_{\rm min} < P < P_{\rm max}$) over which two phases are possible, as a function of FUV radiation field and metallicity. They also estimated the midplane thermal pressure and concluded that the thermal pressure would drop below $P_{\rm min}$ by a Galactic radius of $\sim$12–14 kpc.

The difference between our results and theirs arises in large part as a result of the approximations they made in estimating the pressure. Following Elmegreen (1989), they wrote the total pressure, $P_{\rm tot}$, as being proportional to the product of the gas surface density $\Sigma_{\rm gas}$ and the total (gas plus stars) surface density, $\Sigma_{\rm gas+stars}$, or $P_{\rm tot} \propto \Sigma_{\rm gas}\Sigma_{\rm gas+stars}$. They then assumed that the total surface density is proportional to the gas surface density, $\Sigma_{\rm gas+stars} \propto \Sigma_{\rm gas}$, so that $P_{\rm tot} \propto \Sigma_{\rm gas}^2$, and that the ratio of thermal to total pressure is constant, so that $P_{\rm th} \propto \Sigma_{\rm gas}^2$. Finally, and most importantly, they assumed that $\Sigma_{\rm gas} \propto \exp(-R/H_R)$ with $H_R \sim 4$ kpc. As a result, they obtained $P_{\rm th}/k \approx 10^{5.0}\exp(-2R/H_R)$, which results in a thermal pressure of only $P/k \sim 30$ K cm^{-3} at 16 kpc. In fact, as discussed in § 3, the H I surface density remains above 5 $M_\odot$ pc^{-2} out to $R \simeq 15$ kpc. Our value for the pressure of a pure WNM, $P_{\rm WNM'}$, which is based on the observed H I surface density, is a factor of 67 higher than theirs at 16 kpc. This higher pressure extends the region of cold gas to much greater radial distances than found by Elmegreen & Parravano (1994).

9. SUMMARY AND DISCUSSION

9.1. *Model Assumptions*

Our model for the gas heating and ionization in the Galactic disk is based on a cosmic-ray rate that is constrained by comparisons of observations to chemical models (e.g., van Dishoeck & Black 1986; Federman, Weber, & Lambert 1996; van der Tak & van Dishoeck 2000), direct observations of the local FUV field and soft X-ray field, and a theoretical estimate of the EUV intensity. The soft X-ray and EUV intensity is partly derived from the calculations of Slavin et al. (2000), who find that radiation from cooling SNRs can produce the fractional ionization seen in clouds at high latitude. The intensity used in this paper is an extension of their calculation to the Galactic plane. In addition, a stellar EUV component from Slavin & Frisch (1998) is added so that the total ionizing photon flux from the Galactic disk matches the recombination rate derived from Hα observations. An important component of the EUV and soft X-ray radiation transfer is the opacity produced by the WNM gas component. We have assumed that the opacity is provided by an ensemble of WNM clouds each of column density $N_{\rm cl}$(H I). The radiation fields at the WNM/CNM interface and cloud interior are found by passing the incident radiation through additional columns of $N_{\rm cl}$(H I) and 1×10^{20} cm^{-2}, respectively.

Our confidence in the adopted local parameters is strengthened by our successful modeling of the densities and temperatures in the local WNM and CNM gas. Furthermore, we obtain a good fit to the [C II] cooling rate per hydrogen as derived by UV line absorption and IR line emission studies. The good match between theory and observations further indicates that we have included all the relevant heating and cooling terms in our model, an argument that is especially strong for the CNM phase in which [C II] dominates the cooling; any additional heating sources in our model would emerge as excess [C II] emission. This case is not as strong for the WNM in which the [C II] emission contributes only $\sim$14% of the cooling and is a factor of 16 weaker per hydrogen than in CNM. Additional heating terms do not strongly affect the fine-structure line emission as a result of the strong temperature regulation by Lyα cooling.

To obtain the FUV field in other regions of the Galaxy, we have relied on observations of the gas surface density, metallicity, and OB star distribution, along with a numerical integration for the mean intensity. To check our assumptions, in § 6.3 we compared the infrared emission produced by dust grains heated by the interstellar radiation field with observations taken by the *COBE* satellite. The processes that determine the X-ray and cosmic-ray distributions are certainly more complicated than our models allow. For example, the soft X-ray flux depends on the temperature and emission measure in the hot ionized gas component and the optical depth to the emission regions. The temperatures and emission measures depend on the metallicity, and the optical depth depends on the structure of the ISM. We note, however, that Slavin et al. (2000) find that the intensity of X-rays produced by SNR emission does not depend sensitively on the ambient density of the preshock gas. We have carried through our analysis by adopting a simple approach in which we use plausible arguments for scaling the soft X-ray and cosmic-ray rates to other regions of the

Galaxy based on the distribution of production sources (OB stars) and destruction sinks (various gas components).

Note that we have chosen to extend the OB star distribution with a constant scale length $H_R^{\rm OB} = 3.5$ kpc out to $R = 18$ kpc. Had we adopted the OB star distribution of Bronfman et al. (2000), $P_{\rm min}$ and $P_{\rm max}$ would have been lower and it would have been easier to form CNM in the outer Galaxy. Since the actual OB star distribution in the outer Galaxy is, if anything, below the one we have adopted, our conclusion that CNM must exist in the outer Galaxy is strengthened.

Although the distribution of total H I surface density is constrained by observations, the separate column densities of CNM and WNM gas are not well determined away from the solar neighborhood. In calculating the opacity for EUV and soft X-ray photons, we have assumed that the ratio of WNM to CNM surface densities and scale heights are the solar neighborhood values (Dickey & Lockman 1990) throughout the Galaxy. This in turn implies that the ratio of CNM to WNM volume filling factors in the midplane is held constant with Galactic radius. A somewhat different prescription is given by Ferrière (1998) in which the volume fraction of WNM increases in the outer Galaxy. Note that if we allowed the WNM fraction to increase in the outer Galaxy, then the opacity to soft X-ray and EUV radiation would increase as well, thereby reducing $P_{\rm min}$ and $P_{\rm max}$ and making conditions less favorable for the existence of WNM. Another difference in our H I distributions is that Ferrière (1998) used a constant surface density of $\Sigma_{\rm H\,I} = 5\ M_\odot\ {\rm pc}^{-2}$ in the outer Galaxy to $R = 20$ kpc, whereas our distribution drops below $5\ M_\odot\ {\rm pc}^{-2}$ beyond $R > 15$ kpc. For constant surface density, at $R = 18$ kpc the pressure $P_{\rm WNM'}$ is a factor of $\sim$2 higher than for our H I distribution and would make it more likely that CNM gas can exist. In a future paper we shall compare the calculated [C II] emission with the observational data in an effort to independently derive the volume fractions of CNM and WNM gas. This will be particularly telling for the outer Galaxy, where the relative absence of photodissociation regions and H II regions should permit a clean distinction between WNM and CNM without the confusion of predominantly molecular or ionized gas.

9.2. *Galactic Distribution of Two-Phase ISM*

As discussed in § 6.4, in Figures 12*a*–12*c* we plot $P_{\rm min}$ and $P_{\rm max}$ as a function of position in the Galactic midplane for three values of the WNM cloud column $N_{\rm cl}$. We also plot the thermal pressure $P_{\rm WNM'}$ in the Galactic midplane that would result if all of the H I layer were WNM gas supported by thermal pressure. For the case in which there is no turbulence and the thermal pressure dominates the pressure, regions in which $P_{\rm WNM'} > P_{\rm max}$ *must* have CNM gas. This is because only CNM gas can exist at these pressures, and mass will be converted from the WNM phase to the CNM until the pressure drops below $P_{\rm max}$, where a two-phase medium can exist. Our figures show that this condition is satisfied over much of the Galactic disk.

$P_{\rm WNM'}$ is calculated assuming that all the diffuse gas is WNM and that thermal pressure dominates and determines the vertical scale height, which we calculate in this case locally to be $\sim$80 pc. However, the observed half-height of the "WNM component" seen by Dickey & Lockman (1990) is $\sim$265 pc. This result demonstrates that nonthermal pressure (due to turbulent motions, magnetic fields, and cosmic rays) dominates. We take an analogous approach to analyze the turbulent case. Assuming again that all the H I gas is WNM, we compare the thermal pressure to $P_{\rm min}$ and $P_{\rm max}$. We use the *observed* $\langle n_{\rm H\,I}\rangle$ (which includes the effects of turbulence and the greater scale heights, which lowers $\langle n_{\rm H\,I}\rangle$) to estimate a lower limit $\langle P_{\rm WNM}\rangle$ on the thermal pressure $P_{\rm th,WNM} = \langle P_{\rm WNM}\rangle / f_{\rm H\,I}$, where $f_{\rm H\,I}$ is the volume filling factor of the WNM (the rest is HIM). Since $\langle P_{\rm WNM}\rangle$ exceeds $P_{\rm max}$ in the outer (8 kpc $\lesssim R \lesssim$ 16 kpc) Galaxy, CNM *must* exist in these regions. Since $\langle P_{\rm WNM}\rangle$ exceeds $P_{\rm min}$ (and turbulence likely drives the local pressures above $P_{\rm max}$ occasionally), and since $f_{\rm H\,I} < 1$, we conclude that CNM very likely exists at 3 kpc $\lesssim R \lesssim$ 18 kpc.

It is difficult, however, from our theoretical models, to rule out an ISM with only HIM and CNM (and no WNM) in which the intercloud medium is filled with HIM that maintains a pressure $P > P_{\rm max}$ on the CNM clouds. However, in such a scenario, the volume filling factor of the HIM must be nearly unity. If the HIM does not fill the intercloud medium, CNM would partially convert to WNM to fill the vacuum, and the pressure in the pervasive WNM would adjust such that $P_{\rm max} > P > P_{\rm min}$ (for further discussion see Parravano et al. 2003). We also note that the observation of H I 21 cm emission and absorption throughout the Galaxy strongly suggests the presence of a pervasive WNM.

Assuming that P lies between $P_{\rm min}$ and $P_{\rm max}$, we can use our models to predict the average thermal pressure from equation (22), and the results are given in Table 3. An approximate analytic fit to these results for our fiducial column density of $N_{\rm cl} = 10^{19}\ {\rm cm}^{-2}$ is

$$P_{\rm th,ave}/k = 1.4 \times 10^4 \exp\left(\frac{-R_k}{5.5}\right)\ {\rm K\ cm^{-3}}\ . \qquad (40)$$

We find that at fixed Galactic radius, the pressure does not change by more than a factor of $\sim$3 over our range of cloud columns. For our fiducial column, the pressure drops from about 8200 K cm^{-3} at 3 kpc to 3100 K cm^{-3} at the solar circle and to 600 K cm^{-3} at 18 kpc. The drop in the thermal pressure from 3 kpc to the solar circle (a factor of 2.7) closely matches the drop in the magnetic pressure inferred from radio observations: Beck (2001) estimates that B drops from about 10 μG at 3 kpc to 6 μG locally, corresponding to a pressure drop by a factor of 2.8. (Note that these values for the field are larger than the rms field; as Beck points out, his values of B are $\langle B^{3.9}\rangle^{1/3.9}$.)

We can now test the validity of our assumption that the turbulence parameter $\Upsilon \equiv t_{\rm cool}/t_{\rm shock} \lesssim 1$, so that it is meaningful to discuss a two-phase medium. Our results show that locally $\Upsilon \approx 0.1$ for CNM and $\Upsilon \approx 0.3$ for WNM at a pressure of $P_{\rm th}/k = 3000$ K cm^{-3} (see eq. [5]). As a function of Galactic radius we find that $t_{\rm cool} \propto T/(n\Lambda) \propto \exp(R_k/2.94)$. Ignoring the weak variation of $t_{\rm shock}$ due to the variation in $\Sigma_{\rm WNM}$ and $n_{\rm WNM}^{-0.1}$, we have $t_{\rm shock} \propto \dot{\varsigma}_{\rm SN}^{-1} \propto \exp(R_k/3.5)$. As a result, we find $\Upsilon \propto \exp(R_k/18.4)$, and we conclude that the turbulence parameter is $\lesssim 1$ and weakly dependent on radius throughout the Galactic disk.

In Appendix B we discuss the potential role of turbulence in heating the WNM and CNM phases. Using the admittedly uncertain turbulent heating rate as a function of Galactic radius given by equation (B5), at $R = 17$ kpc we find that $P_{\rm min}$, $P_{\rm th,ave}$, and $P_{\rm max}$ are about a factor of 2 higher than for the nonturbulent heating case. However, since

$\langle P_{\rm WNM}\rangle$ remains above $P_{\rm min}$ to $R = 18$ kpc, turbulent heating does not change our conclusion that turbulent fluctuations will produce cold gas that is thermally stable in the outer Galaxy. The rate of turbulent heating does not exceed the rate of photoelectric heating out to $R \sim 18$ kpc, and from equation (B3) we conclude that our assumption of thermal balance remains approximately valid.

We conclude by summarizing our most important results. We have shown that both observational evidence and our theoretical models presented here indicate that the thermal pressure in the ISM of the Galaxy lies in the relatively narrow range between $P_{\rm min}$ and $P_{\rm max}$ for 3 kpc $< R <$ 18 kpc. We have calculated $P_{\rm min}(R)$, $P_{\rm max}(R)$, and an estimate of the thermal pressure $P_{\rm th,ave}(R)$ in the Galaxy. We have shown that CNM gas must exist out to 18 kpc. We present phase diagrams for several Galactocentric radii and for several cases of varying opacity to EUV and soft X-ray flux. Understanding the neutral phases of the ISM and their dependence on the radiation field is an important step in understanding the formation of molecular clouds and the global star formation rates in a galaxy.

We thank L. Blitz, J. Dickey, C. Heiles, A. Lazarian, H. Liszt, E. Ostriker, and R. Snell for helpful comments, W. Dehnen for providing his code to calculate the Galactic potential, J. Slavin for providing the stellar EUV and SNR X-ray spectra, and T. Sodroski and N. Odegard for the *COBE* Galactic longitude profile. We also thank the referee Don Cox for his insightful comments. M. G. W. is supported in part by a NASA LTSA grant NAG 5-9271. The research of C. F. M. is supported in part by NSF grant AST 00-98365. The research of D. J. H. is supported by NASA RTOP 344-04-10-02, which funds the Center for Star Formation Studies, a consortium of researchers from NASA Ames, University of California at Berkeley, and University of California at Santa Cruz.

APPENDIX A

ANALYTIC SOLUTION FOR THERMALLY SUPPORTED WNM AT SOLAR CIRCLE

We can treat analytically the problem discussed in § 6.4.1 for the thermal support of the WNM if we assume that the mass in the disk is distributed exponentially with height above the plane,

$$\rho_t = \rho_{t0} e^{-z/z_d} , \tag{A1}$$

where z_d is the scale height and ρ_t is the mass density of all the matter: stars, gas, and dark matter. The dominant contribution to the mass in the disk at $R = R_0$ is the "thin disk" of stars with $z_d = 180$ pc (Dehnen & Binney 1998). Solution of the equation of hydrostatic equilibrium for the gas, which is assumed to be isothermal with sound speed $\sigma_{\rm th}$, gives

$$n = n_0 \exp[-\beta x + \beta(1 - e^{-x})] , \tag{A2}$$

where $x \equiv z/z_d$ and

$$\beta \equiv \frac{4\pi G \rho_{t0} z_d^2}{\sigma_{\rm th}^2} \equiv \frac{z_d^2}{h^2} . \tag{A3}$$

In the limit of large x ($z \gg z_d \sim 180$ pc), the distribution becomes an exponential with a scale height $z_d/\beta = h^2/z_d$; in the limit of small x (which is more relevant for the gas distribution in the disk), the gas density approaches a Gaussian,

$$n \rightarrow n_0 \exp\left(-\frac{z^2}{2h^2}\right) . \tag{A4}$$

Numerically, we have $h = 0.89 T^{1/2}$ pc at the solar circle, based on a stellar density in the midplane of 0.115 $M_\odot$ pc^{-3} from Dehnen & Binney (1998) (with the 2.5 $M_\odot$ pc^{-2} augmentation to the thin stellar disk discussed above) and a gas density in the midplane of 0.034 $M_\odot$ pc^{-3} from Dickey & Lockman (1990) and McKee (1990). For an adopted temperature of 8000 K, this gives $h = 80$ pc for the WNM.

As remarked above, the value of the midplane density is determined by requiring that the column density agree with the observed value,

$$N_0 = 2 n_0 h \beta^{1/2} \int_0^\infty \exp[-\beta x + \beta(1 - e^{-x})] dx \equiv (2\pi)^{1/2} n_0 h \phi_\beta . \tag{A5}$$

The fact that the mass is distributed exponentially rather than uniformly increases the Gaussian scale height of the gas from h to $\phi_\beta h$. A little algebra shows that the factor ϕ_β is approximately

$$\phi_\beta \simeq 1 + \frac{1}{3}\left(\frac{2}{\pi\beta}\right)^{1/2} + \frac{1}{12\beta} . \tag{A6}$$

This approximation is accurate to within 2% for $\beta > 1$. For $\beta > 1$ we have $1 < \phi_\beta < 1.35$, so the deviation from Gaussian behavior is not large. With these results, we then find that the pressure the H I would exert in the midplane if it were all WNM

is

$$\frac{P_{\rm WNM'}}{k} = \frac{1.1 N_{\rm H\,I} T}{(2\pi)^{1/2} \phi_\beta h} \ . \tag{A7}$$

For our adopted parameters ($N_{\rm H\,I} = 6.2 \times 10^{20}$ cm^{-3}, $z_d = 180$ pc, $T = 8000$ K, and $h = 80$ pc) we find $P_{\rm WNM'}/k = 7800$ K cm^{-3} at the solar circle. By comparison, the exact numerical solution using the Dehnen & Binney (1998) potential gives $P_{\rm WNM'}/k = 8615$ K cm^{-3}, which is satisfactory agreement.

APPENDIX B

TURBULENT HEATING

In addition to the heating processes we have considered (photoelectric, X-ray, and cosmic-ray heating), turbulent, or mechanical, heating may also be important. Cox (1979) estimated that about 30% of the energy of a supernova would go into the compression of interstellar clouds followed by radiative losses. Numerical simulations (Cowie, McKee, & Ostriker 1981) confirmed this estimate. Spitzer (1982) estimated that about 4% of the energy of a supernova would go into acoustic waves and suggested that the absorption of these sound waves could be an important source of heating for the warm phase of the ISM. Ferrière, Zweibel, & Shull (1988) generalized this discussion to consider the generation and damping of hydromagnetic waves produced by SNRs. Minter & Spangler (1997) used observations of interstellar scintillation to infer the amplitude of fluctuations in the ISM and then set constraints on how these fluctuations damp. Minter & Balser (1997) and Mathis (2000) studied the effect of a turbulent heating rate of $\Gamma \sim 10^{-25}$ ergs s^{-1} H^{-1} on the WIM. Sellwood & Balbus (1999) have estimated the heating rate due to the dissipation of turbulence generated by Galactic differential rotation. Turbulent heating has also been investigated in molecular clouds (e.g., Stone, Ostriker, & Gammie 1998; Mac Low 1999).

Despite more than two decades of work on turbulent heating of the ISM, the rate remains very uncertain. This uncertainty stems directly from our lack of understanding of interstellar turbulence: how it is generated, how it propagates, and how it dissipates. We have already encountered this uncertainty when we tried to estimate Υ, which measures the degree to which nonturbulent heating is in balance with radiative cooling (see § 2). Most of the heating associated with SNRs is very intermittent, with gas being heated by shocks that are separated by long time intervals. As a result, even though about 30% of the energy of an SNR may go into cloud heating, most of this heat may be radiated away in a short time while the gas is substantially hotter than average. This is particularly true for the WNM, which has a rapidly rising cooling rate above 10^4 K as a result of Lyα cooling. The fact that Heiles & Troland (2003) did not find many WNM features with line widths above that corresponding to the temperature we have calculated for the WNM suggests that impulsive heating is not a dominant process in determining the temperature of the interstellar H I. Cox (1979) reached the same conclusion based on the fact that the observed level of turbulence in clouds is relatively small.

In view of the uncertainties associated with turbulent heating in the ISM, we have not included it in our basic models. Here we shall estimate the rate of turbulent heating and determine how it would affect our results.

B1. DISSIPATION OF TURBULENT ENERGY

Let $\dot{\epsilon}$ be the rate of dissipation of turbulent energy per unit mass, which is equivalent to the turbulent heating rate per unit mass. On dimensional grounds, we expect $\dot{\epsilon} \sim \delta v^3/\ell$, where δv is the rms velocity in a region of size ℓ (Landau & Lifshitz 1987; Stone et al. 1998; Mac Low 1999). In other words, the kinetic energy per unit mass is dissipated in a time of order $\ell/\delta v$. A simple global estimate shows that turbulent heating is in fact unimportant in the ISM: the turbulent energy in the ISM is about $0.5 M \delta v^2 \sim 10^{54}$ ergs, where we set $M = 10^9\ M_\odot$ and $\delta v = 10$ km s^{-1}. The scale on which the turbulence in the WNM has an amplitude of 10 km s^{-1} is about 200 pc (§ 2), so the turbulent dissipation time is about 20 Myr.[4] The resulting heating rate is about 1.6×10^{39} ergs s^{-1}, or $4 \times 10^5\ L_\odot$. By comparison, the luminosity of the Galaxy in the C II 158 μm line is $5 \times 10^7\ L_\odot$ (Wright et al. 1991), so turbulent heating is negligible on a Galactic scale. However, as we shall see, it is relatively more important in the outer Galaxy.

We make the dimensional argument for the heating rate exact by introducing the constant $\phi_{\dot{\epsilon}}$,

$$\dot{\epsilon} \equiv \phi_{\dot{\epsilon}} \frac{\delta v^3}{\ell} = 3^{3/2} \phi_{\dot{\epsilon}} \frac{\sigma^3}{\ell} \ , \tag{B1}$$

where σ is the one-dimensional turbulent velocity dispersion. The turbulent heating rate per hydrogen, $\Gamma_{\rm turb}$, is then given by

$$\Gamma_{\rm turb} = \frac{\rho \dot{\epsilon}}{n} = \mu_{\rm H} \dot{\epsilon} = 3^{3/2} \mu_{\rm H} \phi_{\dot{\epsilon}} \frac{\sigma^3}{\ell} \ , \tag{B2}$$

where $\mu_{\rm H} = 2.34 \times 10^{-24}$ g is the mass per hydrogen.

The numerical simulations of Stone et al. (1998) and Mac Low (1999) show that equation (B1) applies to both subsonic and supersonic turbulence. In supersonic turbulence, the energy is dissipated primarily in shocks, so the dissipation is highly

[4] At first glance, it is puzzling that this estimate for the dissipation time exceeds the estimated time interval between shocks in the WNM of about 5 Myr in § 2. However, as discussed above, much of the shock energy is radiated promptly and does not contribute to the level of subsonic turbulence.

localized in space and time. As discussed above, for this reason shocks do not contribute effectively to the general heating of the CNM and WNM, so we are more interested in the subsonic case. In the subsonic, nonmagnetic case, we expect the turbulence to follow the Kolmogorov scaling, in which $\dot{\epsilon}$ is independent of scale ($\sigma \propto \ell^{1/3}$). When magnetic fields are included, Goldreich & Sridhar (1995) found the same scaling, so this should be generally valid in the ISM for scales such that the flow is subsonic. Since $\dot{\epsilon}$ is independent of scale for subsonic turbulence, the turbulent heating in this case should be widely distributed, albeit with substantial fluctuations associated with intermittency. On the other hand, for supersonic turbulence, we expect $\sigma \propto \ell^q$ with $q > \frac{1}{3}$ (Larson 1979; Boldyrev 2002). This scaling is observed in molecular clouds (Heyer & Schloerb 1997), which are highly supersonic. In this case we have $\dot{\epsilon} \propto \sigma \propto \mathscr{M}^{3-1/q}$, where $\mathscr{M}$ is the Mach number of the flow. The fraction of the total turbulent heating that is subsonic and thus widely distributed is thus about $1/\mathscr{M}^{3-1/q}$ for $\mathscr{M} \geq 1$, corresponding to $1/\mathscr{M}$ for $q = \frac{1}{2}$ (Larson 1979) and $1/\mathscr{M}^{1/3}$ for $q = 0.375$ (Boldyrev 2002). The length scale that separates subsonic from supersonic turbulent motions in the WNM, and of CNM clouds in the WNM, is $\ell_P \sim 215$ pc (§ 2).

The parameter $\Upsilon \equiv t_{\rm cool}/t_{\rm shock}$ that describes the strength of the turbulence is directly proportional to $\Gamma_{\rm turb}$. Recall from § 2 that $t_{\rm cool} = (5/2)(1.1nkT)/n^2\Lambda$ for a neutral gas with 10% He; in terms of the isothermal sound speed $\sigma_{\rm th}$, this is $(5/2)(\mu_{\rm H}\sigma_{\rm th}^2/n\Lambda)$. We estimated the shock time to be $t_{\rm shock} = \ell_P/(\sqrt{2}\sigma_{\rm th})$. For a Kolmogorov-type spectrum ($\sigma^3 \propto \ell$), this becomes $t_{\rm shock} = (\sigma_{\rm th}^2/\sqrt{2})(\ell/\sigma^3)$. We then find

$$\Upsilon = \frac{t_{\rm cool}}{t_{\rm shock}} = 0.68\frac{(\Gamma_{\rm turb}/\phi_{\dot{\epsilon}})}{n\Lambda} \ . \tag{B3}$$

Thus, shocks are important in driving the gas away from thermal balance if and only if turbulent heating (evaluated with $\phi_{\dot{\epsilon}} = 1$) is important.

What do numerical simulations say about the value of the parameter $\phi_{\dot{\epsilon}}$? Stone et al. (1998) considered MHD turbulence driven by a range of wavelengths, with the power peaking at a length scale ℓ_d.[5] Their results imply $\phi_{\dot{\epsilon}} = 0.94$ for the case in which the initial field strength was such that the Alfvén velocity $v_{\rm A}$ and the isothermal sound speed $\sigma_{\rm th}$ were equal, as is approximately true in the diffuse ISM. In his study of turbulent dissipation, Mac Low (1999) calculated three models for the case $v_{\rm A} = \sigma_{\rm th}$. He used two slightly different approaches for measuring the dissipation rate, one in terms of the volume-averaged rms velocity and one in terms of the mass-averaged rms velocity. Like Stone et al. (1998), we have used the latter approach. In our notation, Mac Low (1999) found $\phi_{\dot{\epsilon}} = 0.9 \pm 0.13$ dex for this case, in fortuitously good agreement with Stone et al. (1998) (this agreement between the two calculations was not as good for other values of $\sigma_{\rm th}/v_{\rm A}$).

In both these simulations, the turbulence is "balanced," in that the average wave power is the same in both directions along the field. Since the sources of interstellar turbulence are intermittent in space and time, actual interstellar turbulence is likely to be imbalanced, and Cho, Lazarian, & Vishniac (2002) have shown that this can substantially reduce the decay rate of the turbulence. The value $\phi_{\dot{\epsilon}} \sim 1$ found in these simulations is thus an upper limit to the value expected in the ISM. In our work, we shall somewhat arbitrarily adopt $\phi_{\dot{\epsilon}} = 0.5$ as representative of interstellar turbulence.

Recall that we parameterized the strength of the turbulence in terms of the one-dimensional velocity dispersion at a scale of 1 pc, $\sigma(1)$. We estimated this from observation by assuming Kolmogorov scaling, which is reasonable since the motions of the CNM clouds observed by Heiles & Troland (2003) have a velocity dispersion that is very nearly the same as the thermal velocity in the WNM (for $T = 8000$ K, both are $\sim$7.1 km s^{-1}). In order to extend the estimate of the heating rate to other parts of the Galaxy, we assume that σ is approximately constant and that ℓ scales as the thickness of the H I disk, so that $\sigma^3/\ell = \sigma(1; R_0)^3 \propto 1/H_z^{\rm H\,I}$, where $\sigma(1; R_0)$ is the value of $\sigma(1)$ at the solar circle. From equation (B2) we find that the turbulent heating rate is then

$$\Gamma_{\rm turb} = 3.94 \times 10^{-27}\phi_{\dot{\epsilon}}\left[\frac{\sigma(1; R_0)}{1 \text{ km s}^{-1}}\right]^3 \frac{H_z^{\rm H\,I}(R_0)}{H_z^{\rm H\,I}(R)} \text{ ergs s}^{-1} \text{ H}^{-1} \tag{B4}$$

$$= 3.40 \times 10^{-27}\left(\frac{\phi_{\dot{\epsilon}}}{0.5}\right)\left[\frac{\sigma(1; R_0)}{1.2 \text{ km s}^{-1}}\right]^3 \min\left[1, \exp\left(\frac{8.5 - R_k}{6.7}\right)\right] \text{ ergs s}^{-1} \text{ H}^{-1} \ . \tag{B5}$$

Note that the estimated turbulent heating rate inside R_0 is constant, since the scale height of the H I does not change there.

B2. TURBULENT ENERGY FROM DIFFERENTIAL ROTATION

Next, consider the extraction of turbulent energy from differential rotation. As pointed out by Sellwood & Balbus (1999), this process occurs at a rate

$$\rho\dot{\epsilon} = -\left(-\frac{B_r B_\phi}{4\pi} + \rho v_r \delta v_\phi\right)\frac{d\Omega}{d\ln R} \ , \tag{B6}$$

where the rotation velocity is $\Omega R\hat{\phi}$ and the shear is in the radial direction. In a steady state, this rate of extraction of energy from differential rotation will be balanced by dissipation of energy, and so long as the velocities induced by the differential rotation are subsonic, much of this energy should be dissipated in a turbulent cascade. Hawley, Gammie, & Balbus (1995) have carried out MHD simulations of the generation of turbulent velocities and magnetic fields in a shearing box. They present

[5] In comparing with their work, it must be kept in mind that they expressed their results in terms of the size of the simulation box L, not $\ell_d = L/8$, and they left open the question as to whether the dissipation rate is $\sim\delta v^3/L$ or $\sim\delta v^3/\ell_d$. We assume the latter, which is consistent with the subsequent work of Mac Low (1999).

detailed results for one model of a shearing box simulation; using these results, we find that the excitation rate simplifies to

$$\dot{\epsilon} = 0.75\delta v^2 \left(-\frac{d\Omega}{d \ln R} \right) . \tag{B7}$$

Note that this expression is based on the assumption that the velocities are generated by the differential rotation, as may be the case in the outer Galaxy; it may not apply if the velocities are generated by other mechanisms, such as supernovae. Even in regions where the turbulence is primarily due to differential rotation, this expression must be regarded as highly approximate since it does not take into account either the vertical structure or the multiphase nature of the ISM.

The dynamical model of the Galaxy that we have adopted from Dehnen & Binney (1998) has a rotational velocity that declines slowly beyond the solar circle, $d\Omega/d \ln R = (-244 \text{ km s}^{-1})/R$ for $R \gtrsim 8.5$ kpc. We adopt 6 km s^{-1} as a typical velocity dispersion for gas in the outer parts of disk galaxies (e.g., Martin & Kennicutt 2001), somewhat less than the 7 km s^{-1} for the CNM and the 11 km s^{-1} for the WNM in the solar neighborhood (Heiles & Troland 2003). The turbulent heating rate due to differential rotation is then

$$\Gamma_{\rm turb} = 1.50 \times 10^{-26} \left(\frac{\sigma}{6 \text{ km s}^{-1}} \right)^2 \frac{1}{R_k} \text{ ergs s}^{-1} \text{ H}^{-1} \qquad (R_k > 8.5 \text{ kpc}) . \tag{B8}$$

This heating rate is within a factor of 2 of that in equation (B5) for 8.5 kpc $< R_k \lesssim 25$ kpc. Given the uncertainties, these two estimates are in satisfactory agreement. The generic estimate in equation (B5) is about twice that for differential rotation in equation (B8) at the solar circle, consistent with the idea that supernovae are an important source of turbulent motions in the local ISM.

B3. RESULTS

To estimate the effects of turbulent heating in the Galaxy, we adopt equation (B5), since it applies to both the case in which energy is injected by differential rotation and that in which it is injected by explosive events such as supernovae. It should be borne in mind that this estimate for the turbulent heating is quite uncertain, since it is based on highly idealized numerical simulations and an uncertain correction for an imbalanced turbulent cascade; on the other hand, it is reassuring that it is in accord with simple dimensional analysis (eq. [B2] with ϕ_ϵ of order unity). The estimate also depends on the amplitude of the turbulence in the subsonic regime, which is uncertain at present. Our estimate for the turbulent heating in the diffuse H I is about 30 times less than that invoked by Minter & Balser (1997) and Mathis (2000) in their studies of heating of the diffuse H II.

Turbulent heating, unlike heating by cosmic rays, EUV/soft X-rays, and photoelectric heating, is independent of the depth into the cloud, and it therefore becomes more important at high column densities. If turbulent heating at the rate given by equation (B5) occurs throughout the Galactic disk, then for our fiducial column density of 10^{19} cm^{-2}, at $P_{\rm min}$, our estimate of the turbulent heating rate exceeds the cosmic-ray rate for Galactic radii between 3 and 18 kpc and amounts to 70% of the photoelectric heating rate at $R_k = 17$ kpc. For $N = 10^{20}$ cm^{-2}, the turbulent rate is always greater than the cosmic-ray rate and is equal to 93% of the photoelectric rate at $R_k = 17$ pc. The average thermal pressure in a two-phase ISM including turbulent heating is given by

$$\frac{P_{\rm th,ave}}{k} = 1.2 \times 10^4 \exp\left(\frac{-R_k}{7.5} \right) \text{ K cm}^{-3} , \tag{B9}$$

where the fit is good to $\pm 10\%$ between 3 kpc $< R_k <$ 18 kpc except at our $R_k = 11$ kpc model point where the fit overestimates the thermal pressure by 25%.

The turbulent heating has the greatest effect in the outer Galaxy where heating rates based on stellar photons or supernovae are small. With turbulent heating, at $R_k = 17$ kpc, we find $P_{\rm min}/k = 650$ K cm^{-3}, $P_{\rm th,ave}/k = 1370$ K cm^{-3}, and $P_{\rm max}/k = 2900$ K cm^{-3}, which are factors of 1.7, 1.9, and 2.1, respectively, times the nonturbulent case. We find that $P_{\rm WNM'}$ (the thermal pressure in the midplane based on the simple—and incorrect—assumption that the WNM is supported only by thermal pressure) falls below $P_{\rm max}$ at $R_k = 15$ kpc. The "mean" thermal pressure $\langle P_{\rm WNM} \rangle$ (an estimate of the thermal pressure in the midplane based on the assumptions that all the H I is WNM and that the WNM fills space) falls below $P_{\rm max}$ at approximately $R_k = 13.5$. It follows that the H I cannot be all WNM out to $R_k = 13.5$, and a two-phase medium *must* exist out to that point. Since $\langle P_{\rm WNM} \rangle$ remains above $P_{\rm min}$ out to $R = 18$ kpc, we conclude that pressure fluctuations will in fact produce a two-phase medium to these distances.

APPENDIX C

ANALYTIC THERMAL BALANCE MODEL FOR COOL GAS

When gas is in thermal balance, the thermal pressure P can be expressed as a function of either density or temperature. We seek $P(T)$ for the temperature range $T \lesssim 1000$ K, where [C II] 158 μm and [O I] 63 μm radiation dominates the gas cooling, and for $n < n^{\rm H}_{\rm cr}([\text{C II}]) \simeq 3000$ cm^{-3} and $n_e < n^{e}_{\rm cr}([\text{C II}]) \simeq 30$ cm^{-3} so that the [C II] + [O I] cooling is proportional to n^2.

C1. THERMAL BALANCE: HEATING AND COOLING

Cooling rates per unit volume can be written as $n_c n \Lambda_s^c$, where n_c is the density of the collisional agent (n_e or $n_{\rm H}$), n is the hydrogen nucleus density, and Λ_s^c is the cooling rate coefficient, which takes into account the gas-phase abundance of the species at the solar circle (Table 1). We find

$$\Lambda_{\rm C\,II}^{\rm H} = 3.15 \times 10^{-27} e^{-0.92/T_2} Z_g' \text{ ergs cm}^3 \text{ s}^{-1} , \tag{C1}$$

$$\Lambda_{\rm C\,II}^{e} = 1.4 \times 10^{-24} T_2^{-1/2} e^{-0.92/T_2} Z_g' \text{ ergs cm}^3 \text{ s}^{-1} , \tag{C2}$$

and

$$\Lambda_{\rm O\,I}^{\rm H} = 2.5 \times 10^{-27} T_2^{0.4} e^{-2.28/T_2} Z_g' \text{ ergs cm}^3 \text{ s}^{-1} , \tag{C3}$$

where $T_2 = T/(100 \text{ K})$. We assume that H atom collisions dominate electron collisions. Comparison of $n_{\rm H}\Lambda_{\rm C\,II}^{\rm H}$ with $n_e \Lambda_{\rm C\,II}^{e}$ shows that this condition is equivalent to $x_e \equiv n_e/n < 2.3 \times 10^{-3} T_2^{1/2}$.

Assuming that H atoms dominate the excitation of [C II] and [O I], $n < n_{\rm cr} \simeq 3000 \text{ cm}^{-3}$, and 100 K $< T <$ 1000 K [the relevant regime for $T_{(\rm min)}$], we use numerical results using the above cooling coefficients $\Lambda_{\rm C\,II}^{\rm H}$ and $\Lambda_{\rm O\,I}^{\rm H}$ to obtain a simple form for the total cooling coefficient

$$\Lambda_{\rm tot}^{\rm H} = 5.4 \times 10^{-27} T_2^{0.2} e^{-1.5/T_2} Z_g' \text{ ergs cm}^3 \text{ s}^{-1} , \tag{C4}$$

which is good to $\pm 20\%$. A simple form such as this is required, rather than $\Lambda_{\rm C\,II}^{\rm H} + \Lambda_{\rm O\,I}^{\rm H}$, in order to analytically determine $T_{(\rm min)}$.

We modify the grain photoelectric heating rate of Bakes & Tielens (1994) by multiplying by a factor of 1.3, which accounts for a higher PAH abundance (6×10^{-7} by number relative to hydrogen) compared with that assumed in Bakes & Tielens (1994). The heating rate per unit volume for $T \lesssim 1000$ K is given approximately by (see § 5, eq. [19])

$$n\Gamma_{\rm pe} = \frac{1.1 \times 10^{-25} G_0' Z_d' n}{1 + 3.2 \times 10^{-2} \left(G_0' T_2^{1/2} / n_e \phi_{\rm PAH} \right)^{0.73}} \text{ ergs cm}^{-3} \text{ s}^{-1} . \tag{C5}$$

Recall (see § 5) that $\phi_{\rm PAH}$ is a parameter of order unity that scales the PAH collision rates; $\phi_{\rm PAH} = 0.5$ in our standard model.

Note that when the unity term dominates in the denominator, the photoelectric heating is not significantly suppressed by positive charging; i.e., the second term in the denominator represents effects of grain charging. To obtain an analytic solution for $T_{(\rm min)}$ below, we will require the second term to dominate, as it often does for a range of conditions centered on solar neighborhood values.

C2. THE ELECTRON DENSITY n_e

In order to obtain an analytic expression for P under thermal balance conditions, an analytic expression for n_e is required to substitute into the grain photoelectric heating equation (C5). The chemistry leading to steady state electron abundances is quite complex and interesting. We use the results of the numerical code to determine the dominant reaction chains leading to n_e and to determine the major competitors to these reactions. We then find an analytic expression for n_e, along with the conditions required to ensure the assumed reaction chain.

For densities and temperatures near $n_{\rm min}$ and $T_{(\rm min)}$ at the solar circle, H^+ is the dominant ion species and therefore $n_e \approx n_{H^+}$. H^+ is produced mostly by the EUV/soft X-ray photoionization of H with a minor contribution from cosmic rays. We find that $n_{He^+} \approx 0.3 n_{H^+}$ under a variety of conditions at a column of $N_{\rm cl} \simeq 10^{19} \text{ cm}^{-2}$, a result due to the higher photoionization cross section of He at soft X-ray energies counterbalanced by the 0.1 abundance of He relative to H. Since H^+ is a surrogate to obtain the electron abundances, we roughly account for He^+ by increasing the photoionization rate of H by 30% to a rate $1.3 \times 10^{-16} \text{ s}^{-1}$ at $N_{\rm cl} = 10^{19} \text{ cm}^{-2}$ appropriate to the solar neighborhood. The rate ζ_t' is expressed as $\zeta_t' = \zeta_t/10^{-16}$ s^{-1}, where ζ_t is the total ionization rate (including primary and secondary ionizations) of H by photons and cosmic rays. The destruction of H^+ is dominated by reactions with PAH^- or

$$H^+ + PAH^- \rightarrow H + PAH^0 , \qquad \kappa_1 = 8.3 \times 10^{-7} \phi_{\rm PAH} T_2^{-0.5} \text{ cm}^3 \text{ s}^{-1} , \tag{C6}$$

where κ_1 is the rate coefficient calculated from Draine & Sutin (1987) using disk PAHs with $N_{\rm C} = 35$ carbon atoms and the disk radius $a = (N_{\rm C}/1.222)^{0.5}$ Å. Competing reactions are

$$H^+ + PAH^0 \rightarrow PAH^+ + H , \qquad \kappa_2 = 3.1 \times 10^{-8} \phi_{\rm PAH} \text{ cm}^3 \text{ s}^{-1} \tag{C7}$$

and

$$H^+ + e \rightarrow H + h\nu , \qquad \kappa_3 = 8.0 \times 10^{-12} T_2^{-0.75} \text{ cm}^3 \text{ s}^{-1} , \tag{C8}$$

where the reaction coefficients κ_2 and κ_3 are calculated similarly to κ_1. Equating the formation of H^+ to the destruction of H^+, we obtain for the electron density

$$n_e = \frac{1.3 \times 10^{-16} \zeta_t' n}{\kappa_1 n_{\rm PAH^-}} = 1.6 \times 10^{-10} \frac{\zeta_t' T_2^{1/2} n}{\phi_{\rm PAH} n_{\rm PAH^-}} \ {\rm cm}^{-3} \ . \tag{C9}$$

The analytic solution for n_e therefore requires a solution for $n_{\rm PAH^-}$. We simplify PAH ionization state calculations by assuming single-sized PAHs with three ionization states, PAH^-, PAH^0, and PAH^+. We find numerically that, over a wide range of relevant parameter space, neutral PAH^0 dominates the population with $n_{\rm PAH^0} \simeq 0.7 n_{\rm PAH}$, where $n_{\rm PAH} = 6.0 \times 10^{-7} n Z_d'$ is the total density of PAHs in all states. PAH^+ is formed by the FUV photoreaction

$$h\nu + {\rm PAH^0} \rightarrow {\rm PAH^+} + e \ , \qquad \kappa_4 = 7.85 \times 10^{-9} G_0' \ {\rm s}^{-1} \ , \tag{C10}$$

where the rate coefficient κ_4 is calculated from Bakes & Tielens (1994) using $N_{\rm C} = 35$ carbon atoms and assuming a disk geometry. PAH^+ is destroyed primarily by recombination with electrons

$$ {\rm PAH^+} + e \rightarrow {\rm PAH^0} \ , \qquad \kappa_5 = 3.5 \times 10^{-5} \phi_{\rm PAH} T_2^{-0.5} \ {\rm cm}^3 \ {\rm s}^{-1} \ . \tag{C11}$$

The condition that $n_{\rm PAH^+}/n_{\rm PAH^0} < 1$ is then $7.85 \times 10^{-9} G_0'/(\kappa_5 n_e) < 1$. PAH^- is formed by

$$ {\rm PAH^0} + e \rightarrow {\rm PAH^-} \ , \qquad \kappa_6 = 1.34 \times 10^{-6} \phi_{\rm PAH} \ {\rm cm}^3 \ {\rm s}^{-1} \ , \tag{C12}$$

and PAH^- is destroyed primarily by FUV photodetachment

$$ {\rm PAH^-} + h\nu \rightarrow {\rm PAH^0} + e \ , \qquad \kappa_7 = 2.00 \times 10^{-8} G_0' \ {\rm s}^{-1} \ . \tag{C13}$$

The condition $n_{\rm PAH^-}/n_{\rm PAH^0} < 1$ is then $\kappa_6 n_e / 2.0 \times 10^{-8} G_0' < 1$.

Assuming $n_{\rm PAH^0} = 0.7 n_{\rm PAH}$, we find (with n and n_e in units of $\rm cm^{-3}$)

$$n_{\rm PAH^-} = 2.8 \times 10^{-5} n_e n \phi_{\rm PAH} Z_d' G_0'^{-1} \ {\rm cm}^{-3} \ , \tag{C14}$$

or substituting into equation (C9), we find

$$n_e = 2.4 \times 10^{-3} \zeta_t'^{1/2} T_2^{1/4} G_0'^{1/2} Z_d'^{-1/2} \phi_{\rm PAH}^{-1} \ {\rm cm}^{-3} \ . \tag{C15}$$

C3. ANALYTIC EXPRESSION FOR $P(T)$ AND CONDITIONS FOR VALIDITY

We substitute equation (C15) for n_e into equation (C5) for the heating, equate the heating to the cooling given by equation (C4), and obtain for neutral gas in thermal balance with $100 \ {\rm K} \lesssim T \lesssim 1000 \ {\rm K}$

$$\frac{P}{k} = 1.1 n T = \frac{2240 G_0' (Z_d'/Z_g') T_2^{0.8} e^{1.5/T_2}}{1 + 2.6 (G_0' T_2^{1/2} Z_d'/\zeta_t')^{0.365}} \ . \tag{C16}$$

This equation is valid if all of the following conditions are met:

1.

$$\frac{G_0' T_2^{1/2} Z_d'}{\zeta_t'} < 17 \ . \tag{C17}$$

Condition 1 ensures that H^+ is mostly destroyed by PAH^-, and not PAH^0. This condition and the rest below are derived by using the rate coefficients above, along with equation (C15) for n_e.

2.

$$\frac{G_0' T_2^{1/2} Z_d'}{\zeta_t'} < 112 \ . \tag{C18}$$

Condition 2 ensures that neutral PAH^0, and not PAH^+, dominates the PAH population. Note that if condition 1 is satisfied, condition 2 is automatically satisfied.

3.

$$\frac{G_0' \zeta_t'}{T_2^{1/2} Z_d'} < 0.9 n^2 \phi_{\rm PAH}^2 \ . \tag{C19}$$

Condition 3 ensures that H atoms, and not electrons, dominate collisional excitation of [C II] 158 μm. In these equations, the hydrogen nucleus number density n is in cm^{-3}.

4.

$$\frac{G_0'}{Z_d' T_2^{1/4}} < 2.9 n \phi_{\rm PAH}^2 \ . \tag{C20}$$

Condition 4 ensures that H^+ is destroyed by PAH^-, and not by electron recombination.

5.

$$\frac{G_0' Z_d'}{T_2^{1/2} \zeta_t'} > 2.5 \times 10^{-2} \ . \tag{C21}$$

Condition 5 ensures that neutral PAH^0, and not PAH^-, dominates the PAH population.

6.

$$\frac{G_0' Z_d' T_2^{1/2}}{\zeta_t'} > 9.5 \times 10^{-3} \ . \tag{C22}$$

Condition 6 ensures that FUV dominates the destruction of PAH^-, and not reactions with H^+. Note that for $T_2 \simeq 1$–10, condition 5 automatically ensures condition 6.

7.

$$\frac{G_0' \zeta_t' T_2^{1/2}}{Z_d' Z_g'^2} > 3.5 \times 10^{-3} n^2 \phi_{\rm PAH}^2 \ . \tag{C23}$$

Condition 7 ensures that the dominant ion is H^+, and not C^+, which is ignored in the analytic analysis. These conditions ensure the validity of equation (C16) for $P(T)$.

Although the number of conditions is large, inspection of each of them reveals that for $n \sim 10$ cm^{-3} and $\phi_{\rm PAH} = 0.5$, all of the conditions are met for a wide range of conditions centered on solar neighborhood values. The motivation for deriving $P(T)$ is to find an analytic solution for $P_{\rm min}$, $T_{\rm (min)}$, and $n_{\rm min}$. Thus, the range of validity is centered on $T \simeq T_{\rm (min)} \simeq 250$ K and $n \simeq n_{\rm min} \simeq 10$ cm^{-3}, as we shall derive below. To calculate $P_{\rm min}$, we take $dP/dT = 0$ and solve for $T_{\rm (min)}$. Substitution of $T_{\rm (min)}$ into equation (C16) gives $P_{\rm min}$. No analytic solution is possible unless we simplify the denominator of $P(T)$ (eq. [C16]). If conditions 1–7 are satisfied, then the second term in the denominator is usually larger than unity. The denominator originates from the grain photoelectric heating equation, and the second term corresponds to the effects of positive charging on the grains/PAHs. The condition that the second term dominates (condition 8) is

$$\frac{G_0' Z_d' T_2^{1/2}}{\zeta_t'} > 0.072 \ . \tag{C24}$$

Note that condition 8 and condition 5 are nearly identical, for $T_2 \sim 2.5$. With all eight conditions satisfied, we find the solutions for $T_{\rm (min)}$, $P_{\rm min}$, and $n_{\rm min}$ given in the main text. Substitution of $n_{\rm min}$ (with the factor of unity in the denominator removed) and $T_{\rm (min)}$ into the eight conditions gives the simplified set of conditions given in the text.

REFERENCES

Afflerbach, A., Churchwell, E., Acord, J. M., Hofner, P., Kurtz, S., & DePree, C. G. 1996, ApJS, 106, 423
Afflerbach, A., Churchwell, E., & Werner, M. W. 1997, ApJ, 478, 190
Allamandola, L. J., Tielens, A. G. G. M., & Barker, J. R. 1989, ApJS, 71, 733
Anantharamaiah, K. R. 1985, J. Astrophys. Astron., 6, 203
Bakes, E. L. O., & Tielens, A. G. G. M. 1994, ApJ, 427, 822
———. 1998, ApJ, 499, 258
Beck, R. 2001, Space Sci. Rev., 99, 243
Begelman, M. C. 1990, in The Interstellar Medium in Galaxies, ed. H. A. Thronson, Jr., & J. M. Shull (Dordrecht: Kluwer), 287
Bennett, C. L., et al. 1994, ApJ, 434, 587
Bertsch, D. L., Dame, T. M., Fichtel, C. E., Hunter, S. D., Sreekumar, P., Stacy, J. G., & Thaddeus, P. 1993, ApJ, 416, 587
Black, J. H., & van Dishoeck, E. F. 1987, ApJ, 322, 412
Blitz, L., & Spergel, D. N. 1991, ApJ, 370, 205
Blum, R. D., & Pradhan, A. K. 1992, ApJS, 80, 425
Bock, J. J., et al. 1993, ApJ, 410, L115
Bohlin, R. C., Savage, B. D., & Drake, J. F. 1978, ApJ, 224, 132
Boldyrev, S. 2002, ApJ, 569, 841
Boulares, A., & Cox, D. P. 1990, ApJ, 365, 544
Brand, J., & Blitz, L. 1993, A&A, 275, 67
Braun, R. 1997, ApJ, 484, 637
Braun, R., & Walterbos, R. A. M. 1992, ApJ, 386, 120
Bregman, J., Parriott, J., & Rosen, A. 1999, in Interstellar Turbulence, ed. J. Franco & A. Carramiñana (New York: Cambridge Univ. Press), 120
Bronfman, L., Casassus, S., May, J., & Nyman, L.-Å. 2000, A&A, 358, 521
Bronfman, L., Cohen, R. S., Alvarez, H., May, J., & Thaddeus, P. 1988, ApJ, 324, 248
Burton, M. G., Hollenbach, D. J., & Tielens, A. G. G. M. 1992, ApJ, 399, 563
Burton, W. B. 1985, A&AS, 62, 365
Cardelli, J. A., Meyer, D. M., Jura, M., & Savage, B. D. 1996, ApJ, 467, 334
Carilli, C. L., Dwarakanath, K. S., & Goss, W. M. 1998, ApJ, 502, L79
Chen, L.-W., Fabian, A. C., & Gendreau, K. C. 1997, MNRAS, 285, 449
Cho, J., Lazarian, A., & Vishniac, E. T. 2002, ApJ, 564, 291
Colgan, S. W., Salpeter, E. E., & Terzian, Y. 1988, ApJ, 328, 275
Corbelli, E., & Salpeter, E. E. 1988, ApJ, 326, 551
Cowie, L. L., McKee, C. F., & Ostriker, J. P. 1981, ApJ, 247, 908
Cox, D. P. 1979, ApJ, 234, 863
———. 1995, in ASP Conf. Ser. 80, The Physics of the Interstellar Medium and Intergalactic Medium, ed. A. Ferrara, C. F. McKee, C. Heiles, & P. R. Shapiro (San Francisco: ASP), 317
Cox, D. P., & Smith, B. W. 1974, ApJ, 189, L105
Cuillandre, J.-C., Lequeux, J., Allen, R. J., Mellier, Y., & Bertin, E. 2001, ApJ, 554, 190
Dalgarno, A., Black, J. H., & Weisheit, J. C. 1973, Astrophys. Lett., 14, 77
Dame, T. M. 1993, in Back to the Galaxy, ed. S. S. Holt & F. Verter (New York: AIP), 267
Dehnen, W., & Binney, J. 1998, MNRAS, 294, 429
de Vaucouleurs, G. 1983, ApJ, 268, 451

Dickey, J. M., & Brinks, E. 1993, ApJ, 405, 153
Dickey, J. M., & Lockman, F. J. 1990, ARA&A, 28, 215
Dickey, J. M., Mebold, U., Stanimirovic, S., & Staveley-Smith, L. 2000, ApJ, 536, 756
Digel, S., de Geus, E., & Thaddeus, P. 1994, ApJ, 422, 92
Dixon, W. V. D., Hurwitz, M., & Bowyer, S. 1998, ApJ, 492, 569
Draine, B. T. 1978, ApJS, 36, 595
Draine, B. T., & Lee, H. M. 1984, ApJ, 285, 89
———. 1987, ApJ, 318, 485
Draine, B. T., & Sutin, B. 1987, ApJ, 320, 803
Elmegreen, B. G. 1989, ApJ, 338, 178
———. 1997, ApJ, 480, 674
Elmegreen, B. G., & Parravano, A. 1994, ApJ, 435, L121
Federman, S. R., Weber, J., & Lambert D. L. 1996, ApJ, 463, 181
Ferguson, A. M. N., Wyse, R. F. G., Gallagher, J. S., & Hunter, D. A. 1998, ApJ, 506, L19
Ferrière, K. 1998, ApJ, 497, 759
Ferrière, K. M., Zweibel, E. G., & Shull, J. M. 1988, ApJ, 332, 984
Fich, M., & Silkey, M. 1991, ApJ, 366, 107
Field, G. B. 1965, ApJ, 142, 531
Field, G. B., Goldsmith, D. W., & Habing, H. J. 1969, ApJ, 155, L149
Fitzpatrick, E. L., & Spitzer, L., Jr. 1994, ApJ, 427, 232
———. 1997, ApJ, 475, 623
Flannery, B. P., Roberge, W., & Rybicki, G. B. 1980, ApJ, 236, 598
Froese Fischer, C., & Saha, H. P. 1985, Phys. Scr., 32, 181
Galavis, M. E., Mendoza, C., & Zeippen, C. J. 1997, A&AS, 123, 159
Garmire, G. P., Nousek, J. A., Apparao, K. M. V., Burrows, D. N., Fink, R. L., & Kraft, R. P. 1992, ApJ, 399, 694
Garnett, D. R., Shields, G. A., Skillman, E. D., Sagan, S. P., & Dufour, R. J. 1997, ApJ, 489, 63
Garwood, R. W., & Dickey, J. M. 1989, ApJ, 338, 841
Gibson, S. J., Taylor, A. R., Higgs, L. A., & Dewdney, P. E. 2000, ApJ, 540, 851
Ginzburg, V. L., & Syrovatskii, S. I. 1964, The Origin of Cosmic Rays (Oxford: Pergamon)
Goldreich, P., & Sridhar, S. 1995, ApJ, 438, 763
Gry, C., Lequeux, J., & Boulanger, F. 1992, A&A, 266, 457
Gummersbach, C. A., Kaufer, A., Schäfer, D. R., Szeifert, T., & Wolf, B. 1998, A&A, 338, 881
Haardt, F., & Madau, P. 1996, ApJ, 461, 20
Habing, H. J. 1968, Bull. Astron. Inst. Netherlands, 19, 421
Haffner, L. M., Reynolds, R. J., & Tufte, S. L. 1999, ApJ, 523, 223
Hartmann, D., & Burton, W. B. 1997, Atlas of Galactic Neutral Hydrogen (New York: Cambridge Univ. Press)
Hawley, J. F., Gammie, C. F., & Balbus, S. A. 1995, ApJ, 440, 742
Heiles, C. 1994, ApJ, 436, 720
———. 2001, ApJ, 551, L105
Heiles, C., Reach, W. T., & Koo, B.-C. 1996, ApJ, 466, 191
Heiles, C., & Troland, T. H. 2003, ApJ, 586, 1067
Hennebelle, P., & Pérault, M. 1999, A&A, 351, 309
———. 2000, A&A, 359, 1124
Heyer, M. H., Brunt, C., Snell, R. L., Howe, J. E., Schloerb, F. P., & Carpenter, J. M. 1998, ApJS, 115, 241
Heyer, M. H., Carpenter, J. M., & Snell, R. L. 2001, ApJ, 551, 852
Heyer, M. H., & Schloerb, F. P. 1997, ApJ, 475, 173
Hunter, S. D., et al. 1997, ApJ, 481, 205
Jenkins, E. B. 1987, in Interstellar Processes, ed. D. Hollenbach & H. A. Thronson, Jr. (Dordrecht: Reidel), 533
Jenkins, E. B., Jura, M., & Loewenstein, M. 1983, ApJ, 270, 88
Jenkins, E. B., & Shaya, E. J. 1979, ApJ, 231, 55
Jenkins, E. B., & Tripp, T. M. 2001, ApJS, 137, 297
Kaufman, M. J., Wolfire, M. G., Hollenbach, D. J., & Luhman, M. L. 1999, ApJ, 527, 795
Kerr, F. J., Bowers, P. F., Jackson, P. D., & Kerr, M. 1986, A&AS, 66, 373
Knee, L. B. G., & Brunt, C. M. 2001, Nature, 412, 308
Kobayashi, N., & Tokunaga, A. T. 2000, ApJ, 532, 423
Kolpak, M. A., Jackson, J. M., Bania, T. M., & Dickey, J. M. 2002, ApJ, 578, 868
Korpi, M. J., Brandenburg, A., Shukurov, A., Tuominen, I., & Nordlund, Å. 1999, ApJ, 514, L99
Krolik, J. H., McKee, C. F., & Tarter, C. B. 1981, ApJ, 249, 422
Kulkarni, S. R., Blitz, L., & Heiles, C. 1982, ApJ, 259, L63
Kulkarni, S. R., & Fich, M. 1985, ApJ, 289, 792
Kulkarni, S. R., & Heiles, C. 1987, in Interstellar Processes, ed. D. Hollenbach & H. A. Thronson, Jr. (Dordrecht: Reidel), 87
Kulsrud, R. M., & Cesarsky, C. J. 1971, Astrophys. Lett., 8, 189
Kuntz, K. D., & Snowden, S. L. 2000, ApJ, 543, 195
Landau, L. D., & Lifshitz, E. M. 1987, Fluid Mechanics (New York: Pergamon)
Larson, R. B. 1979, MNRAS, 186, 479
———. 1981, MNRAS, 194, 809
Launay, J. M., & Roueff, E. 1977, A&A, 56, 289
Lazarian, A., & Pogosyan, D. 2000, ApJ, 537, 720
Lepp, S., Dalgarno, A., van Dishoeck, E. F., & Black, J. H. 1988, ApJ, 329, 418
Linsky, J. L., & Wood, B. E. 1996, ApJ, 463, 254
Liszt, H. S. 1992, in The Center, Bulge, and Disk of the Milky Way, ed. L. Blitz (Dordrecht: Kluwer), 111
Liszt, H. S., Braun, R., & Greisen, E. W. 1993, AJ, 106, 2349
Lockman, F. J. 1988, in The Outer Galaxy, ed. L. Blitz & F. J. Lockman (New York: Springer), 79
———. 2003, in ASP Conf. Ser. 276, Seeing through the Dust: The Detection of H I and the Exploration of the ISM in Galaxies, ed. A. R. Taylor, T. Landecker, & A. Willis (San Francisco: ASP), in press
Mac Low, M.-M. 1999, ApJ, 524, 169
Mac Low, M.-M., Balsara, D., Avillez, M. A., & Kim, J. 2001, ApJ, submitted
Malhotra, S. 1995, ApJ, 448, 138
Martin, C. L., & Kennicutt, R. C. 2001, ApJ, 555, 301
Mathis, J. S. 2000, ApJ, 544, 347
Mathis, J. S., Mezger, P. S., & Panagia, N. 1983, A&A, 128, 212
Mathis, J. S., Rumpl, W., & Nordsieck, K. H. 1977, ApJ, 217, 425
Matsuhara, H., Tanaka, M., Yonekura, Y., Fukui, Y., Kawada, M., & Bock, J. J. 1997, ApJ, 490, 744
McKee, C. F. 1989, in Interstellar Dust, ed. L. J. Allamandola & A. G. G. M. Tielens (Dordrecht: Kluwer), 431
———. 1990, in ASP Conf. Ser. 12, The Evolution of the Interstellar Medium, ed. L. Blitz (San Francisco: ASP), 3
McKee, C. F., & Ostriker, J. P. 1977, ApJ, 218, 148 (MO)
McKee, C. F., & Williams, J. P. 1997, ApJ, 476, 144
Mebold, U., Duesterberg, C., Dickey, J. M., Staveley-Smith, L., & Kalberla, P. 1997, ApJ, 490, L65
Mebold, U., Winnberg, A., Kalberla, P. M. W., & Goss, W. M. 1982, A&A, 115, 223
Meyer, D. M., Jura, M., & Cardelli, J. A. 1998, ApJ, 493, 222
Millar, T. J., Farquhar, P. R. A., & Willacy, K. 1997, A&AS, 121, 139
Minter, A. H., & Balser, D. S. 1997, ApJ, 484, L133
Minter, A. H., & Spangler, S. R. 1997, ApJ, 485, 182
Olling, R. P., & Merrifield M. R. 1998, MNRAS, 297, 943
Parker, E. N. 1969, Space Sci. Rev., 9, 651
Parravano, A. 1987, A&A, 172, 280
———. 1988, A&A, 205, 71
———. 1989, ApJ, 347, 812
Parravano, A., Hollenbach, D. J., & McKee, C. F. 2003, ApJ, 584, 797
Pottasch, S. R., Wesselius, P. R., & van Duinen, R. J. 1979, A&A, 74, L15
Rachford, B. L., et al. 2002, ApJ, 577, 221
Reynolds, R. J. 1983, ApJ, 268, 698
———. 1984, ApJ, 282, 191
———. 1992, ApJ, 392, L35
———. 1995, in ASP Conf. Ser. 80, The Physics of the Interstellar Medium and Intergalactic Medium, ed. A. Ferrara, C. F. McKee, C. Heiles, & P. R. Shapiro (San Francisco: ASP), 388
Reynolds, R. J., Tufte, S. L., Haffner, L. M., Jaehnig, K., & Percival, J. W. 1999, Publ. Astron. Soc. Australia, 15, 14
Rolleston, W. R. J., Smartt, S. J., Dufton, P. L., & Ryans, R. S. I. 2000, A&A, 363, 537
Rudolph, A. L., Brand, J., de Geus, E. J., & Wouterloot, J. G. A. 1996, ApJ, 458, 653
Salama, F., Bakes, E. L. O., Allamandola, L. J., & Tielens, A. G. G. M. 1996, ApJ, 458, 621
Savage, B. D., Drake, J. F., Budich, W., & Bohlin, R. C. 1977, ApJ, 216, 291
Savage, B. D., Lu, L., Weymann, R. J., Morris, S. L., & Gilliland, R. L. 1993, ApJ, 404, 124
Scoville, N. Z., & Sanders, D. B. 1987, in Interstellar Processes, ed. D. Hollenbach & H. A. Thronson, Jr. (Dordrecht: Reidel), 21
Sellwood, J. A., & Balbus, S. A. 1999, ApJ, 511, 660
Sembach, K. R., & Danks, A. C. 1994, A&A, 289, 539
Shaver, P. A., McGee, R. X., Newton, L. M., Danks, A. C., & Pottasch, S. R. 1983, MNRAS, 204, 53
Shull, J. M. 1987, in Interstellar Processes, ed. D Hollenbach and H. A. Thronson, Jr. (Dordrecht: Reidel), 225
Simpson, J. P., Colgan, S. W. J., Rubin, R. H., Erickson, E. F., & Haas, M. R. 1995, ApJ, 444, 721
Slavin, J. D., & Cox, D. P. 1993, ApJ, 417, 187
Slavin, J. D., & Frisch, P. C. 1998, in The Local Bubble and Beyond, ed. D. Breitschwerdt, M. J. Freyberg, & J. Truemper (New York: Springer), 305
Slavin, J. D., McKee, C. F., & Hollenbach, D. J. 2000, ApJ, 541, 218
Smith, D. A., Allen, R. J., Bohlin, R. C., Nicholson, N., & Stecher, T. P. 2000, ApJ, 538, 608
Smith, L. F., Biermann, P., & Mezger, P. G. 1978, A&A, 66, 65
Snell, R. L., Carpenter, J. M., & Heyer, M. H. 2002, ApJ, 578, 229
Snowden, S. L., Egger, R., Finkbeiner, D. P., Freyberg, M. J., & Plucinsky, P. P. 1998, ApJ, 493, 715
Sodroski, T. J., et al. 1994, ApJ, 428, 638
Sofia, U. J., Cardelli, J. A., Guerin, K. P., & Meyer D. M. 1997, ApJ, 482, L105
Solomon, P. M., Rivolo, A. R., Barrett, J., & Yahil, A. 1987, ApJ, 319, 730
Spitzer, L., Jr. 1968, in Nebulae and Interstellar Matter, ed. B. M. Middlehurst & L. H. Aller (Chicago: Univ. Chicago Press), 1

Spitzer, L., Jr. 1978, Physical Processes in the Interstellar Medium (New York: Wiley)
———. 1982, ApJ, 262, 315
Spitzer, L., Jr., & Fitzpatrick, E. L. 1993, ApJ, 409, 299
Spitzer, L., Jr., & Jenkins, E. B. 1975, ARA&A, 13, 133
Stark, A. A., Gammie, C. F., Wilson, R. W., Bally, J., Linke, R. A., Heiles, C., & Hurwitz, M. 1992, ApJS, 79, 77
Sternberg, A., McKee, C. F., & Wolfire, M. G. 2002, ApJS, 143, 419
Sternberg, A., & Neufeld, D. A. 1999, ApJ, 516, 371
Stone, J. M., Ostriker, E. C., & Gammie, C. F. 1998, ApJ, 508, L99
Taylor, J. H., & Cordes, J. M. 1993, ApJ, 411, 674
Tielens, A. G. G. M. 1995, in ASP Conf. Ser. 73, Airborne Astronomy Symposium on the Galactic Ecosystem: From Gas to Stars to Dust, ed. M. R. Haas, J. A. Davison, & E. F. Erickson (San Francisco: ASP), 3
Tielens, A. G. G. M., & Hollenbach, D. J. 1985, ApJ, 291, 722
Tielens, A. G. G. M., Hony, S., van Kerckhoven, C., & Peeters, E. 1999, in The Universe as Seen by *ISO*, ed. P. Cox & M. F. Kessler (ESA-SP 427; Noordwijk: ESA), 579
Torres-Peimbert, S., & Peimbert, M. 1977, Rev. Mexicana Astron. Astrofis., 2, 181
Twarog, B. A., Ashman, K. M., & Anthony-Twarog, B. J. 1997, AJ, 114, 2556
Vallerga, J. V. 1996, Space Sci. Rev., 78, 277
van der Tak, F. F. S., & van Dishoeck, E. F. 2000, A&A, 358, L79
van Dishoeck, E. F., & Black, J. H. 1982, ApJ, 258, 533
———. 1986, ApJS, 62, 109
Van Steenberg, M. E., & Shull, J. M. 1988, ApJ, 330, 942
Vázquez-Semadeni, E., Gazol, A., Passot, T., & Sánchez-Salcedo, J. 2003, in Turbulence and Magnetic Fields in Astrophysics, ed. E. Falgarone & T. Passot (New York: Springer), in press
Vázquez-Semadeni, E., Gazol, A., & Scalo, J. 2000, ApJ, 540, 271
Wang, L., Höflich, P., & Wheeler, J. C. 1997, ApJ, 483, L29
Watson, W. D. 1972, ApJ, 176, 103
Weaver, H., & Williams, D. R. W. 1973, A&AS, 8, 1
Weingartner, J. C., & Draine, B. T. 2001a, ApJ, 563, 842
———. 2001b, ApJS, 134, 263
Welty, D. E., & Hobbs, L. M. 2001, ApJS, 133, 345
Williams, J. P., & McKee, C. F. 1997, ApJ, 476, 166
Wolfire, M. G., & Cassinelli, J. P. 1986, ApJ, 310, 207
Wolfire, M. G., & Churchwell, E. 1994, ApJ, 427, 889
Wolfire, M. G., Hollenbach, D., McKee, C. F., Tielens, A. G. G. M., & Bakes, E. L. O. 1995a, ApJ, 443, 152 (WHMTB)
Wolfire, M. G., McKee, C. F., Hollenbach, D., & Tielens, A. G. G. M. 1995b, ApJ, 453, 673
Wouterloot, J. G. A., & Brand, J. 1989, A&AS, 80, 149
Wouterloot, J. G. A., Brand, J., Burton, W. B. & Kwee, K. K. 1990, A&A, 230, 21
Wright, E. L., et al. 1991, ApJ, 381, 200